Structural Health Monitoring of Arch Dams Using Dynamic and Static Measurements

Report to the
Water Research Commission

by

Pilate Moyo[1] & Chris Oosthuizen[2]
[1] Department of Civil Engineering, University of Cape Town
[2]Department of Water Affairs

WRC Report No. 2025/1/13
ISBN 978-1-4312-0453-3

September 2013

Obtainable from

Water Research Commission
Private Bag X03
Gezina, 0031

orders@wrc.org.za or download from www.wrc.org.za

EXECUTIVE SUMMARY

Background

Dam failures in the late 1800s resulted in loss of life, and raised awareness about the need for legislation on dam safety. Notable examples include the collapse of Dale Dyke Dam in the United Kingdom, Sheffield in 1864 and the collapse of Mill River Dam in USA, Massachusetts in 1874. Many countries have since introduced legislation on dam safety primarily to ensure periodic safety evaluation of large dams. In South Africa, the Department of Water Affairs is responsible for Dam Safety as stipulated in the National Water Act, Section, 123(1), 1998.

Dam safety evaluation includes structural assessment through dam surveillance and monitoring data and finite element analysis. Static surveillance and monitoring of dams, that is, continuous or periodic monitoring of static structural parameters such as strain and temperature is now well established. In recent years it has been shown that monitoring of the dynamic behaviour of civil engineering infrastructures can provide essential information for determining their safety. Therefore, in many civil engineering applications it has become important to identify the dynamic characteristics of structures and also monitor these dynamic characteristics in the operation phase through ambient vibration testing. While this technology has grown in many civil engineering applications, its viability in dam safety has not been fully investigated. One of the reasons for the limited use of ambient vibration testing in arch dams is that early trials such as Brownjohn et al. (1982) concluded that it was difficult to apply this approach to dams owing to their high stiffness. However since that time, there have been substantial improvements in sensing technologies and data processing algorithms. This has led to the development and maturity of a new discipline in structural health monitoring, now often referred to as operational modal analysis (OMA). This discipline deals with ambient vibration testing of structures and the analysis of resulting data.

Finite element analysis (FEA) plays an important role in safety evaluation of dams as it allows the application of various load combinations which are not always observed through surveillance and monitoring. The challenge in FEA is generating a finite element model that is representative of the as-built dam with respect to dynamic behaviour. The most commonly adopted approach for dynamic analysis of dams is the so called Westergaard approach. While this approach has been used successfully for investigating the dynamic performance of dams under seismic loading, it has not been applied in finite element model updating based on ambient vibration testing. The essential difference between the two situations is the magnitude of accelerations induced on the structure by the excitation force. In a seismic event, large accelerations are experienced compared to the normal operating environment. Thus the applicability of the Westergaard approach in finite element model updating of arch dams based on ambient vibration testing needs to be established.

Cyclic seasonal temperature and associated thermally induced stresses have been found to contribute significantly to long term degradation of strength and stiffness of concrete dams. Thus accurate modelling of thermally induced stresses is critical in dam safety evaluation. Also thermal stresses may affect the dynamic behaviour of concrete arch dams. Consequently this aspect needs to be investigated.

Key objectives

This project focused on three key objectives namely;

i). The applicability ambient vibration testing to concrete arch dams. A concrete arch dam was monitored periodically over a three year period. A high resolution, low noise vibration measuring system was used.

ii). The applicability of the Westergaard approach in finite element model updating of arch dams based on ambient vibration testing. Another aspect of finite element modelling that strongly influences the behaviour of arch dams is the foundation-wall system. Here the challenge is generally what size of the foundation is necessary to model the system with minimal error. FEA software, ABAQUS, was used.

iii). Temperature modelling for arch dams, and the influence of seasonal temperature variations on dynamic properties of arch dams. FEA software, ABAQUS, was used.

Findings

The following findings were obtained;

i). Ambient vibration testing is a viable methodology for surveillance and monitoring of arch dams.

ii). The Westergaard method tends to overestimate the added mass of water for divergent and/or skewed reservoirs. This method cannot be directly applied to dams with divergent and/or skewed reservoirs.

iii). In order to accurately model the effect of seasonal temperature variations on arch dams, the temperature model must include seasonal reservoir level variations. The results of the temperature analysis show that it is critical to include temperature effects for dynamic analysis of arch dams. However once the initial thermal stresses have been introduced, the influence of seasonal temperature variations on dynamic characteristics is negligible.

Recommendations

Based on the findings of this research the following recommendations are made;

i) Revise the Westergaard method to account for skew/divergent reservoirs in estimation of added mass.

ii) Further investigate the effect of thermal stresses in concrete dams.

iii) The current study confirmed the viability of the application of ambient vibration testing of dams. It is recommended to install permanent monitoring systems for dam surveillance based on ambient vibration testing.

ACKNOWLEDGEMENTS

The authors acknowledge funding and support from the Water Research Commission. Special acknowledgement to Mr Wandile Nomquphu and his team for managing the project effectively and diligently.

We are also grateful to the Department of Water Affairs for providing access to the dams and necessary information.

The contribution of the reference group, Prof Mark Alexander, Prof Jan Wium, Mr Jeremiah Mutamba, Mr Piet Naude and Mr Heinrich Elges, is acknowledged.

Thanks to Prof Alexander for reviewing this document.

We acknowledge the contribution of the following students Mr Patrick Bukenya, Mr Tony Meri, Mr Makha Ramonate, Mr Mbongeni Nzuza and Mr Bongani Sibanda, Mr Chad Ludwig and Miss Fiona Budlender.

TABLE OF CONTENTS

LIST OF TABLES

LIST OF FIGURES

LIST OF SYMBOLS AND ABBREVIATIONS

Latin Upper Case

A	amplitude of air temperature fluctuations
A_u	amplitude of reservoir temperature fluctuations
A_0	amplitude of reservoir surface temperature fluctuations
A_m	amplitude of foundation temperature fluctuations
$\boldsymbol{B}$	strain displacement matrix
B_m	annual mean air temperature
C	capacitance matrix
C_s	Stefan-Boltzmann constant
$°C$	degree celsius
D_m	concrete thermal diffusivity
D_{gm}	foundation thermal diffusivity
$\boldsymbol{D}$	generalised material thermal conductivity matrix
$\overline{D}$	stress-strain matrix
E	material elastic modulus
$\vec{f}$	vector of nodal force
I	total incident solar radiation
I_h	Hourly incident solar radiation
H_d	sky diffused radiation
H	depth of reservoir
H_0	monthly average global solar radiation on horizontal surface
H_b	direct radiation / global irradiance
H_d	diffuse radiation / diffuse irradiance
H_r	reflected radiation / direct irradiance
H_e	extra-terrestrial radiation
I_{sc}	solar constant
$\boldsymbol{K}$	stiffness matrix

$\boldsymbol{K_{cd}}$	thermal conductivity matrix
$\boldsymbol{K_c}$	convection matrix
$\boldsymbol{K_r}$	radiation matrix
K_T	monthly average index of cloud cover
K	degrees Kelvin
L	dam thickness
N	array of shape functions
P	period of cycle
Q	heat source
T	temperature of concrete
$\bar{T}$	boundary prescribed temperature
T_{ini}	initial temperature state
$\dot{T}$	rate of temperature change
T_a	air temperature
$\bar{T}_a$	mean air temperature
T_w	reservoir temperature
T_m	mean annual reservoir temperature
T_b	reservoir temperature at the bottom
T_t	reservoir temperature at the top/surface
T_g	ground temperature
T_s	ground surface temperature
T_0	annual mean ground surface temperature
T^*	absolute zero temperature
V	wind speed
W	watts
C_{ijkl}	rank four material stiffness tensor

Latin Lower Case

a	surface absorptivity of solar radiation
c	material specific heat capacity
$\{\boldsymbol{d}\}$	vector array of nodal temperatures
e	surface emissivity
f	evaporation fraction
h_s	sunrise / sunset hourly angle
h	hourly angle
h_r	radiation coefficient
h_c	convection coefficient
k	material thermal conductivity
m	meters
n	maximum number of time steps
p	average coefficient of reflection from surrounding
q	heat flux
q_s	surface heat flux
q_a	heat flux due to solar radiation
q_c	convection heat transfer rate
q_r	radiation heat transfer rate
$\vec{q}$	heat flux vector
$\bar{q}$	boundary prescribed heat flux
r^2	correction factor for solar constant
r_h	relative humidity
s	seconds
t	time
w	test / weighting function
x, y, z	Cartesian coordinate system
y	reservoir depth

z	foundation depth
$\bar{z}$	damping depth of ground temperature oscillations

Greek Upper Case

∇^2	Laplacian operator for temperature
ΔR	
Δt	time step length
Γ_T	temperature imposed boundary
Γ_q	flux imposed boundary
Ω	finite element domain

Greek lower Case

α	coefficient of thermal expansion
β	sloping angle of dam surface
δ	solar declination
φ	latitude of location
ω	angular frequency
ε_{ts}	thermal strain vector
ε_{kl}^{e}	strain tensor
$\bar{\sigma}$	thermal creep stress caused by temperature difference
σ_{ij}	stress tensor

1. INTRODUCTION

A well-managed water resource system helps to sustain society, commerce and industry of any country. Dams constitute significant and critical discrete components of a water resource system and they are among the most expensive investment asset of any country's civil infrastructure. They also have a long service life compared with most commercial products and are rarely replaceable once they are built. Dam failure often leads to both economic loss and loss of human life. Therefore, given these severe consequences of failure of any dam, it is imperative to maintain dams in such a way that they function reliably and efficiently throughout their service life. To this end all dams with a safety risk (i.e. dams with a maximum wall height that exceeds 5,0 m and with a storage capacity of more than 50 000 m3) in South Africa is subject to appropriate monitoring and surveillance to alert authorities about any safety risks to the dams. A major aspect of these monitoring systems is to form an opinion about the behaviour of the dams compared to the design parameters.

A useful tool that has not been fully exploited in dam monitoring and surveillance is dynamic testing. Dynamic testing involves the measurement of dynamic properties of a dam such as natural frequencies, mode shapes and damping ratios which can be related to structural parameters such as modal mass, stiffness and damping. Thus by determining the dynamic properties of a dam, one gains insight into as-built structural behaviour of the dam. The measured dynamic properties can therefore be used for calibrating theoretical finite element models and also tracking the behaviour of the dam over extended periods of time. A major drawback in the implementation of dynamic testing has been the need to measure excitation forces during testing in order to extract dynamic parameters (natural frequencies, damping ratios, modal mass, etc.) from measurements. To do this, heavy machinery should be set-up on the dam, making dynamic testing a very expensive exercise.

The development of the so-called output-only techniques (ambient vibration testing) for extracting dynamic properties has expanded the applications of dynamic testing (Brincker et al. 2001, Peeters and De Roeck 2001). Output-only techniques do not require the input force to be measured in order to extract dynamic properties of a system. Thus ambient vibration testing lends itself well to testing of large structures such as dams. For these types of structures, excitation is provided by such effects as wind and waves.

Early ambient vibration testing of dams was reported by Ellis et al. (1982) and Brownjohn et al. (1986). Their findings highlighted the challenges of identifying natural frequencies of large stiff structures from ambient vibration testing. Kemp et al. (1996), Loh and Wu (1996) and Darbre et al. (2000) reported successful short term ambient vibration testing of Ruskin, Fei-Tsui and Mauvoisin dams respectively. Darbre (2002) performed periodic monitoring of Mauvoisin dam for a period of about 180 days. These studies indicate that there have been significant improvements in ambient vibration testing of dams since early trials in the 1980s. The improvements can be attributed to developments in instrumentation and signal processing algorithms.

The integration of ambient vibration testing with static monitoring (stress, temperature, strain, inclination) provides a holistic overview of dam behaviour and performance. The challenges of static monitoring lie in the interpretation of measurements and extraction of useful features from the measurements (Sohn et al. 2001; Moyo and Brownjohn 2002) . By integrating dynamic testing and static monitoring it would be possible to identify the critical loading conditions on the dam.

The present proposal is for the installation and operation of a combined dynamic and static monitoring system on Roode Elsberg dam located in the Western Cape, South Africa. The overall goal is an in-depth understanding of the structural condition and structural performance of the dam. The project draws from successful demonstration of applicability of ambient vibration testing to dams cited above. However, unlike the previous studies, the present study will focus on the long-term monitoring of the behaviour and performance of the dam. Long-term monitoring will provide information on the influence of different loading regimes (e.g. temperature load and hydrostatic load) on the behaviour and hence state of 'health' of the dam. The experience gained from ambient dynamic testing and monitoring of Roode Elsberg dam will be used in the development and implementation of similar strategies for other dams in the country.

2. OBJECTIVES

Although the potential of ambient vibration testing for dynamic testing of dams has been demonstrated, its application is not widespread. Hence there are no best-practice procedures for ambient vibration testing of dams.

Thus the present project will seek to investigate;

i) the applicability of ambient vibration testing to concrete arch dams. A concrete arch dam was monitored periodically over a three year period.
ii) the applicability of the Westergaard approach in finite element model updating of arch dams based on ambient vibration testing. Another aspect of finite element modelling that strongly influences the behaviour of arch dams is the foundation-wall system. Here the challenge is generally what size of the foundation is necessary to model the system with minimal error.
iii) temperature modelling for arch dams and the influence of seasonal temperature variations on dynamic properties of arch dams.

Roode Elsberg Dam, was chosen as a subject structure to investigate and demonstrate the potential of dynamic monitoring of concrete dams using ambient vibration testing. The dam was chosen owing to its proximity to the University of Cape Town and ease of access.

3. BACKGROUND

Structural health monitoring of dams has become an integral part of the safety assessment of large dams. The main goal of structural health monitoring is to identify any abnormal behaviour which could lead to structural failure as early as possible, thereby allowing sufficient time for the implementation of appropriate corrective measures. Structural health monitoring involves the use of instrumentation to measure the actual in-service structural condition of a dam, and inference of its ability to function reliably, using data processing and interpretation techniques. Structural health monitoring of dams can be continuous or periodic. Continuous monitoring tracks the condition and behaviour of a dam using permanently installed instrumentation and serves to detect and characterise unusual structural behaviour. On the other hand, periodic monitoring is usually performed at selected intervals to assess the fitness for purpose of a dam. The following are the key steps in SHM:

i) Acquisition of the monitoring information, i.e. measurements from instruments as well as qualitative information from visual inspections.

ii) Interpretation and assessment of the information

iii) Taking decisions

iv) Archiving the results.

A comprehensive SHM system should have internal intelligence, operational intelligence, and presentational intelligence Aktan (1996). Internal intelligence is the ability of the SHM system to function in a reliable manner, to be self-diagnosing of internal faults and to notify users of any malfunctions in the system. Operational intelligence is the ability of the SHM system to obtain proper data and not to miss data collection during critical events or periods in the life of the structure. Presentational intelligence is concerned with the ability of the SHM system to pass on only those data which are useful to the user, in a user-friendly manner. In order to accomplish these roles, a typical SHM system should consist of a host computer and sensor excitation hardware, an integrated system of sensors, software and communication hardware (Figure 3.1). The host computer performs the task of controlling data acquisition and interpretation hardware in addition to storing recorded data in its hard disk, analysing the data, and communicating with remote computers. The sensor excitation and data interpretation hardware provides the link between the sensors and the host computer. This data acquisition hardware excites sensors and converts signals from sensors to appropriate engineering units such as strain, temperature, etc. Sensors are the nerves of the system, logging sensed data to the host computer via the data acquisition system. Their selection for a particular system is governed by application, sensor sensitivity, power requirements, robustness and reliability. The software plays the important role of controlling the operating system, sensors, data analysis and communication. Data analysis involves reducing the data into minimal and useable information and presenting the data in meaningful formats for the user. Communication capabilities form an important component of a health monitoring system; the user must be able to communicate with the host computer from a remote site as well as a portable computer connected up to the system in the field. Possible communication links include, a modem and telephone line, a cellular connection, the internet, and telemetry or radio link.

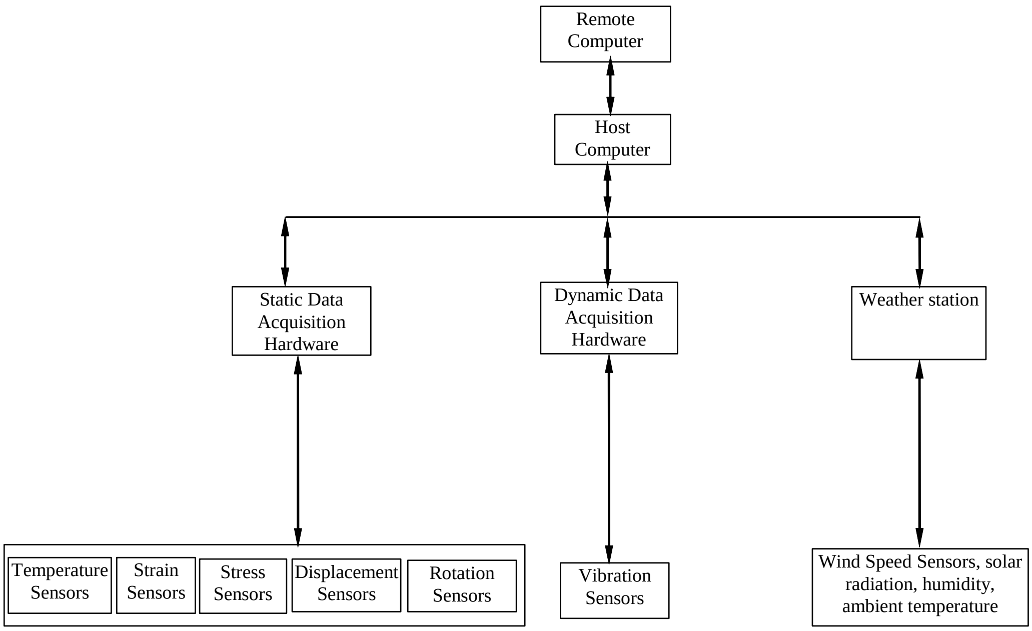

Figure 3.1: Typical Instrumentation for Structural Health Monitoring

The present project is viewed in the context of an integrated dam management system in which structural health monitoring forms part of a broader system incorporating visual inspections and analytical/numerical models (Figure 3.2). The heart of such a system is synthesis and interpretation of data from various modules. This project focuses on dynamic based SHM and analytical modelling of concrete arch dams. The integration and interpretation of data from these modules is explored.

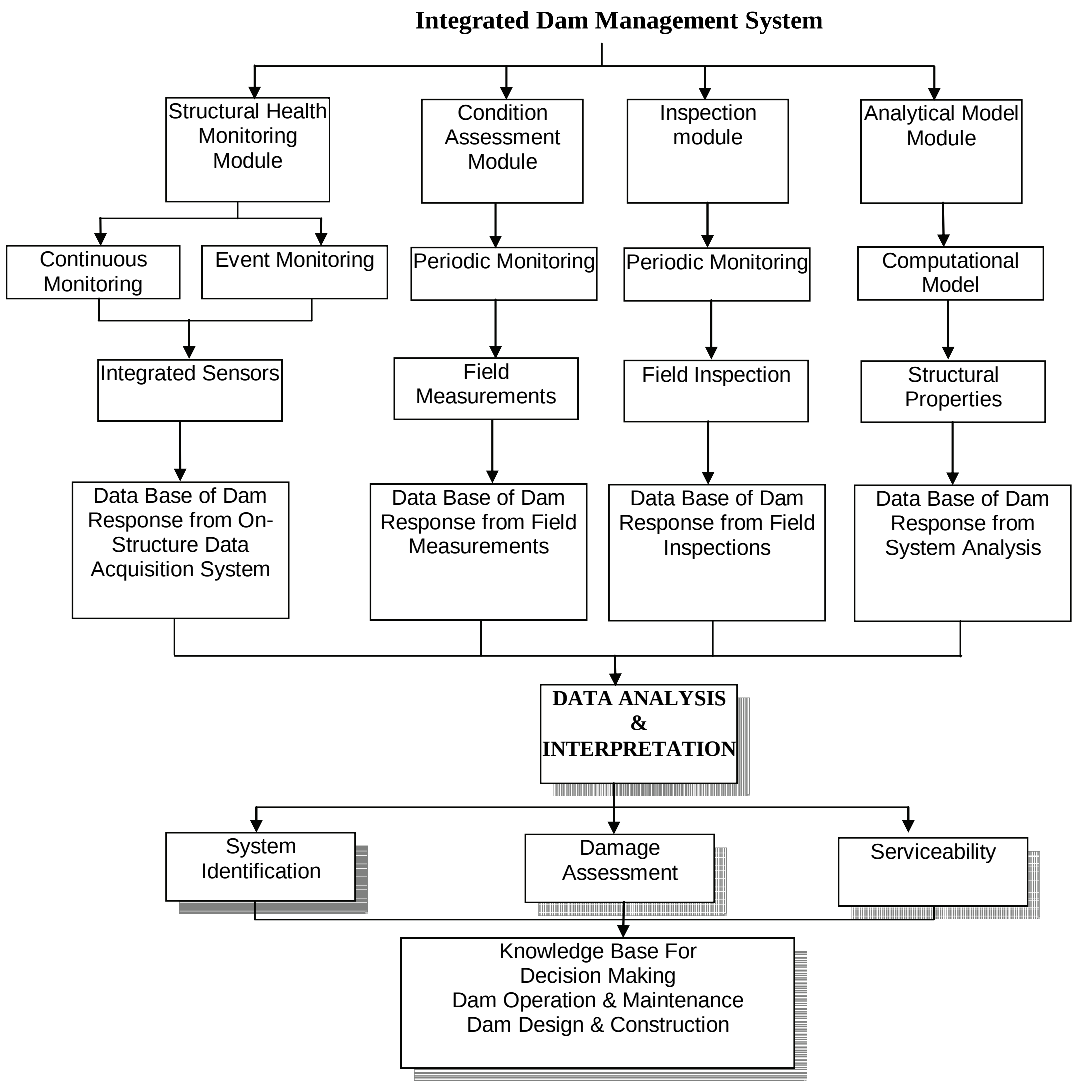

Figure 3.2: Integrated dam management system

4. AMBIENT VIBRATION TESTING

4.1. Background

Dynamic characterization of structures is of significant importance in civil engineering structures such as dams, buildings and bridges as it provides useful information about the as-built behaviour of these structures. The basis of dynamic based monitoring is that the dynamic properties such as natural frequencies, mode shapes, and damping ratios are related to structural parameters such as mass, stiffness and damping. A change in the dynamic characteristics may therefore be related to structural damage. While finite element analysis (FEA) can be used to compute dynamic properties, the results never perfectly match the as-built parameters owing to modelling and computational errors. Thus measured dynamic characteristics can be used to fine-tune finite element (FE) models to match, as closely as possible, the as-built behaviour of a dam. Dynamic monitoring and testing thus serves to assess structural performance of dams as well as update FE models. Updated FE models play a key role in the condition assessment of dams and this is done by comparing updated models to the design model.

The main goal of dynamic testing is to extract dynamic properties, also referred to as modal parameters, of a structure from vibration measurements. Two approaches are commonly used to extracted the modal parameters namely experimental modal analysis (EMA), also referred to as forced vibration testing (FVT) and ambient vibration testing (AVT), commonly referred to as operational modal analysis (OMA).

EMA requires the measurement of the excitation force in order to measure the frequency response function. This is expensive and time consuming for large structures such as dams which require large forces to excite. Thus EMA is not an attractive method for dynamic testing of dams. OMA on the other hand, does not require the measurement of excitation forces and uses ambient or operational forces for the excitation of a structure. In dams, such excitation is provided by water waves, wind and sometimes ground motions. This methodology has become attractive for testing large structures such as dams due to a number of advantages:

i) Testing is fast and cheap to conduct since no excitation equipment is needed
ii) It does not interfere with the normal use of the structure.
iii) It allows identification of modal parameters which are representative of the whole system in its actual operational conditions.

In case of OMA, the excitation process being unknown, the response signals must be recorded simultaneously to assure the same testing conditions. The deterministic knowledge of the input is usually replaced by the assumption that the input is a realization of a stochastic process (i.e. stationary zero mean Gaussian white noise uniformly exciting the structure over the complete frequency range). This assumption means that the input is characterized by a flat spectrum in the frequency range of interest and, therefore, it gives a broadband excitation, so that all modes are excited. As a result, the output spectrum contains full information about the structure, since all modes are equally excited. From a mathematical point of view, signals are completely described by their correlation functions or by their counterpart in the frequency domain, the auto and cross power spectra.

The main challenges in the development of OMA have been extracting modal parameters from measured data. To this end many modal parameter estimation techniques have been proposed. Parameter estimation methods directly based on time histories of the output signals are referred to as time domain methods, while those based on Fourier transform of signals are referred to as frequency domain methods. A review of these techniques is given in the following section.

4.2. Modal Parameter Estimation Techniques in OMA

Although OMA techniques are derived from EMA procedures, they are developed in a stochastic framework, due to the assumptions about input. There are a number of modal parameter estimation methods in OMA broadly divided into two categories, namely frequency domain methods and time domain methods. Frequency domain methods are based on the Fourier transform while time domain methods are extract modal parameters from time histories of the output signals. This chapter reviews the most commonly used OMA methods and new methods are also presented.

4.2.1. Frequency domain methods

Peak Picking

One of the first techniques to be used for modal parameter estimation is the so-called peak picking technique. The method is based on output-only frequency response functions (FRFs) and consists of identifying the natural frequencies as the peaks of the FRF curves. Damping ratios are obtained using the half-power bandwidth method, and the FRFs amplitude at the peak can be considered as an estimate of the mode shape.

Identification of actual natural frequencies can be carried out by looking not only at peaks of the spectra but also by inspecting the coherence function between two signals, defined as:

$$\gamma_{xy}^{2}(f)=\frac{\left|G_{xy}(f)\right|^{2}}{G_{xx}(f)G_{yy}(f)} \qquad 4.1$$

and assuming values between 0 and 1; $G_{xy}(f)$ is the value of the cross spectrum between signals *x* and *s* at the frequency *f*, while $G_{xx}(f)$ and $G_{yy}(f)$ are the values of the auto-spectra of signal *y* and signal *s*, respectively, at the same frequency. If *f* is a natural frequency, the coherence function is close to 1 because of the high signal-to-noise ratio at that frequency. This characteristic is helpful in identifying the correct natural frequencies.

The method is probably the easiest and the most widely-used technique for fast modal parameter estimation and has been successfully applied to civil engineering structures (Felber 1993, Danielle and Taylor 1999). However, peak picking method suffers some drawbacks as it works well when damping is low and modes are well-separated. If these conditions are violated erroneous results are expected. The method identifies the so-called operational deflection shapes (which are a combination of all mode shapes: they are a good approximation of actual mode shapes only if one mode is dominant at the considered frequency) instead of actual mode shapes. In case of closely-spaced modes, this shape is the superposition of multiple modes which may not be the exact mode shapes. The second drawback is that the selection of natural frequencies can become a subjective task if the spectrum peaks are not very clear. The last drawback is the need of a fine frequency resolution in order to obtain a good estimation of the natural frequency.

Frequency domain decomposition

The main drawbacks of the peak picking method have been overcome by the introduction of the frequency domain decomposition (FDD) technique (Brincker et al. 2000). This method was originally applied to output only FRFs and was known as complex mode indicator function (CMIF) in order to point out its ability to detect multiple roots and, therefore, the possibility to count the number of modes present in the measurement data. FDD technique is based on the input and output power spectrum density (PSD) relationship (equation 4.2) for stochastic process

$$G_{yy}(j\omega) = \overline{H}(j\omega)G_{xx}(j\omega)H(j\omega)^{P} \tag{4.2}$$

Where $G_{xx}(j\omega)$ is the input PSD, $G_{yy}(j\omega)$ is the output PSD, $H(j\omega)$ is the FRF which is expressed as partial fractions (equation 4.3) form via poles λ_k and residues R_k containing information about mode shapes (Zhang et al. 2005).

$$H(j\omega) = \sum_{k=1}^{n} \frac{R_k}{j\omega - \lambda_k} + \frac{\overline{R}_k}{j\omega - \overline{\lambda}_k} \tag{4.3}$$

Where

$$R_k = \phi_k \gamma_k^T \tag{4.4}$$

ϕ_k and γ_k^T are the mode shape vector and the modal participation vector respectively.

When all output measurements are taken as references, then the FRF becomes a square matrix and $\gamma_k = \phi_k$. If the input is assumed to be white noise, i.e. its PSD is a constant matrix ($G_{xx}(j\omega) = C$, then equation 4.2 becomes (Brincker et al.2000):

$$G_{yy}(j\omega) = \sum_{k=1}^{n}\sum_{s=1}^{n} \left[\frac{R_k}{j\omega - \lambda_k} + \frac{\overline{R}_k}{j\omega - \overline{\lambda}_k} \right] \times C \left[\frac{R_s}{j\omega - \lambda_s} + \frac{\overline{R}_s}{j\omega - \overline{\lambda}_s} \right]^{p} \tag{4.5}$$

Using Heaviside partial fraction theorem, multiplying the two partial fractions, the output PSD can be reduced to a pole/ residue form as shown below:

$$G_{yy}(j\omega) = \sum_{k=1}^{n} \frac{A_k}{j\omega - \lambda_k} + \frac{\overline{A}_k}{j\omega - \overline{\lambda}_k} + \frac{B_k}{-j\omega - \lambda_k} + \frac{\overline{B}_k}{-j\omega - \overline{\lambda}_k} \tag{4.6}$$

where A_k is the k^{th} residue (m x m) matrix of the output PSD also known as the Hermitian matrix (Brincker et al. 2000) given by:

$$A_k = R_k C \left(\sum_{s=1}^{n} \frac{R_s^p}{-\lambda_k - \overline{\lambda}_s} + \frac{\overline{R}_s^p}{-\lambda_k - \overline{\lambda}_s} \right) \tag{4.7}$$

The contribution to the residue from the *kth* mode is given by

$$A_k = \frac{R_k C \overline{R}_k^p}{2\alpha_k} \tag{4.8}$$

where α_k is the negative of the real part of the pole $\lambda_k = -\alpha_k + j\omega_k$. It appears this term becomes dominating when the damping is light, and, thus, for case of light damping, the residue becomes proportional to the mode shape vector (Brincker et al. 2000):

$$A_k \alpha R_k C R_k = \phi_k \gamma_k^p C \gamma_k \phi_k^p = d_k \phi_k \phi_k^p \tag{4.9}$$

Where $d_k = \gamma_k^p G_{xx} \gamma_k$, is a real scalar for white noise excitation. In the vicinity of a natural frequency, PSD can be approximated by modal decomposition (Zhang et al. 2005):

$$G_{yy_{\omega \to \omega_k}}(j\omega) \approx \phi_k \frac{2d_k}{j\omega - \lambda_k} \phi_k^p = \alpha_k \phi_k \phi_k^p \tag{4.10}$$

The FDD method is the backbone of frequency domain decomposition-type methods. It uses the output PSD as the peak-peak method but it carries out singular value decomposition (SVD) of the output PSD, estimated at discrete frequencies $\omega = \omega_i$ (Brincker et al. 2000) This decomposition is performed to identify single degree of freedom models of the system (Batel, 2002)

The singular value decomposition of an m x n complex matrix A is the following factorization:

$$A = U \Sigma V^H \tag{4.11}$$

Where U and V are unitary and Σ is a diagonal matrix that contains the real singular values.

$$\Sigma = diag(s_1,....,s_r)$$
$$r = \min(m,n) \tag{4.12}$$

The superscript *H* on the matrix *V* denotes a Hermitian transformation (transpose and complex conjugate). In the case of real valued matrices, the *V* matrix is only transposed. The s_i elements in the matrix S are called the singular values and their following singular vectors are contained in the matrices *U* and *V*.

This singular value decomposition is performed for each of the matrices at each frequency and for each measurement taken. The spectral density matrix is then approximated to the following expression after SVD decomposition:

$$[G_{yy}(j\omega)] = [\Phi][\Sigma][\Phi]^H \tag{4.13}$$

(with $$[\Phi]^H[\Phi] = [I]$$

$[\Sigma]$ being the singular value matrix and $s_1, \ldots, s_r$ the singular vectors unitary matrix and $[\Phi]$ being a vector of mode shapes at a specific mode.

The SVD has the ability of separating signal space from noise space, the modes can be indicated from SV plots, and closely spaced modes or even repeated modes can easily be detected (Zhang et al. 2005). The FDD has the advantages of calculating closely spaced modes, being user friendly, but it cannot give modal damping ratios.

The second generation of FDD is called enhanced FDD which estimates not only natural frequencies and mode shapes, but damping ratios (Brincker et al. 2001). From equation (4.13), the first singular vector is an estimate of the mode shape and the corresponding singular value is the auto power spectral density function of the corresponding single degree of freedom system. EFDD allows the natural frequency and damping of a particular mode to be extracted by computing auto-and cross-correlation functions (Batel, 2002). The natural frequency and damping ratios are obtained from the fully or partially identified SDOF auto spectral density function. The modal parameters are obtained by taking the spectral density function back to time domain by inverse FFT. From the free decay domain function, which is also the auto correlation function of the SDOF, the natural frequency and damping ratio is found by estimating crossing times and logarithmic decrement. First all the extremes p_k both peaks and valleys on the correlation function are found. The logarithmic decrement δ is given by:

$$\delta = \frac{2}{k} In\left(\frac{p_0}{|p_k|}\right) \tag{4.14}$$

where p_0 is the initial value of the correlation function and p_k is the k^{th} extreme. Since only truncated data, i.e. the data near the peak of the SV plot, are used for the inverse FFT to calculate the approximate correlation function of a corresponding

SDOF system, bias error in damping estimation maybe introduced. Moreover, when dealing with closely spaced modes, the beat phenomena would be encountered, and this can lead to inaccurate estimation of damping ratio by logarithm decrement technique. Jacobsen et al. (2005) extended the concept of EFDD method into detecting harmonics in a set of data. Procedures such as kurtosis, short time Fourier transform were proposed for this.

The third generation of FDD, i.e. Frequency-Spatial Domain Decomposition (FSDD), was proposed by (Zhang et al. 2005). FSDD makes use of the singular vector, computed via SVD of output PSD with spatial measurements, to enhance the PSD. In most cases the enhanced PSD in the vicinity of a mode can be approximated as SDOF system, and therefore an SDOF curve fitter can be adopted to estimate relevant modal frequency and damping ratio.

The main drawback of the FDD methods is that it relies on the observation of the analyst to detect modes and hence estimate modal properties and leakage due to fast Fourier transform. Good knowledge of optimisation procedures for parameter estimation is necessary before application of the FDD method, that is the user must be know how to choose the appropriate frequency resolution for FDD, modal assurance criterion (MAC) rejection level and correlation factors for SDOF bell identification.

Least square complex frequency (LSCF)

The least-square complex frequency domain (LSCF) method was formulated to find initial values for the iterative maximum likelihood frequency domain method (Guillaume et al. 1998). The LSCF method was found to give quite accurate estimation of modal parameters with lower computational effort and, thus could be used as a modal parameter estimation technique. The main drawbacks of this method are (1) its inability to deal with closely spaced poles which are shown as a single pole and (2) mode shapes and modal partition factor are difficult to obtain by reducing the residues to a rank-one matrix using the SVD. Guillaume et al. (2003) introduced a poly-reference version of the LSCF (pLSCF) method which eliminated the aforementioned drawbacks. The poly-reference LSCF also known as PolyMAX (Peeters and Van der Auweraer 2005, Peeters et al. 2004) has an advantage of producing very clear stabilization diagrams.

Janssen et al. (2006) presented the operational PolyMAX based on half spectra from and it takes the form:

$$S_{yy}(\omega)=\sum_{i=1}^{n}\frac{\{v_i\}\langle g_i\rangle}{j\omega-\lambda_i}+\frac{\{v_i^*\}\langle g_i^*\rangle}{j\omega-\lambda_i^*} \tag{4.15}$$

Where *n* is the number of modes, * conjugate of a matrix, $\{v_i\}$are related to mode shapes, $\langle g_i\rangle$ are the operational reference factors which replace the modal participation factors in case of output data. λ_i are the pole and are related to eigen frequencies and ξ_i damping ratios as follows.

$$\lambda_i, \lambda_i^* = -\xi_i\omega_i \pm j\sqrt{1-\xi_i^2\omega_i} \qquad 4.16$$

Like the original LSCF method, it is a two-step method (identification of mode shapes must be preceded by identification of modal frequencies and damping ratios) which leads to very clear and, thus, easy-to-interpret stabilization diagrams. For an exhaustive literature about this method and the mathematics behind it the reader can refer to several publications available in the literature (Guillaume et al. 1998, Guillaume et al. 1996, Parloo 2003, Cauberghe 2004).

4.2.2. Time domain methods

NExT type methods

Natural Excitation Technique (NExT) type techniques were initially developed in the deterministic framework of traditional input-output modal analysis. In their original formulation, these worked on the impulse response functions (IRF) of the system determined through tests. However, in OMA the data utilized for modal parameter estimation are correlation functions of the random response of the structure under natural excitation. In fact, it is possible to show that the correlation function can be expressed as a summation of decaying sinusoids, each one characterized by a damped natural frequency, damping ratio and mode shape coefficient identical to those of the corresponding structural mode. Correlation functions can therefore be used as IRF for the estimation of modal parameters. The NExT-type of procedures are two-stage time domain modal identification methods , i.e. estimation of the time response function as the first stage, and extraction modal parameters from time response function data as the second stage. The time response function can be estimated by (i) correlation function estimated directly from stochastic response via a correlogram, or from power spectrum density (PSD) via inverse FFT (ii) random decrement signature which is computed from random response data (Asmussen , 1997). The NExT type methods then use the traditional EMA time domain modal parameter estimation algorithms such as poly-reference least square complex exponential (pLSCE) method (Brown et al. 1979), multiple reference Ibrahim time domain (MRITD) method (Fukuzono 1986) and eigensystem realization algorithm (Juang and Pappa 1984).

The idea underlying pLSCE is that the correlation function is written as:

$$R_{ij}(k.\Delta t) = \sum_{r=1}^{n} e^{\mu_r k\Delta t} C_{ij} + \sum_{r=1}^{n} e^{\mu_r^* k\Delta t} C_{rj}^* \qquad 4.17$$

Where μ_r is the system pole related to natural frequency and damping ration of the r^{th} mode. C_{rj} is constant associated with the r^{th} mode for the j^{th} response signal, n is the number modes, Δt is the sampling time step and * is the complex conjugate.

Since μ_r appears in complex conjugate forms, there exists a polynomial order 2n

(Prony's equation) of which $e^{\mu_r \Delta t}$ are roots. In order to find the coefficients (β) of this polynomial, the Prony's equation is written for 2n times starting at subsequent time samples thus obtaining a linear system of equations. Using least squares and pseudo inverse techniques of unknown coefficients (β) modal parameters can be determined. The least squares method has also been used to detect harmonics (Mahonty, 2004).

The Multiple Reference Ibrahim Time Domain method basically starts from arranging correlation functions in two Hankel matrices, [H_0], and [H_1], shifted in time by one time interval. A recurrence matrix [A] is then computed by solving the following equation:

$$[\mathbf{A}][\mathbf{H_0}] = [\mathbf{H_1}] \tag{4.18}$$

in a least square sense by applying pseudo inverse, thus obtaining:

$$[\mathbf{A}] = [\mathbf{H_1}][\mathbf{H_0}]^{+} \tag{4.19}$$

where the superscript + denote pseudo-inverse. By computing the eigenvalues of this matrix, the poles of the system, and therefore modal frequencies and damping ratios, can be extracted. The eigenvectors are, instead, residues from which mode shapes can be determined. The Ibrahim Time Domain is a low order method and as a consequence, the number of responses should not be more than the number of modes that can be identified. If, instead the number of modes is larger than the responses, there will be some computational modes. More details about the MRITD method can be found in (Ibrahim and Mikulcik 1977, Fukuzono 1986).

Juang and Pappa (1985) developed ERA from a system realization viewpoint. It is a MIMO algorithm that can be used for modal parameter identification and model reduction of dynamical systems. The first step of this algorithm is to formulate a generalized *Hankel* matrix, which contains the *Markov* parameters. Then the realization matrices, which can reproduce system's input-output relationship, are derived. Modal parameters are extracted from the realized system matrices. The detailed derivation of ERA can be found in (Juang and Pappa 1985).

It is also worth noting that, even if these algorithms were originally obtained as separate methods, a common mathematical derivation can be obtained by applying the unified matrix polynomial approach (UMPA) proposed by Allemang and Brown (Allemang and Brown 1998). Moreover, it is worth noticing that the first two techniques are the results of improvements carried out over the years by several authors with respect to their original formulations, basically in order to deal with close or repeated roots: such resulting techniques are now applied in the OMA framework.

Auto regressive moving average (ARMA) models

The ARMA model type methods can also be used in estimating modal parameters in OMA of a structure from measured random responses. The basic idea behind this method is to identify a system and predict its present and future response from the information of its past inputs and outputs. In case of multiple natural excitations, multi-dimensional ARMA model, i.e. Vector ARMA or ARMAV model should be applied.

The ARMAV model can be used to represent the dynamics of a vibrating system (Huang, 2001). It is shown that the difference equation for an ARMAV time series is

$$y_{k+1} - \sum_{j=1}^{f} \alpha_j y_{k+f-j} = \sum_{j=1}^{f} \beta_j e_{k+f-j} \qquad 4.20$$

The left side of this equation is the vector autoregressive (AR) part and the right side is the vector moving average (MA) part. The AR part describes the system dynamics and contains all the modal information of the vibrating system while the MA part is related to the external noise as well to the excitation. If m is the number of sensors, y*k* is an *(m* × 1*)* vector of observations at time *k* : $y_k = [y_{1k}, y_{2k}, \ldots, y_{mk}]^T$, where the superscript T denotes the transpose. Also, e_k is an *(m* ×1*)* zero-mean vector white noise process, α_j's are the AR parameter matrices *(m × m)* and β_j's are the MA parameter matrices *(m × m).* Only the AR parameter matrices are necessary in order to identify the modal parameters of the vibrating system. Using eigenvalue decomposition, eigenvalues and eigenvectors are decomposed. These eigenvalues are related to natural frequencies and damping ratios of the structure and the eigenvectors are related to the mode shapes. Ljung (1999) described a Prediction-Error method (PEM) approach in which the modal parameters are obtained by minimizing the prediction error. This algorithm results in a highly nonlinear optimization problem due to which its utility is severely affected. The algorithm is sensitive to initial values, is computationally intensive, and convergence is not guaranteed. This makes it unsuitable for OMA purposes, especially for analysing large structures. Modal parameters can be computed from the ARMAV model by the coefficient matrices of the AR polynomials. PEM-ARMAV type OMA procedures have two main drawbacks, i.e. computationally intensive and the requirement of initial "guess" for the parameters to be identified. Petsounis and Fassois (2001) proposed a method which would overcome some of the difficulties that have rendered ARMAV identification. This method has come to be known as Linear Multi-Stage (LMS) ARMAV method and is effective in the presence of noise. Andersen, (1997) proposed a MIMO version of the PEM-ARMAV and applied it to civil engineering structures. It was shown that the ARMA model is a good representation of a linear, time-invariant structure vibrating under unknown input forces which can be modelled as a zero mean Gaussian white noise process.

Stochastic Subspace-based Procedures

Stochastic Subspace Identification (SSI) modal estimation algorithms have been around for more than a decade by now. The real break-through of the SSI algorithms happened in 1996 with the publishing of the book by van Overschee and De Moor (1996). The techniques fit parametric models directly to the measured time responses. They are based upon the stochastic state space model described by:

$$x_{t+1} = [A]x_t + w_t$$
$$y_t = [C]x_t + v_t \qquad 4.21$$

where x_t is the state vector at time t, [A] is the system matrix (state matrix), y_t is the response vector at time t, and [C] is the observation matrix. The response is generated by two stochastic processes w_t and v_t called the process noise and the measurement noise respectively.

The steps in the SSI techniques from the time responses y_t, via optimal predictors of x_t, least square error estimates of [A] and [C] etc. to the estimated modal parameters are described in several references, including (Brincker and Andersen, 2006, Moller et al. 2005 and Andersen 2010). Modal models are estimated for the different state space dimensions up to a selected maximum state space dimension. The setting of maximum state space dimension depends upon the number of modes, which is searched for, the excitation, the number of sinusoidal components in the response signals and the number of noise modes needed to fit (predict) the measured response signals. The results are achieved by a singular value decomposition of the full observation matrix, which is a matrix calculated from the measured responses, and extracting a subspace holding the modes in the model. Three different algorithms are often used in the SSI techniques, the Unweighted Principal Component (UPC), the Principal Component (PC) and the Canonical Variate Analysis (CVA) algorithms.

A stabilization diagram for the modal models is used for selecting a model (at a certain state space dimension). Responses predicted from the models are compared with the measured responses in order to validate the selected model. The normalized singular values of the weighted observation matrix (or weighted common SSI input matrix) indicate the rank of the matrix on a scale from 0 to 1 and this value can therefore also be used as a guideline for the state space dimension required for the modelling. Is it difficult, however, to say how low this number should be and it is different for the three algorithms.

SSI has advantages of having no leakage because in model estimation there is no reliance on Fourier transformation, there are no problems with harmonics as modal parameters are extracted directly by fitting parameters to the raw measured time histories, it has less random errors because the SSI algorithms are based on linear least-squares fitting techniques, fitting state space systems with correct noise modelling and lastly all modal parameters are fitted in one operation hence taking advantage of the noise cancellation techniques of the orthogonal projection of SSI. However, SSI method provides a challenge in choosing the best method amongst the three (UPC, PC and CVA). Also the selection of state space order, deviation of frequency, damping, mode shape MAC and then choice of projection channels which requires user's experience. Lastly, in presence of several setups, the method is normally applied independently for each setup and then final estimates of the modal parameters are determined globally.

4.2.3. Special methods

Beside the above described methods, which can be considered as classical, new approaches for OMA are appearing in the literature. Some of them can be, in a way, classified within the traditional classes of time domain or frequency domain methods; some others, work in different domains. These include, wavelet transform, transmissibility functions and blind source separation method. This section describes these new OMA techniques.

Transmissibility functions

This technique for modal identification in output-only conditions is based on the use of transmissibility functions. Transmissibility functions are a kind of FRF which, however, are not obtained from conjugate variables (output vs. input) but from like variables (for example, two motion records). Since the mathematical structure is one of FRFs, this approach can in a way be classified as a frequency domain one.

FRFs are widely used functions in the field of experimental modal analysis: nevertheless, transmissibility functions have recently made their appearance in the field of OMA (Devriendt and Guillaume 2007). The main difference with respect to FRFs is that transmissibility functions can be measured without knowledge about the excitation forces. Even if they are estimated in the same way as FRFs, transmissibility functions are actually the ratio between two response spectra, i.e. X_i (ω) and a reference response signal X_j (ω), instead of an excitation signal as in the case of FRFs:

$$T_{ij}(\omega) = \frac{X_i(\omega)}{X_j(\omega)} \qquad 4.22$$

Since the reference output is present in all transmissibility functions, it must be properly chosen, in a way that it carries the maximum amount of information about structural modes.

It can be easily shown, by recalling the relation between FRFs and Fourier transforms of input and output and the structure that the system poles disappear when computing the ratio between two responses, namely transmissibility: as a consequence, in transmissibility measurements each resonance is represented by a flat zone instead of a peak. However, the most important property of transmissibility functions is that they approach a constant value when converging to a system pole and, in particular, such value is directly related to mode shape components at measurement points *i* and *j*. Devriendt and Guillaume (2006) concluded that the limit value of the transmissibility functions is independent of the input, and it relates to the same responses but obtained from two tests characterized by different loading cross each other exactly at resonances and, therefore, their difference is zero. By considering the inverse of such a difference, a function characterized by poles equal to the system poles is again obtained based on transmissibility measurements. By applying a frequency domain estimator (Pintelon et al. 1994, Peeters et al. 2004), natural frequencies and damping ratios of the system under test can be obtained. Based on the results of this first step, mode shapes can then be obtained from transmissibility functions. One of the main advantages of the use of transmissibility functions for OMA with respect to more traditional approaches is related to the fact that they do not depend on the nature of the forces and this circumstance reduces the risk of wrongly identifying the modal parameters in presence of non-white excitations (Devriendt et al. 2008). The disadvantage of a transmissibility function, defined by taking the ratio of two response spectra, in a multiple input situation raises when different inputs of the same order of magnitude with uncorrelated noise are exciting the structure.

Blind Source Separation

Blind Source Separation (BSS) techniques were initially developed in the early 80's for signal processing in the context of neural network modelling. During the last two decades, numerous studies were achieved on this topic diversifying the application fields. This success certainly comes from two of the BSS intrinsic features:

First, the aim of any BSS technique is to reveal the underlying structure of a set of observed phenomena (e.g. random variables, measurements or signals). Recovering initial (and unobservable) signals from measured data is a generic problem in many domains.

Secondly, a small number of assumptions is required about the signals. The term 'blind' means that the source signals are extracted from the rough data even though very little, if anything, is known about the nature of those initial components. The methods are said to be versatile in the sense that the analyzed data can originate from various domains, and that no a priori knowledge is required about the physical phenomenon of interest.

The desired signals, denoted s, are named sources or components of the system. They are of primary interest because they concentrate the valuable information of the system. Unfortunately, this information is diluted within the measured signals, denoted x, that are essentially mixtures of the sources. The following assumptions are made while dealing with separation sources

The sources are assumed as statistically independent. The mathematical definition of statistical independence, based on the joint probability density functions

The unknown mixing matrix is usually assumed to be square. The number nx of sensors is then assumed to be equal to the number ns of sources.

The simplest BSS model assumes the existence of ns sources $\{s_1(t)\ldots s_{ns}\ (t)\}$ and the observation of as many mixtures $\{x_1(t)\ldots.x_{nx}\ (t)\}$, where nx = ns . Mathematically, the BSS model can be expressed as follows

$$x(t) = [\mathbf{A}]s(t) \qquad 4.23$$

where the observed data x(t) are assumed to be linear combinations of unknown sources s(t). The matrix A is referred to as the mixing matrix. Equation (4.23) can also be defined as

$$x_i(t) = \sum_{j=1}^{n_s} a_{ij} s_j(t) \qquad 4.24$$

Knowing the signals x(t), the BSS problem then consists in estimating the sources. Because both mixing coefficients a_{ij} and sources s_i are unknown, the estimation problem is considerably more difficult. Noise may also corrupt the data and, in this case, the noisy model can be expressed as

$$x_i(t) = \sum_{j=1}^{n_s} a_{ij} s_j(t) + \sigma_{noise}(t) \;\; i = 1,\ldots,n_x \qquad 4.25$$

where σ_{noise} is the noise vector corrupting the data.

Since by definition, BSS techniques work only on output responses to identify either their sources or the system (mixing matrix) without any knowledge about them, it is logical that these techniques can be used in OMA. Recently, it has been shown that BSS techniques can be utilized for the purpose of modal analysis (Poncelet et al. 2006, Randall and Holley, 2006).

Antoni (2005) discussed the different issues associated with the application of BSS techniques for vibration signals in detail. BSS techniques and their applicability for output-only modal analysis can be found in (Kerschen et al. 2007, Poncelet et al. 2007, Belouchrani et al. 1997). It is worth emphasizing that, among BSS techniques, a very promising one in the field of OMA seems to be the so called Second Order Blind Identification (SOBI): it is a kind of two-step method where, mode shapes are identified at the first step while natural frequencies and damping ratios are recovered from the second step. Mode shapes are directly provided by the columns of the mixing matrix while other modal parameters (natural frequencies and damping ratios) are evaluated using post processing techniques such as FFT to the identified sources. More details about SOBI can be found in (Poncelet et al. 2007, Belouchrani et al. 1997, Poncelet et al. 2008).

However SOBI has limitations in that sensors should always be chosen in a number greater or equal to the number of active modes and it is suitable for lightly damped systems

Wavelet transform

The wavelet transform is, instead, defined from a basic wavelet, the so called mother wavelet ψ, which is an analyzing function located in both time and frequency. From the mother wavelet a set of analyzing functions b can be obtained simply by scaling (parameter a) and translation (parameter b). The wavelet transform of a signal s is thus defined as:

$$W_s(a,b)=\frac{1}{\sqrt{a}}\int_{-\infty}^{+\infty}s(t)\psi^*\left(\frac{t-b}{a}\right)dt \qquad 4.26$$

where the superscript * denotes complex conjugation. In order to interpret the wavelet transform in terms of time-frequency analysis, a relation the scale parameter *a* and the frequency *f* has to be established.

Several applications of wavelet transform in the field of OMA are reported (Ruzzene et al. 1997; Lardiès 1997; Staszewski 1997; Gouttebroze and Lardiès 2001), yielding accurate estimations of natural frequencies and damping. Moreover, a wavelet-based output-only modal analysis procedure for extraction also of mode shapes has been proposed (Han et al. 2005). The main advantage of wavelet transforms is related to the possibility to process non-stationary signals (for example, transient signals): for this reason, they are also widely applied within vibration based damage detection procedures. WT has been successfully applied in the time-frequency analysis of engineering structures, and it has been extensively studied both in the linear and nonlinear systems for the purpose of mode parameters identification (Ruzzene et al. 1997; Brincker et al. 2000).

The main drawback of the wavelet transform is that it does well in estimating natural frequencies and damping ratios but not for mode shape extraction and also is not valid for weak damping. Furthermore, the success of these techniques depends on the ability of the frequency localisation of the wavelet transform to decompose the responses of multiple modes accurately into the responses of the single mode of interest. Mode decomposition is typically difficult for close modes with severe modal interference

Combined methods

With the random decrement (RD) technique (Cole, 1968), the structural responses to ambient loads are converted into RD functions. The process of evaluation of the RD functions is a rather simple technique of averaging time segments of the measured structural responses, with a common initial or triggering condition. Initially (Brincker et al. 2000) the RD functions were interpreted as free vibration responses of a system, but later (Asmussen, 1997, Brincker, 1995 and Brincker et al. 1992) it has been proved that, under the assumption that the analyzed responses are a realization of a zero mean stationary Gaussian stochastic process, the RD functions are proportional to the correlation functions of the responses and/or to their first derivatives in relation to time.

The interpretation of the RD functions as free vibration responses is almost intuitive, if one thinks that the response of a system to random input loads is, in each time instant *t*, composed by three parts: the response to an initial displacement; the response to an initial velocity; and the response to the random input loads between the initial state and the time instant *t*. By averaging time segments of the response with the same initial condition, the random part of the response will have a tendency to disappear from the average, and what remains is the response of the system to the initial conditions. Since the experimentally measured structural responses always have some noise content, the time segments averaging of the RD technique, also has an effect of reducing the noise in the resulting RD functions.

Additionally to auto RD functions, where the triggering condition and the time segments to be averaged are defined in the same response signal, it is also possible to evaluate cross RD functions, where the triggering condition is defined in one response signal and the time segments to be averaged are taken from the other simultaneous response signals. One can therefore evaluate a complete matrix of RD functions, or like in the spectral density functions matrix, a reference-based approach can be adopted, where only a few reference response measurements are considered to apply the triggering conditions.

The RD technique is also computationally efficient. For instance, in terms of evaluation of correlation functions, comparisons (Brincker et al. 1992) have been made of different techniques, including the direct method, the FFT based method and the RD technique, showing that the RD technique is faster than the direct method and in many situations faster than the FFT based one (eventually for long estimates of the correlation functions the FFT based method is more competitive).

RD functions can be interpreted as free vibrations of a system, therefore, it seems reasonable to evaluate the spectra of the RD functions, using the FFT algorithm, and to apply the frequency domain output-only modal identification methods to the spectral density functions obtained in such way.

However there are problems associated with the discrete Fourier transform, namely the effects of leakage. To avoid the effects of leakage, the RD functions must be computed with a total length that allows them to have a complete decay within that length. If this condition is fulfilled then the FFT algorithm can be applied directly to the RD functions, without the need to use signal-processing windows.

An averaged spectral density functions matrix can be evaluated as the mean of the spectral matrices computed from each column or line of the RD functions matrix. The three frequency domain output-only modal identification methods can then be applied to that averaged spectral density functions matrix, in a similar manner as they are applied to the spectral densities estimated by the more usual Welch's procedure (Welch, 1967). The resulting identification methods can be named as RD-BFD, RD-FDD and RD-EFDD since they correspond to a combination of the RD technique with the methods BFD, FDD and EFDD. The advantage in doing this combination is clearly visible in the results that will be presented below, and is a consequence of the noise reduction from the averaging of time segments that is performed in the RD technique, and also from avoiding the effects of leakage (if the RD functions are evaluated with enough length to have a complete decay within that length).

OMA in presence of eXogenous inputs (OMAX approach)

In some in-operational testing applications, exciters are used to inject more energy in the system. This is for instance done during flight flutter tests, where artificial forces are applied on the wings of the airplane using special equipment. In that case, input signals are available and it is again possible to use classical EMA identification techniques to estimate the modal parameters from the input/output (or FRF) measurements. However, by doing so, the effect on the natural forces will be treated as ambient `noise'.

However, in OMA, the mode shapes cannot be scaled in an absolute sense, e.g. to unit modal mass, unless a second measurement is performed after adding or removing a significant amount of mass to or from the structure (Parloo et al. 2002), which is rather cumbersome for heavy structures such as dams. Another disadvantage of OMA is that the frequency content of the ambient forces may be narrow banded, which makes that the number of modal parameters that can be determined from an OMA test may be limited. For these reasons, there is an increasing interest in the last few years towards combined deterministic-stochastic system identification methods where both measured and unmeasured forces are accounted for. The resulting modal analysis is called ‘‘Operational Modal Analysis with eXogenous (or deterministic) inputs’’ (OMAX)

It permits the determination of the modal scaling factors, whereas it is still possible to have low excitation levels due to the applied artificial forces. It should be noted that absolute mode scaling is also possible by performing two different OMA tests, adding a known mass to the structure during the second test. Traditional EMA techniques will remove this `noise' by averaging the measurements. This is in contradiction to the output-only approach where the modal parameters are estimated using response data due to the ambient excitation only. Clearly, the ambient noise is not just `noise' but it contains useful information about the system. To make an optimal use of the operational data, both measured (artificial) and unmeasured (natural) forces should be taken into account. By doing so, all the available information in the measured data can be optimally used. Cauberghe et al. (2003) proposed an OMAX algorithm called Combined non-linear least squares frequency method on input output spectra which is recently known as OMAX maximum likelihood estimation (Guillaume et al.2006) Reynders and De Roeck (2008) extended the OMAX to a reference based combined deterministic-stochastic subspace identification in OMA. This new method has an advantage of exciting a complete set of modes of the structure which could not be excited by ambient conditions only.

4.3. Concept of stabilisation diagram

A stabilisation diagram (Figure 4.1) is a standard tool in modal analysis (Ewins 2000, Peeters and De Roeck, 2001) used for removing part of the bias error in estimating modal parameters. It is constructed by choosing a wide range of model orders *n* for the identification and by plotting all identified modes in a frequency vs. model order diagram. The idea is then, to remove the following parts of the bias using the diagram.

Bias of the model: spurious modes can be removed with the stabilization diagram. Two types of spurious modes are; (i) noise modes, that arise due to physical reasons, for example, excitation and noise colour; and (ii) mathematical modes that arise due to an over-estimation of the system order.

Bias of the modes: the part of the bias that is due to an under-estimation of the system order, which makes that a single identified mode may in reality be a combination of different modes (true or noisy), can be detected with a stabilization diagram if sufficiently high values of the model order *n* are considered.

Ideally, most of the mathematical modes can be removed from the diagram using so-called stabilization criteria: modes, for which the distance in modal parameters between two consecutive model orders is higher than certain threshold values, are not plotted in the diagram. The idea behind this is that modes that do not meet the stabilization criteria are not physical, since there is apparently no reason why they should appear at different model orders. For the eigenfrequencies and damping ratios, the ‘distance’ is usually defined as a relative difference, and for the mode shapes, as one minus their modal assurance criteria (MAC) value.

The mathematical modes that pass the stabilization criteria, as well as the noise modes, should be removed based on other validation criteria. The bias of the modes that arises due to under-specifying the model order can be removed by selecting the mode at a model order that is high enough.

The stabilization diagram, commonly used in commercial software, is a traditional way of picking out the genuine modes. The basic idea is to perform several identifications for different model orders. For each considered order, the identified eigenfrequencies are plotted in the diagram in which they can be compared to the poles of the lower-order models. If the variations of the eigenfrequencies, the damping ratios and the mode shapes are lower than pre-set values, the poles are said to be ’stable’. Finally a pole is identified as genuine if it is stable for several consecutive system orders (Maia and Silva, 1997)

Even though it is widely used, the stabilization diagram possesses important drawbacks. First, it requires several modal identifications, the number of computed orders being directly related to the number of active modes in the frequency range. Second, the selection of the stabilized modes is time consuming and requires good user’s expertise. Therefore the results might vary according to the user interpretation. Peeters (2000) illustrated that finding an automatic procedure for the selection of the modal parameters remains a challenging issue for dynamics operators.

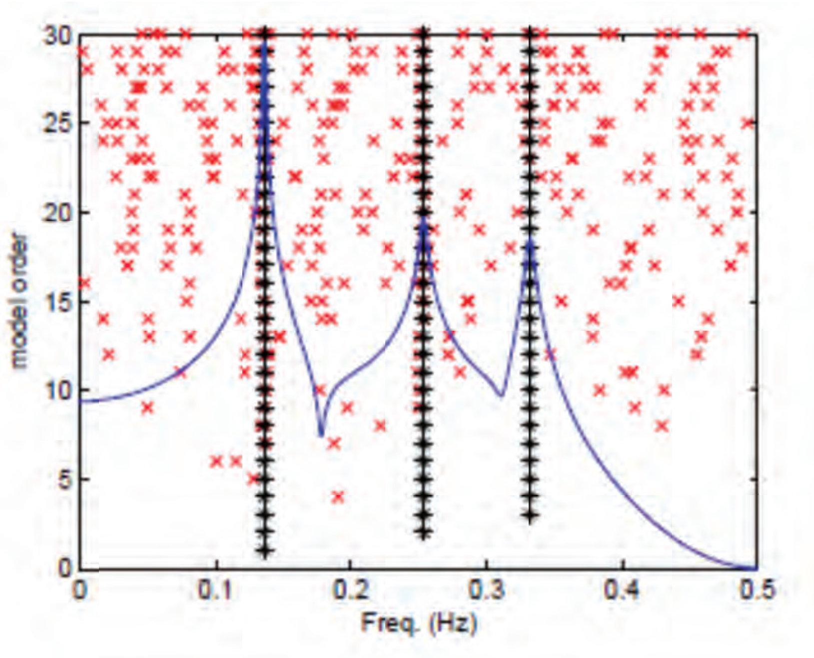

Figure 4.1: Typical stabilization chart

The stabilization chart being a very effective method in determining modal parameters and distinguishing between mathematical and spurious modes, it has some disadvantages.

i) First, the modal parameters are computed and identified as many times as considered system orders. This iterative process may lead to high computational load.
ii) Second, the stabilization diagram analysis can quickly become tedious in case of complex industrial structures containing numerous natural frequencies.
iii) Thirdly, because the user's interpretation is required to extract the genuine modes, an inconsistency between estimates of different operators according their expertise may appear.
iv) Finally, for data with large noise levels, stabilization charts must be applied with caution, since the damping values can be underestimated.

4.4. Automation of OMA

Classical modal analysis takes advantage of very relevant and effective tools, such as the stabilization diagram, which leads to distinguish physical from mathematical modes. Selection of physical poles is not a trivial task. It may be difficult and time consuming depending on the quality of data, the performance of the estimator (even if there are interesting advancements in this field (Lanslots et al. 2004 and Chauchan and Tchernaik, 2009) and the experience of the user. Nevertheless, extensive interaction between tools and user is basically inappropriate for monitoring purposes which created a need for automation of OMA.

Peeters and De Roeck (2001) proposed a basic criterion for automated modal parameter identification via stochastic subspace identification (SSI) and applied to monitor the environmental and damage effects on the dynamic behaviour of the Z24 Bridge in Switzerland. It is based on the definition of the stabilization diagram and on the selection of just those poles that are at least five times stable. This basic criterion has been also recently applied in order to track the effects of changing environmental conditions on the modal parameters of Tamar bridge.

Verboven et al. (2002) made the first proposal for automated identification of modal properties. However, in the last four years there has been an increasing attention paid to this issue, with formulation of algorithms for automated identification and tracking of modal parameters (Brincker et al. 2007, Rainieri et al. 2007 and Deraemaeker et al. 2008) relying on OMA methods based conventional signal processing.

The least square complex frequency (LSCF) method was the base for development of the first approach to automated modal identification (Verboven et al. 2003). In this case, selection of physical poles from a high order model is based on a number of deterministic and stochastic criteria and a fuzzy clustering approach. However, the algorithm for pole selection is quite complex and demanding from a computational standpoint.

Andersen et al. (2007) proposed a fully automated method for extraction of modal parameters adopting SSI. It is based on the clear stabilization diagram obtained according to a multipatch subspace approach. Pole extraction is carried out by the graph theory. This algorithm seems to be very fast, so that it can be used as a monitoring routine, but further improvements are under investigation to increase the reliability and robustness of the method.

Brincker et al. (2007) presented an algorithm for automation of the frequency domain decomposition (FDD) procedure in order to remove any user interaction and use it as modal information engine in SHM systems has been presented. It is based on identification of the modal domain around each identified peak in the singular value plot according to predefined limits for the so-called modal coherence function and modal domain function. A good initial value for such limits would be 0.8. However, even if the limit value for the modal coherence indicator is somehow justified on the basis of the standard deviation of correlation between random vectors and on the number of measurement channels, few suggestions are reported for the modal domain indicator. Recently, the approach to automated modal parameter identification proposed by Brincker et al. (2007) has been slightly modified and applied to the permanent monitoring of the Infante D. Henrique bridge (Magalhaes et al. 2008). In this case, also an automated procedure based on covariance driven SSI (Cov-SSI) and on a clustering algorithm for stable pole selection was proposed (Magalhaes et al. 2009)

The automated OMA procedure using transmissibility functions is, instead, based on the combination of singular value decomposition (SVD) and stabilization diagram for selection of structural modes (Deverient et al. 2008). Computation of the stabilization diagram from transmissibility functions resulted in stable vertical lines but not all of them correspond to actual system poles, even if they are related to structural characteristics. Thus, another selection tool is needed. In the context of the proposed procedure, the SVD of a two column matrix is computed, where each column consists of a transmissibility function evaluated for a particular load condition. Since all transmissibility functions converge to the same unique values at the system poles, the matrix will be of rank one in correspondence with each system pole. Thus, by looking at the plot of the inverse of the second singular value, it is possible to distinguish actual structural modes from its peaks. Peak selection is carried out through a threshold definition. However, in the presence of measurement noise this approach is not very reliable. In order to overcome this drawback, the use of a smoothing function has been proposed (Deverient et al. 2008) but it has to be used carefully to avoid distortion. Further refinements of the proposed algorithm are, therefore, needed. Deraemaeker et al. (2008) presented another automated operational modal analysis procedure based on the SSI technique. It is suitable as a tracking method but it always requires user interaction because an initial set of modal parameters, using stochastic subspace identification and stabilization diagram, has to be identified before launching the tracking procedure.

Automated modal identification algorithms have been recently proposed also for the second order blind identification (SOBI) method and for the transmissibility-based method. About SOBI (Poncelet et al. 2008), identification of structural modes is based on rejection of all modes out of the frequency range of interest and of time series of sources characterized by a fitting error higher than 10%; finally, selection of actual structural modes is based on the computation of a confidence factor. The main advantage of the proposed procedure is a lower computational load with respect to SSI methods; moreover, selection of model order is not necessary. Conversely, the main drawback is related to the need of a number of sensors greater than or equal to the number of active modes. At present the algorithm has been applied only against simulated data, so that effectiveness in the case of real systems and measures has to be analysed.

The main drawbacks of existing automated modal identification methods can be, therefore, summarized as follows: (1) most of them move from a threshold-based peak detection; as a consequence, a first calibration phase is needed for its proper definition; however, only some of the identified peaks correspond to actual modes; performance of peak detection algorithms can get worse in the presence of measurement noise; (2) identification of actual modes is based on a number of parameters so that a time-consuming calibration process for each monitored structure is required.

4.5. Brief review of ambient vibration testing of concrete dams

The application of ambient vibration testing of concrete dams started in the early 1980. Ellis et al. (1983) were among the first reported applications of ambient vibration testing of concrete dams with the aim of understanding the overall structural behaviour of dams. Ellis et al. (1983) carried out ambient vibration tests on a 220m high arch dam called Contra dam (Figure 4.2) located in Ticino Switzerland. During these tests, heavy rainfall resulted in rapid rise of the reservoir water level which caused natural frequencies to vary substantially during the tests.

Figure 4.2: Contra dam

Brownjohn et al. (1986) investigated the feasibility of ambient vibration testing of dams. Schaevitz servo-accelerometers placed on the crest of the dam were used together with a purpose built power supply and signal conditioning unit. Each test lasted about 133 minutes. The signals were recorded on a magnetic tape and analysed using a Solartron 1200 twin channel spectrum. Aries IEEE interface module and a microcomputer was used for communication with the spectrum analyser. Eight upstream-downstream modes were extracted in the frequency range 1.8-4.2 Hz and damping ratio in the range 2.72-4.33%. The natural frequencies were determined by picking peaks on the auto-spectrum while the mode shapes were obtained from the output only transfer functions between the travelling and reference accelerometers. Test results showed that natural frequencies of the measured modes increased with a decline in the reservoir level and that the excitation process was directly related to hydro-electricity generating activity. Brownjohn et al. (1986) concluded that the ambient vibration testing of stiff structures can be expected to provide a limited amount of information about dynamic responses, unless both sensitive, low noise accelerometers and a reasonable level of excitations are available.

Brownjohn (1990) carried out ambient vibration tests on Hermitage dam (Figure. 3) a concrete gravity dam located on the Wag River, Kingston, Jamaica. The study was performed to investigate the safety and stability of the dam and validate a finite element model of the dam. Schaevitz LSOC14 inclinometers and Sundstrand QA700 accelerometers were used in the acquisition of signals during testing. One Sundstrand accelerometer was used as a reference accelerometer while the Shaevitz and Sundstrand accelerometers were moved to selected locations on the dam crest. The signals from the Shaevitz-type accelerometer were noisy and had to be discarded and the ambient tests had to be repeated using only Sundstrand accelerometers due to their very high resolution and low threshold and internal noise. Signals were recorded on a magnetic tape using a RACAL store 4DS tape recorder.

Figure 4.3: Hermitage dam

Natural frequencies in the range of 7-30 Hz picked from peaks of the auto-spectra were compared with the analytical natural frequencies obtained from the finite element model of the dam. The report concluded that although there were some discrepancies between the predictions of the mathematical model and the experimental results, the agreement was good enough to justify the usage of the mathematical model. At the end of the tests, it was also observed that even for dams with low levels of ambient excitation, it is possible to make sensible estimates of modal parameters derived by sensitive instruments.

Loh and Wu (1996) obtained the dynamic characteristics of the Fei-Tsui dam using seismic response data and ambient vibration data. Fei-Tsui dam (Figure 4.4) is concrete arch dam 122.5m high and 510m long located in Taiwan. SSA-1 type strong motion seismometers were used to measure the responses at the crest of the dam. The modal parameters were extracted for the upstream-down direction. Random decrement method and auto regressive model with least-squares method were used to estimate modal parameters of the dam. Two modes were identified with the first and second having average frequencies of 2.49 Hz and 3.33 Hz and damping ratio in the range 2.38-4.24%. The conclusion of the tests was that the dynamic characteristics obtained from ambient vibration data were consistent with those obtained during the seismic excitations. The authors however did not comment on the performance of the different modal parameter estimation methods.

Figure 4.4: Fei-Tsui dam

Kemp (1996) conducted ambient vibration tests on the Ruskin dam (Figure 4.5) a 58 m high concrete gravity dam located in British Columbia, Canada. The main objective of these tests was to determine the suitability of ambient vibration testing and analysis as part of seismic evaluation studies of concrete gravity dams. The dynamic properties of Ruskin dam were used to calibrate a numerical model of the dam. Kinemetrics model FBA-11 accelerometers with 5V/g sensitivity and resolution of 0.2µg were used. The natural frequencies in the range of 6.5-14 Hz for the high reservoir and 8.5-14.5 Hz for low reservoirs were obtained from the peaks of average normalized power spectral densities (ANPSDs). Following these tests, it was concluded that dynamic properties of the Ruskin dam identified using ambient vibration testing and analyses were useful in calibration of the finite element model of the dam.

Figure 4.5: Ruskin dam

Danielle and Taylor (1999) presented results of ambient vibration tests conducted on a 56 m high gravity dam called Claewern dam (Figure 4.6). The tests were carried out to measure the dam's modal properties for validating a finite element model for the dam-reservoir foundation system. Sundstrand Q-Flex type QA-700 accelerometers mounted on steel blocks on the dam crest were used to acquire the signals. The signals were digitized and stored on the hard disk of a portable computer. Six lateral modes were identified in the frequency range 6.1-11.8 Hz. Natural frequencies were picked from the peaks of average normalized power spectral densities. The finite element model was analysed using EACD-3D program. The computed mode shapes and natural frequencies compared well with the experimental results. The study demonstrated that ambient vibration testing can offer a viable alternative to forced vibration testing when only the modal properties of a dam are required.

Figure 4.6: Claewern dam

The arch dam of Mauvosin (Figure 4.7) was subjected to a number of investigations with an aim of identifying natural frequencies for various reservoir levels (Darbre et al. 2000). Mauvoisin dam is a doubly curved 250.5 m high arch dam and is located in the Swiss Alps. Ambient vibration tests on Mauvoisin dam marked the beginning of long term ambient vibration monitoring of dams. Seven ambient vibration tests at different water levels were carried out between 1995 and 1996. An automated system was set up on the dam and ambient vibrations were recorded twice daily for 6 months (Darbre and Proulx, 2000). Tri-axial force-balanced accelerometers with a sensitivity of 5V/g were used to capture the responses of the dam.

Figure 4.7: Arch dam of Mauvosin

Natural frequencies were obtained by peak picking on normalized power spectral densities of individual acceleration. Results showed that the natural frequencies initially increased with rising water level and then decrease with further rise. This was contributed to the two competing features of increasing mass of water (reduction of natural frequencies) and of dam stiffening due to closing of vertical construction joints.

Mivehchi and Ahmad (2003) carried out ambient vibration tests on Shahid-Rajaee (Figure 4.8) and Saveh dams (Figure 4.9), two concrete arch dams located in Iran. The purpose of the tests was to verify the results obtained from mathematical model used regularly in the Iranian dam design practice by comparing with the behaviour of the actual as-built structures. The ambient tests were conducted during winter of 1999 to autumn of 2000. At this time the water level in the reservoir of Shahid-Rajaee dam was at 18 m below the crest while that of Saveh dam was at 47.5 m below the crest.

Figure 4.8: Shahid-Rajaee dam

Figure 4.9: Saveh dam

Facilities from the International Institute of Earthquake Engineering and Seismology (IIEES) were used in the measurement and recording of the vibrations of the two dams. Because of limited number of sensors and in order to determine different mode shapes, the tests were performed in several stages of equipment arrangements. Each set of three sensors closely spaced are named as *A*, *B*, *C* (travelling set) and *R* (as the reference set) so that for instance stations are called as *A*1, *A*2, and *A*3, or *R*1, *R*2, and *R*3. Partial and rapid opening and closing of the bottom outlet gates of the dam body provided artificial excitation during the ambient vibration tests. These were helpful in exciting any weak modes which could not be realized with ambient tests only. Modal parameters from both dams were extracted from peaks of auto power spectra. Natural frequency range of Shahid-Rajaee and Saveh dams were reported as 1.46-3.58 Hz and 3.91-7.91 Hz respectively. The damping ratios of Shahid-Rajaee and Saveh dams were 0.95-1.32% and 0.9-1.74%, respectively. Authors concluded that ambient vibration tests will be used in the seismic safety evaluation of other Iranian dams and also be used in the design enhancement of new dams.

Two ambient vibration tests were carried out in 2002 and 2003 with an objective of developing a continuous dynamic monitoring system for Cabril dam (Oliviera et al. 2004). Cabril arch dam (Figure 4.10) is double curvature dam with a height of 130 m and crest length of 290 m. The dam is located on the Zezere River in the centre of Portugal and was constructed for hydropower electricity generation. Kinemetrics ES-U force balance accelerometers were used to detect signals from the dam and these were installed in the radial upstream-downstream direction in the gallery close to the crest. Data acquisition hardware and software used during the testing were from National Instruments. The results from these two tests have been used for different purposes; (i) influence of reservoir levels and the thermal load on the variation of modal parameters with time (Mendes et al. 2004) (ii) demonstrate that it is possible to characterize the dynamic response of arch dams with good precision owing to the development of sensors and data acquisition systems (Oliviera et al. 2004) (iii) develop a pioneer monitoring system of the dam (Mendes et al. 2007) (iv) investigate the influence of contraction joints on dynamic behaviour of Cabril dam (Lemos et al. 2008) and (v) study the influence of an intake tower dynamic behaviour on modal identification of the dam (Mendes and Oliveira 2009).

Figure 4.10: Cabril dam

Frequency domain decomposition (FDD) and stochastic subspace identification (SSI) techniques were used to extract modal parameters of the dam and also to cross-validate results. Numerical results from 3D finite element models were compared with the experimental results. Results showed that there was a need to develop a continuous monitoring system for the dam so that the finite element models would be calibrated. The performance of the different modal estimation methods on Cabril dam was not evaluated.

Okuma et al. (2008) evaluated the seismic safety of Hitotsuse arch dam in Japan and collected fundamental data for developing structural damage detection based on long term ambient vibration testing. Hitotsuse arch dam (Figure 4.11) is a concrete arch dam, 130 m high and consists of twenty seven blocks. The dam was built for hydropower electricity generation. The long term vibration testing was done to evaluate the changes of the natural frequencies of the whole dam due to macroscopic damage caused by aging effects. Tri-axial accelerometers installed on the dam crest were used to detect signals from the dam. The measuring system was configured to record continuously at a sampling rate of 200 Hz and store data measured every after 30 minutes. Natural frequencies were identified from the cross spectrum of autoregressive moving average models. Results showed that the identified natural frequencies were in good agreement with the earthquake observation records, and the identified natural frequencies of three modes strongly correlated with the water level of the dam.

Figure 4.11: Hitotsuse arch dam

Sevim et al. (2010) presented a finite element model calibration of Berke arch dam using operational modal analysis. Berke arch dam (Figure 4.12) is a double curvature concrete arch dam located on the Ceyhan River in Osmaniye, Turkey. Ambient vibration tests were conducted on the dam to obtain the vibration characteristics. B&K 8340 type uni-axial accelerometers with a sensitivity of 10V/g were used to measure the responses from the dam. Wind and water pressure were the source of excitation during ambient vibration testing of Berke dam. Two types of tests were done, i.e. the first three tests were performed in the second gallery, 50m below the crest and the other three tests were performed on the crest. Using enhanced frequency domain decomposition modal parameters of the dam were obtained.

Figure 4.12: Berke arch dam

Eight natural frequencies ranging between 2.74-9.66 Hz were determined with a range of damping ratio being 0.15 -0.84%. For analytical purposes, a 3D finite element model of Berke arch dam reservoir system using ANSYS software. The analytical model was calibrated to match with the measured dynamic characteristics of the dam.

Ellis et al. (2010) reported ambient vibration tests which were performed on Gem Lake dam. The Gem Lake dam (Figure 4.13) is a multiple concrete arch dam located on Rush Creek, California, USA. The objective of the tests was to measure the dynamic response characteristics of the entire dam. Ambient vibrations in the dam crest and gallery were acquired using Honeywell Q-Flex Model QA-700 and QA-750 current output accelerometers with nominal sensitivities of 10.7 V/g and 12.3 V/g respectively. Spectral analysis techniques that included the fast Fourier transform and the maximum entropy method, coupled with waterfall plot analyses, were effective in the identification of individual arch and full dam model behaviour. Natural frequencies of the arches ranged from 13.18 Hz to 27.71 Hz. Numerical modelling of the dam was carried out to gain an insight of how the dam behaves and was used to develop a suitable field test procedure. It was concluded that a practical field test approach based on ambient vibration testing can be adopted for large multiple arch dams.

Figure 4.13: Gem Lake dam

4.6. Summary

The field of ambient vibration testing (AVT) has grown tremendously in the last two decades, particularly in the area of modal parameter identification. Now there exists a wide range of techniques for parameter identification ranging from frequency domain techniques to time-frequency techniques. AVT has been applied successfully to dams, with most reported applications employing frequency domain modal parameter identification techniques. There are limited examples of the application of time domain techniques in AVT of dams. There are no reported studies on the performance of AVT modal parameter extraction techniques with respect to dam monitoring. Based on reported AVT measurements, there has been substantial improvement in instrumentation as well as AVT measurement procedures since early trials in the 1980s.

5. HYDRODYNAMIC BEHAVIOUR OF ARCH DAMS

The arch dam wall and the water body interact with each other dynamically, with the independent solution of any one system being impossible without simultaneous solution of the other (Zienkiewicz and Taylor, 2000). According to Leung et al. (2008), the inertia effect of the fluid medium on the dynamic characteristics, such as natural frequencies, of immersed structures can be significant. This is especially true of structures having large areas of contact with the surrounding fluid. Leung et al. (2008) further state that any movement of the dam wall and foundation will impart motions to the water in the reservoir and in turn the pressure generated in the water will cause forces on the dam wall.

The dynamic problem of a linear multi degree of freedom dam structure subjected to time varying force vectors, $\boldsymbol{F_g}$ and $\boldsymbol{F_p}$ is defined as in equation 5.1:

$$[\boldsymbol{M_s}]\{\ddot{\boldsymbol{u}}\} + [\boldsymbol{C_s}]\{\dot{\boldsymbol{u}}\} + [\boldsymbol{K_s}]\{\boldsymbol{u}\} = \dot{\left\{\{\boldsymbol{F_g}(\boldsymbol{t})\} + \{\boldsymbol{F_p}(\boldsymbol{t})\}\right\}} \quad 5.1$$

$\mathbf{M_s}$, $\mathbf{C_s}$ and $\mathbf{K_s}$ refer to the mass, damping and stiffness matrices of the dam structure and $\boldsymbol{u}$ is a vector of relative displacements. The overdots denote the derivatives of $\boldsymbol{u}$ with respect to time. $\boldsymbol{F_g}$ and $\boldsymbol{F_p}$ are the force vectors generated by the ground accelerations vector $\boldsymbol{u_g}$ and by the hydrodynamic pressures $\boldsymbol{P}$ on the upstream side of the dam wall respectively. The two force vectors are further defined as follows;

$$\boldsymbol{F_g} = -\mathbf{M}_{\boldsymbol{s}}\ddot{\boldsymbol{u}}_{\boldsymbol{g}} \quad 5.2$$

$$\boldsymbol{F_p} = Q\boldsymbol{P} \quad 5.3$$

Q in equation 5.3 is the transformation matrix which converts nodal pressures into hydrodynamic forces. For ambient vibration of arch dams, the ground accelerations force term $\boldsymbol{F_g}$ can be assumed to be zero as ground motions are negligible. The force vector due to the hydrodynamic pressures is small for ambient vibrations but it is not negligible.

It is important to point out at this stage that, this study is not concerned with the full solution of the dynamic equation 5.1. The full solution of equation 5.1 involves the solution of both the pressures in the upstream side and the displacements. The study is however about the extraction of the natural frequencies and mode shapes of a system that is described by equations 5.1 and 5.3.

Alternatively, the free vibration version of equation 5.1 can be described in terms of the mode shapes $\boldsymbol{\phi}$ and natural frequencies ω of the dam structure as in equation 5.4 below. The expression in equation 5.4 is based on several assumptions, notably the following; linear behaviour, the damped natural frequency is very close to the undamped natural frequency and that after the initial disturbance, the motion of the dam is harmonic and all the points vibrate with the same frequency but different amplitudes.

$$([\boldsymbol{K_s}] - \omega^2 \dot{[}\boldsymbol{M_s}])\boldsymbol{\phi} = \mathbf{0} \quad 5.4$$

Normally, for simple dynamic systems, equation 5.4 would be adequate to allow for the correct extraction of the natural frequencies and mode shapes. In arch dams, the fluid structure interaction generates the hydrodynamic pressures ***P*** on the upstream wall which affect the deformations of the dam wall, which in turn influence the pressures (USACE, 2003). Thus there is a coupled pressure-displacement relationship.

Chopra (1987) showed that the complete formulation of the fluid-structure interaction produces frequency-dependent hydrodynamic pressures that can be interpreted as an added force, an added mass and an added damping. The added force normally does not affect the natural frequencies and mode shapes of the dam. It has already been assumed above that damping does not change the dynamic properties considerably. Hence, the only parameter which changes the dynamic properties that is altered by the fluid structure interaction is the mass of the structure.

In light of this information, equation 5.4 can be written as follows;

$$([\boldsymbol{K_s}] - \omega^2[\dot{\boldsymbol{M_s}} + \boldsymbol{M_a}])\boldsymbol{\phi} = \boldsymbol{0} \qquad 5.5$$

Where ***M_a*** is the added mass of water due to the hydrodynamic interaction of structure and the water body. The added mass concept is however only valid if the water in the dam is assumed to be incompressible (Chopra, 1967).

The two most common added mass formulations applicable to arch dams are the Westergaard method and the fluid-structure coupled finite element added hydrodynamic mass model. These two formulations estimate the added mass ***M_a*** in equation 5.5 differently. However, of note is that both methods first focus on the hydrodynamic pressures estimation which can then be converted to added mass. The estimation of ***M_a*** allows for the solution of the equation for the mode shapes and natural frequencies.

Besides the added mass formulations, there are also Lagrangian and Eulerian approaches which are used to solve the fluid-structure interaction problem in arch dams using finite elements. These two approaches both model the water body using finite elements. In the Eulerian approach normally the displacements are variables in the dam wall and pressures are variables in the fluid, while in the Lagrangian approach the displacements are both variables in the fluid as well as the solid. Some examples of these formulations are described in the next sections.

5.1. Westergaard Method

Westergaard (1933) published the added equivalent mass theory which can be used to estimate the dynamic action of the water on the dam. Several assumptions were made in the derivation of this theory, which include the following;

i) a 2-dimensional system is assumed
ii) the reservoir extends to infinity in the upstream direction
iii) the dam is rigid and has a vertical upstream face
iv) deformations are small

v) the effect of the surface waves of the homogenous water body can be neglected
vi) ground motions which excite the dam are harmonic and in the downstream-upstream direction. The ground motion's period is also assumed to be more than the natural period of the reservoir.

The harmonic excitation forces imply that the motion of the dam is also harmonic. It is the responsive movement of the dam that Westergaard (1933) estimated using the added equivalent mass theory. The problem of the dynamic action of the mass of the dam was transformed into an equivalent problem of statics from which it was observed that the generated pressures were the same as if a certain body of water were forced to move back and forth with the dam while the remainder of the reservoir is left inactive.

This approach allows the forces exerted on the upstream surface of the dam to be represented as inertia forces like those due to the moving mass of the dam itself. The shape of the body of water that is considered to move with the dam is determined such that the inertia forces become equal to the pressures actually exerted by the water due to the dynamic loading.

Westergaard (1933) concluded that a body of water enclosed by a dam wall and an upside down parabola which intersects with the horizontal bottom of the reservoir at a distance of seven-eighths of the water depth away from the dam wall base can give a good approximation of the inertia forces which would equal the hydrodynamic pressures. The graphical representation of Westergaard theory is shown in Figure 5.1.

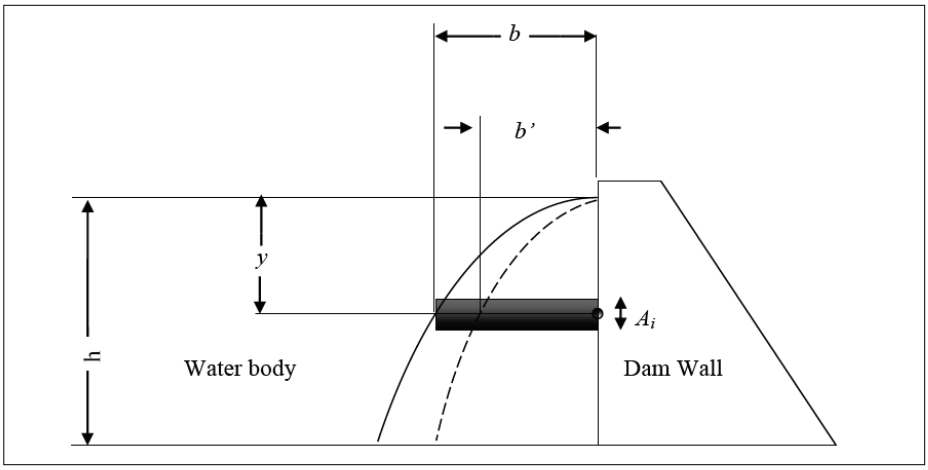

Figure 5.1: Body of water which may be considered to move with the dam wall shown by a bold curve. The dotted curve shows equivalent body of concrete.

The parameter y refers to the depth of the water from the water surface to the point of interest while the parameters b and b' are the depth dependent dimension which describe the respective parabolas for the masses of the water or equivalent concrete which move with the dam. The depth of the water in the reservoir is defined by the parameter h.

$$\boldsymbol{b'} = \mathbf{0.38} \times \sqrt{(\boldsymbol{h} \times \boldsymbol{y})} \quad 5.6$$

$$\boldsymbol{b} = \frac{\mathbf{7}}{\mathbf{8}} \times \sqrt{(\boldsymbol{h} \times \boldsymbol{y})}) \quad 5.7$$

The added mass of water m_{ai} at point *i* is obtained by multiplying the mass density of water ρ_w by the volume of water tributary to point *i*. This derivation was for a 2-dimensional case hence it can be assumed that dam section extends one unit into the page and A_i is the height of the small water volume which is tributary to point *i*.

$$m_{ai} = \frac{7}{8} \times \rho_w \times A_i \sqrt{(h \times y)}) \quad 5.8$$

The calculated added mass matrix for the wetted upstream points is then added to the mass matrix of the structure as mentioned in equation 5.5.

The USBR Design of Arch Dams Manual (1977) extends the application of the Westergaard method to 3-dimensional cases. This was done in order to make possible the use of the Westergaard method for arch dams' dynamic analysis. It is not advisable for any analysis of arch dams to be executed in 2-dimensions only as their crown cantilever's behaviour is not always representative and critical; this is normally the case in gravity dams.

The USBR Manual (1977) notes that the amount of water that is assumed to move with the dam is actually different for the different modes of vibration of the dam. For example, in this approach the dimensions *b* and *b'* given in equations 5.6 and 5.7 above respectively only apply for the dam's first mode of vibration. The dimension *b* for the mass of water that moves in the second mode of vibration for any point in contact with the water is given in equation 5.9.

$$b = \frac{2X}{3L} \times \sqrt{(h \times y)} \quad 5.9$$

The parameters *h* and *y* are as described as in Figure 5.1: . *L* is the length of contact of the water with the face of the dam at the height of point of interest and *X* is the distance measured from the vertical axis of the dam horizontally to the point of interest.

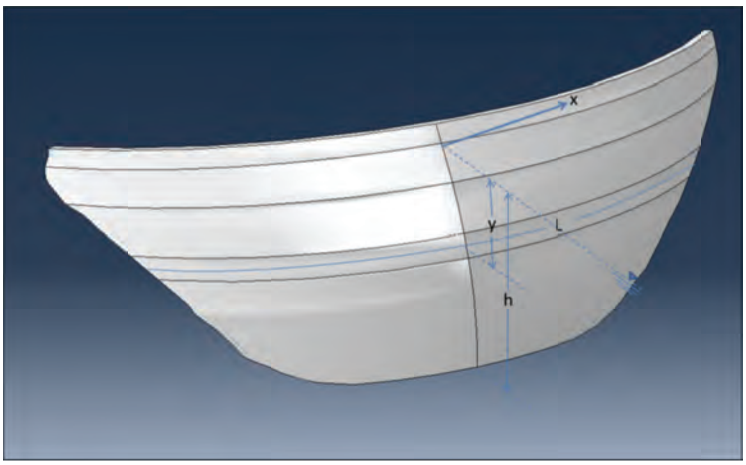

Figure 5.2: The parameters used to describe the added mass in the USBR Manual.

The USBR Manual method modifies the original Westergaard method by considering the flexibility of the dam wall. Clearly, once the flexibility of the dam is considered, it would imply that the added mass function would then depend upon the shape of the vibration mode considered. So, no one function will be exactly valid for all vibration modes of the dam. However it has been shown that the formulations for a rigid dam can still be used to an acceptable degree of accuracy to account for the hydrodynamic effects for all modes of a flexible structure (Goyal and Chopra, 1989 cited by Davey et al. (2006)).

Kuo (1982) extended the original Westergaard method to allow the method to account for both flexibility and curvature and hence extend the application of the method to other dam types. This formulation by Kuo is often referred to as the generalized Westergaard method.

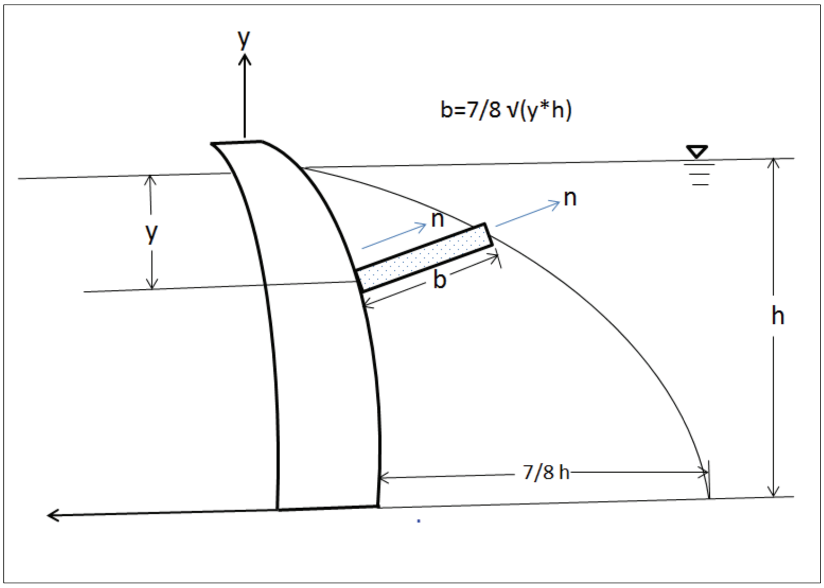

Figure 5.3: A curved upstream face on which the generalized Westergaard method is applicable.

The generalized Westergaard method recognises that the hydrodynamic pressure exerted on any point of the upstream face of the dam, due to the total acceleration normal to the dam face at that point, is equal to the inertia force produced by a prismatic body of water of unit cross section with length *b,* which is defined as in equation 5.7. This water body is assumed to be attached strongly normal to the dam face at that point and moving back and forth with the dam in the normal direction without friction (Kuo 1982).

It is also of importance to note that at any wetted point on the upstream wall the normal hydrodynamic pressure $\boldsymbol{P}_n$ is said to be proportional to the total normal acceleration $\ddot{\boldsymbol{u}}_{\boldsymbol{n}}$ at that point (Federal Energy Regulatory Committee, 1999).

In mathematical form:

$$\{\boldsymbol{P}_{\boldsymbol{ni}}\} = \alpha\{\ddot{\boldsymbol{u}}_{\boldsymbol{n}}\} \qquad 5.10$$

$$\alpha = \frac{7}{8}\rho_w\sqrt(h \times y) \tag{5.11}$$

The parameter α is known as the Westergaard pressure coefficient. It is the product of the length parameter *b,* which has already been described in equation 5.7, and the density of water ρ_w.

$\ddot{\boldsymbol{u}}_{\boldsymbol{n}}$, the total normal acceleration at a node "*i*" is resolved into a sum of the ground acceleration $\ddot{\boldsymbol{u}}_{\boldsymbol{g}}$ and acceleration at node "*i*" relative to the base of the dam which is $\ddot{\boldsymbol{u}}$. In order for this to occur, use is be made of the row vector of direction cosines of the normal vector λ_i at a point of interest "*i*" and a transformation matrix β_i.

β_i, a (3×3) displacement transformation matrix of which the entry β_{jk} stands for the acceleration of node "i" in the j-direction due to a unit ground acceleration in k-direction while the dam is undergoing rigid body motion, is also needed for the resolving of the total normal acceleration (Kuo, 1982).

$$\{\ddot{\boldsymbol{u}}_{\boldsymbol{n}}\} = \lambda_i(\{\ddot{\boldsymbol{u}}\} + [\beta_i]\{\ddot{\boldsymbol{u}}_{\boldsymbol{g}}\}) \tag{5.12}$$

Combining equations 5.10 and 5.12 results in equation 5.13 below; remembering that the normal force $\boldsymbol{F}_{\boldsymbol{ni}}$ at a node *i* is a product of the normal pressure and the surface area A_i tributary to point *i* also gives the hydrodynamic force formulation in equation 5.14.

$$\{\boldsymbol{P}_{\boldsymbol{ni}}\} = \alpha\,\{\ddot{\boldsymbol{u}}_{\boldsymbol{n}}\} = \alpha\,\lambda_i(\{\ddot{\boldsymbol{u}}\} + [\boldsymbol{\beta}_{\boldsymbol{i}}]\{\ddot{\boldsymbol{u}}_{\boldsymbol{g}}\}) \tag{5.13}$$

$$\boldsymbol{F}_{\boldsymbol{ni}} = -\boldsymbol{P}_{\boldsymbol{ni}}A_i = \alpha\,\lambda_i(\{\ddot{\boldsymbol{u}}\} + [\boldsymbol{\beta}_{\boldsymbol{i}}]\{\ddot{\boldsymbol{u}}_{\boldsymbol{g}}\})A_i \tag{5.14}$$

The last step involves resolving the normal force $\boldsymbol{F}_{ni}$ into Cartesian components. This is done using equation 5.15. The positive direction in this derivation is assumed to be outward and normal from the dam face.

$$F_i = \lambda_i^T\boldsymbol{F}_{\boldsymbol{ni}} \tag{5.15}$$

Combining equation 5.14 and 5.15 results in the following;

$$F_i = -\alpha A_i\lambda_i^T\lambda_i(\{\ddot{\boldsymbol{u}}\} + [\boldsymbol{\beta}_{\boldsymbol{i}}]\{\ddot{\boldsymbol{u}}_{\boldsymbol{g}}\}) \tag{5.16}$$

Where

$$M_{ai} = \alpha A_i\lambda_i^T\lambda_i \tag{5.17}$$

M_{ai} is a full (3×3) added mass matrix associated with a node *i* on the upstream face of the dam (Ghanaat, 1993). The difference between the original and generalized Westergaard methods is the presence of the symmetric matrix in the latter. This matrix will be referred to as a matrix *f* for the rest of this report.

The component of the normal acceleration which relates to the ground motions can be assumed to be almost zero for non-seismic excitations. This is because there are hardly any ground motions during normal operation of the dam unless the limited ones that may occur due to the water that might overspill the spill-way when the dam is full.

At this stage, it is important to highlight that all of the Westergaard method express were formulated on the basis of an earthquake induced movement which is very different from the ambient dynamic behaviour of the dam. However, the method has been used for both earthquake and ambient behaviour where it has been observed that it overestimated the added mass leading to inaccurate results especially for seismic analysis (Lemos et al. 2008).

The magnitudes of the accelerations experienced by the dam during both earthquake and ambient conditions are significantly different. Data of peak accelerations extracted from Mauvoisin dam shows that during an earthquake of magnitude 4.6 that occurred on 31^{st} March 1996, peak accelerations that were observed at the dam crest had a magnitude of about 0.013g. On the other hand, typical time-history from a continuous automated ambient vibration monitoring of the same dam for an acceleration record close to the crest show a peak value of 11μg (Darbre and Proulx, 2002).

The significance of the different peak acceleration magnitudes is that higher magnitudes experienced during seismic activities result in greater pressures on the water forcing it to vibrate immensely such that the compressibility of the water cannot be ignored anymore. It turns out that for such cases the dynamic pressures depend on magnitude and the nature of the exciting acceleration (Pani and Battacharyya, 2008). On the other hand, during ambient day to day operation of the dam, modest pressures are observed and these pressures do not depend on the magnitude of the exciting acceleration. In this case, the water can be assumed to be incompressible since the dynamic deformations are relatively small.

The Westergaard added mass assumes the water in the dam is incompressible. With this in mind, the authors postulate that for the case of the ambient day-to-day dynamic behaviour of an arch dam for which the dynamic pressures and deformation are relatively small, the method can still be used to give reasonable results. The Westergaard method has been used throughout the years as an easily applicable method and an alternative to a more cumbersome approach of using fluid finite elements. Improvements, criticisms and evaluations of the method have been done over the years and this study also attempts to contribute positively to the use of the method.

5.2. Fluid structure interaction approach

As in the Westergaard added mass method, this approach attempts to estimate the hydrodynamic pressures generated from the incompressible fluid-structure interaction. Once they are found, the pressures are lumped into equivalent hydrodynamic nodal forces, the forces from which the added mass coefficient matrix can be deduced (Kuo, 1982).

This method resorts to the pressure wave equation for incompressible and inviscid fluid as given in equation 5.18 for the solution of the pressures. ∇^2 is the Laplace operator in three dimensions and $\boldsymbol{P}$ is the hydrodynamic pressure in excess of the static pressure in the fluid domain.

$$\nabla^2 \boldsymbol{P} = 0 \qquad 5.18$$

The boundary condition assumptions made in the solution of this pressure wave equation are very important. Most reservoirs are generally irregular in geometry which makes it very difficult to find closed form solutions of equation 5.18. Therefore, a numerical solution based on the Finite element method is used. A finite element mesh of a fluid domain which extends the distance which is three times the height of the dam in the upstream is assumed to be good enough to be representative of the entire reservoir.

In general, when the Westergaard method is compared to the Finite element based Galerkin method, the Westergaard method gives higher hydrodynamic pressures and hence higher added masses (Kuo, 1982). The effect of the diverging reservoir wall angles can be captured by the boundary conditions in the modelling when the Galerkin Finite element method is used but when the Westergaard method is used the effect cannot be captured. This is one of the reasons these two methods can give different results.

5.2.1. Extraction of natural frequencies using Decoupled Modes

For the case of a compressible water and flexible dam wall, the fluid and structure interaction of the impounded water and the dam wall results in a coupled system. The coupled system of a can be described with the help of equation 5.19 which has been written in the standard Galerkin variation formulation of pressures and displacements (Tiliouine and Seghir, 1998). This formulation can be used in finite elements.

$$\begin{bmatrix} \boldsymbol{M_s} & \boldsymbol{0} \\ \rho_w \boldsymbol{Q^T} & \boldsymbol{M_F} \end{bmatrix} \begin{Bmatrix} \ddot{\boldsymbol{u}} \\ \ddot{\boldsymbol{P}} \end{Bmatrix} + \begin{bmatrix} \boldsymbol{C_s} & \boldsymbol{0} \\ \boldsymbol{0} & \boldsymbol{C_F} \end{bmatrix} \begin{Bmatrix} \dot{\boldsymbol{u}} \\ \dot{\boldsymbol{P}} \end{Bmatrix} + \begin{bmatrix} \boldsymbol{K_S} & -\boldsymbol{Q} \\ \boldsymbol{0} & \boldsymbol{K_F} \end{bmatrix} \begin{Bmatrix} \boldsymbol{u} \\ \boldsymbol{P} \end{Bmatrix} = \begin{Bmatrix} \boldsymbol{F_g} \\ \boldsymbol{0} \end{Bmatrix} \qquad 5.19$$

Equation 5.19 is not really made out of 2x2 matrices but it is represented so as to show the distinction between terms associated with the displacement, ***u*** and terms associated with the pressure, ***P***. The symbols **M**, **C** and **K** still have the usual meaning they have in structural dynamics while ρ_w is the water density. The terms with the subscript *s* refer to the dam wall while those with the subscript *F* refer to the impounded water body. $\mathbf{F_g}$ refers to the driving force and **Q** is the transformation matrix which converts nodal pressures into hydrodynamic forces (Tiliouine and Seghir, 1998).

This Eulerian based equation is especially difficult to solve since the matrices are not symmetric. Even though there are unsymmetrical eigen-solvers available, they are very time-consuming from the execution point of view and also complicated from programming aspects. Furthermore, even though symmetrisation of the matrices is possible, it requires introduction of additional variables which creates complications in computer programming (Tiliouine and Seghir, 1998).

Sani and Lotfi (2010) solve the dynamic problem of the arch dam-reservoir system by introducing fictitious decoupled systems whose mode shapes are found and then used to compute the actual mode shapes. The fictitious mode shapes are known as ideal coupled modes as they represent mode shapes of ideal systems. The two ideal systems are the incompressible fluid system and the massless dam wall system. The analysis of the incompressible fluid system generates mode shapes of the dam with the reservoir water assumed to be incompressible while the massles dam wall system analysis will generate mode shapes of the reservoir with rigid walls everywhere except at the free surface (Sani and Lofti, 2007). Of much interest to this project, is the first system which is made out of an incompressible fluid.

This analysis is based on the Eulerian approach of solving the structure-fluid interaction problem (Figure 5.4). In the Eulerian formulation normally the displacements are variables in the dam wall and pressures are variables in the fluid (Bayraktar et al. 2011).

In this ideal-coupled modal approach, the dam is discretized by solid finite elements, while, the reservoir is divided into parts, a near-field region in the vicinity of the dam and a far field part assumed as a prismatic channel, which extends to infinity. The former region is discretized by fluid finite elements, while the three-dimensional fluid hyper-elements are utilized to model the reservoir far-field region. It is said that the hyper-elements help in treating the radiation condition rigorously. The hyper-element has an arbitrary geometry shape in the vertical plane, and it actually consists of several sub-channels, which extends to infinity in the upstream direction and all nodes of this semi-infinite fluid element are located on that vertical plane (Sani and Lotfi, 2010).

The main aim of ideal-coupled modal approach method is to provide a better solution method in terms of programming, for the fluid-structure dynamic interaction formulation in equation 5.19 (Sani and Lotfi, 2010).

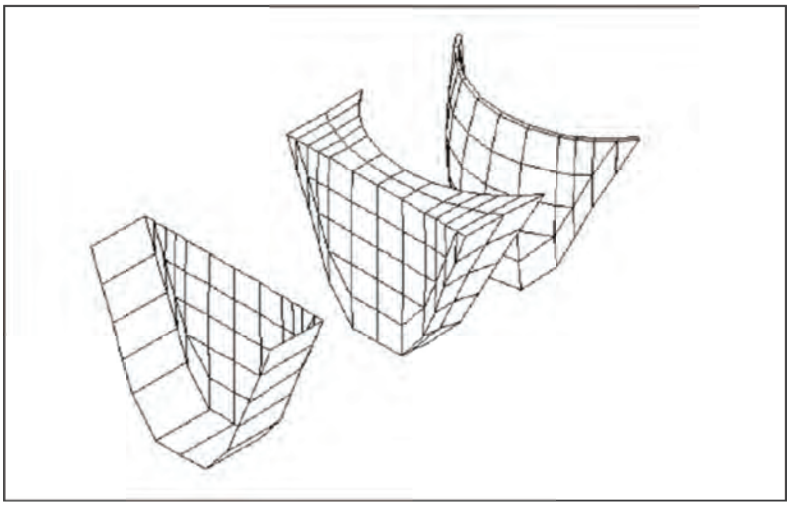

Figure 5.4: Shows the finite element mesh of a dam body, far right. The fluid domain finite elements in the middle and the fluid hyper-element which extends to infinity in the upstream direction, far left. Courtesy of Sani and Lofti, (2007).

The procedure for the ideal-coupled modal approach is outlined below for a dam with a finite reservoir system.

The free vibration form of equation 5.19 without the damping is outlined in equation 5.20 below. It can also be assumed that the dam's response in the form of displacements and pressures will be harmonic (Sani and Lotfi, 2010);

$$\begin{bmatrix} -\boldsymbol{\omega}^2\mathbf{M_S} + \mathbf{K_S} & -\mathbf{Q} \\ -\boldsymbol{\omega}^2\rho\mathbf{Q}^\mathrm{T} & -\boldsymbol{\omega}^2\mathbf{M_F} + \mathbf{K_F} \end{bmatrix} \begin{Bmatrix} \boldsymbol{u} \\ \boldsymbol{P} \end{Bmatrix} = \begin{Bmatrix} \mathbf{0} \\ \mathbf{0} \end{Bmatrix} \qquad 5.20$$

Considering only the lower partition of equation 5.20 and letting $\mathbf{M_F}$ be equal to zero for the assumed incompressibility of water. One would have:

$$-\boldsymbol{\omega}^2\rho\mathbf{Q}^\mathrm{T}\mathbf{u} + \mathbf{K_F}\mathbf{P} = \mathbf{0} \qquad 5.21$$

Solving equation 5.20 for the pressure in terms of the displacement field yields the following:

$$\boldsymbol{P} = \boldsymbol{\omega}^2\rho\, \boldsymbol{K_F^{-1}}\, \mathbf{Q}^\mathrm{T}\, \mathbf{u} \qquad 5.22$$

Substituting this relation in the upper partition equation of equation 5.20 results into the following simplified form of the first ideal eigenproblem:

$$\left(-\boldsymbol{\omega}^2(\mathbf{M_s} + \mathbf{M_a}) + \mathbf{K_S}\right)\mathbf{u} = \mathbf{0} \qquad 5.23$$

With the following matrix definition being used:

$$\boldsymbol{M_a} = \rho\boldsymbol{Q}\;\; \boldsymbol{K_F^{-1}}\, \mathbf{Q}^\mathrm{T} \qquad 5.24$$

Matrix $\boldsymbol{M_a}$ is referred to as added mass matrix that is usually obtained for fluid-structure interaction problems in the case of incompressible fluid assumption (Sani and Lotfi, 2010). This is almost an equivalence of the added mass methods discussed earlier. The difference is that the added mass in this case is added through the use of fluid finite elements in an Eulerian approach.

The second stage of this ideal eigen-problem involves using the assumption of the massless dam wall, i.e. the corresponding mode shapes are entirely due to the water body restrained from all sides. This corresponds to omitting the matrix $\mathbf{M_S}$ in equation 5.20. Having omitted $\mathbf{M_S}$, the task is then to use the upper partition of equation 5.20 to solve for the displacements $\boldsymbol{u}$ in terms of the pressures $\boldsymbol{P}$. This leads to:

$$\boldsymbol{u} = \boldsymbol{K_S^{-1}}\boldsymbol{Q}\,\boldsymbol{P} \qquad 5.25$$

Thereafter, substitute this relation in the lower partition equation of equation 5.20 to obtain the simplified form of the second ideal eigen-problem:

$$\left(-\boldsymbol{\omega}^2(\mathbf{M_F} + \mathbf{G_a}) + \mathbf{K_F}\right)\mathbf{P} = \mathbf{0} \qquad 5.26$$

Where $\mathbf{G_a}$ is defined as:

$$\boldsymbol{G_a} = \;\boldsymbol{\rho}\, \mathbf{Q}^\mathrm{T}\, \boldsymbol{K_S^{-1}}\, \mathbf{Q} \qquad 5.27$$

Sani and Lotfi (2010) suggest that the two ideal eigen-problems represented by both equations 5.23 and 5.26 may be combined in one relation to yield the following:

$$\begin{bmatrix} \left(-\boldsymbol{\omega}^2(\mathbf{M_s}+\mathbf{M_a})+\mathbf{K_S}\right) & 0 \\ 0 & -\boldsymbol{\omega}^2(\mathbf{M_F}+\mathbf{G_a})+\ \mathbf{K_F} \end{bmatrix} \begin{Bmatrix} \boldsymbol{u} \\ \boldsymbol{P} \end{Bmatrix} = \begin{Bmatrix} \mathbf{0} \\ \mathbf{0} \end{Bmatrix} \qquad 5.28$$

Due to the symmetry of the matrix in equation 5.28, the solution to the above combined eigen-value can be easily found by standard multiple degree of freedom dynamic systems solving techniques provided that the matrices are computed correctly. Having outlined the procedure for a dam for its near field reservoir, the effects of the reservoir far-field region are then added to what has been discussed for the near field region (Sani and Lotfi, 2010).

It has been mentioned that the hyper-elements help in treating the radiation condition. The radiation condition refers to the propagation and absorption of the hydrodynamic waves upstream. These waves are unlikely to be significant in ambient conditions hence the use of the hyper-elements is not of great importance in ambient modal analysis of arch dams using the ideal-coupled method.

The ideal-coupled modal approach was discussed to illustrate that for the case of an ideal system of an incompressible fluid, the ideal-coupled modal approach show some similarities to the added mass methods discussed before. This is through the use of the near-field part of the reservoir in the ideal modal coupled approach. If the far field area is ignored, the ideal modal coupled approach's incompressible water set would still give comparable results to the Westergaard method.

5.3. Arch dam Foundation Models

This section will describe models used to represent the foundation behaviour during a dynamic activity. The problems normally encountered in the modelling of foundation-dam wall dynamic behaviour will also be discussed together with their respective solution methods.

5.3.1. Massless foundation approach

Much of the work that has been done on the dynamic interactions between the dam and the foundation is biased towards safety of dams under seismic loads. Earthquake effects are transferred from the source in the form of underground waves. The dam then experiences the effect of the earthquake as a result of the movement of the foundation. In order to accurately assess the safety of dams in the event of earthquakes, the magnitude of the critical acceleration that can be experienced by a dam needs to be known to a reasonable degree of accuracy. The magnitude of these accelerations on an already existing dam can be measured by the help of seismometers which are normally located at the interface of the dam wall with the foundation.

It is therefore clear that in order to correctly formulate the dynamic response analysis for a dam, it is necessary to include a significant amount of the foundation material in the dam model. Having included the foundation in the modelling; the major challenge that follows is then ensuring that the seismic input to the foundation is specified as accurately as possible. It also needs to be ensured that the propagation of the seismic input waves inside the foundation model is as close to the actual field scenario as possible.

Generally, either of two different approaches is used to specify the seismic input to models: it may be defined as motions applied at the boundaries of the foundation, or it may be prescribed as 'free-field' motions of the interface between dam and foundation. These 'free-field' motions are the ones that would have occurred at the nodes of the foundation block in contact with the dam if the dam were not present (Zienkiewicz et al. 1984).

The massless foundation model assumes the mass of the foundation block is simply zero. The foundation block in this case functions simply as a spring system in the interaction mechanism; without mass the rock does not develop vibration waves to modify the properties of the waves as they propagate through the foundation (Zienkiewicz et al. 1984).

Normally, in this method ground level accelerations measured from previous earthquakes which are also known as free-field accelerations time history are applied uniformly at the truncated foundation base. Since the wave propagation velocity in the assumed massless rock is approaching infinity, the input motions are transmitted instantaneously through the foundation rock to the dam-foundation interface, and the motion at the interface would be the same as the input one. This makes the method highly favourable in that aspect as it allows for the use of the actually measured earthquake motions at the free field surface as the boundary input (Chuhan et al. 2009).

Hence, the massless foundation model avoids one of the major difficulties inherent in the boundary input approach and has been used extensively for that reason. However, Chuhan et al. (2009) mention that this massless foundation approach only considers the foundation flexibility and ignores the dam-foundation inertial interaction. One other disadvantage with this method as indicated by Chuhan et al. (2009), is that it overestimates the response of the dam both in the linear and the non-linear analyses.

Literature indicates that the EACD-3D and the Smeared Crack Arch Dam Analysis programs which were developed by Fok et al. (1986) and Hall (1996) respectively use this assumption of a massless foundation. In a study done by Proulx et al. (2004) in which numerical analyses of earthquake responses of three dams was done and compared with results from in-situ measurements, it was found that higher damping ratios as 8-15% (while the normal range of damping ratio of dams is about 5% in design practice) were needed for approximately matching the field response records of the dams which further highlights the inaccuracy of the massless foundation assumption.

5.3.2. Foundation with mass approach

There are generally two earthquakes data input methods available for use with the foundation with mass approach, namely the deconvolution and the free-field input methods.

Deconvolution Input Method

As mentioned earlier, the free field surface motions are significantly different from the motions at depth. The former are considerably amplified by reflections as compared to the latter. Seismometers located at the surface of the ground measure the free field surface motions.

If the mass of the foundation is to be considered in the analysis then it is highly advisable that the earthquake motions at depth are known so that they can be introduced accordingly at the truncated foundation base. The difficulty normally encountered is how to determine these at depth motions given the free field ones. The procedure of determining this is known as the deconvolution analysis.

In the deconvolution analysis, first the foundation block alone is analysed alone to determine the motion at depth that would have produced the measured free field surface motions. The result of this preliminary analysis which is performed in the frequency domain is then used as the input to the boundary of the foundation block supporting the dam (Zienkiewicz et al. 1984).

Free-Field Input Method

In this method, the equations of motion are formulated directly in terms of the free-field input. Earthquake excitations are therefore imposed as the free-field motions at the dam-foundation interface directly. Both the latter two methods, namely the deconvolution input and the free-field input models are equivalent if the radiation damping and input mechanisms are considered appropriately (Chuhan et al. 2009).

5.3.3. Foundation size models

The preceding sub-topic has outlined how important it is to include the foundation in the dynamic analysis of arch dams. When this is done, at some depth at which the boundary of this hypothesized portion of the foundation rock lies; the conditions are usually assumed to be rigid. This is one of the limitations associated with this approach in that in concrete dam sites where rocks usually extend to large depths, there is no obvious rigid boundary.

However, studies have been done which show that depending on the ratio of foundation’s deformation modulus to the dam’s elastic modulus the extent of the representative foundation model can be estimated. Whether a foundation model is representative or not is decided upon on the basis of whether the increase of dimensions of which affects any of the deflections, stresses or natural frequencies in the dam. For example, for a ratio of the foundation’s deformation modulus to the dam’s elastic modulus of about 1, the minimum radius of the semi-circular foundation can be chosen to be equivalent to the dam wall height (U.S. Army Corps of Engineers, 1994).

These artificial boundary conditions have an effect of reflecting radiation waves from the dam model, which is not what exactly happens on site. Radiation waves produced by the ambient dynamic motions of the dam are unlikely to be that great such that they can reach the bottom of the reservoir while they are still very intense in their magnitude.

However for earthquake induced radiation waves, in order to avoid their reflections in models, truncated foundation with non-reflecting boundaries needs to be introduced such that the radiated waves can propagate through towards infinity. The viscous spring boundary input model is one such input method which ensures that waves can propagate through towards infinity.

5.3.4. Viscous-spring boundary input model

Chuhan et al. (2009) use the viscous-spring input model to study the arch dam-foundation interaction. They argue that this method is very efficient and convenient to incorporate in the finite element code and has sufficient accuracy without much increase in computational efforts. In this method, pairs of dashpots and springs are installed in all nodes of artificial boundaries. Each node on the artificial boundary contains three pairs of dashpots and springs, i.e. one in the normal direction of the boundary plane and the other two in the tangential directions. The dashports and the spring are both assigned values of viscous damping and stiffness respectively in all three directions. It is said that the acceleration time histories which normally act as an input parameter are, in this method, replaced by equivalent force input on the artificial boundaries.

5.4. Summary

Dynamic behaviour of arch dams involves the interaction between the water body, the dam and the foundation of the dam. The numerical solution to this complex fluid structure interaction problem is computationally intensive and can be time consuming. The Westergaard method provides a simplified approach to the solution of the fluid-structure interaction problem by eliminating fluid elements and introducing additional mass to the dam. However this approach was developed for dams under seismic excitation. This project explores application of Westergaard method to the dynamic behaviour of dams under operational loading.

6. TEMPERATURE MODELLING FOR CONCRETE DAMS IN OPERATION

Concrete arch dams in operation are permanently subjected to thermal action due to seasonal temperature variation (Agullo, Aguado, & Mirambell, 1991). The variation in seasonal temperatures and climatic conditions has significant influence in temperature field patterns that are observed within arch dams. A significant portion of deterioration of arch dams has been observed to be a result of temperature loading (Daoudu, Galanis and Ballivy, 1997). The temperature loads are modelled in finite element computational software which comes in various packages. Temperature modelling largely depends on the thermal conductivity of concrete, coefficient of thermal expansion, diffusivity and specific heat. To study the performance of operational concrete arch dams, static and dynamic analysis are the prime analyses that are considered. In static analysis, the focus is on temperature field patterns, stresses and displacements. In dynamic analysis, the focus is on obtaining the dynamic properties if the dam and responses of the dam to dynamic forces such as seismic action.

Heat analysis is performed via three main temperature mechanisms namely radiation, conduction and convection. In finite element modelling of concrete dams, thermal boundary conditions have to be applied to specify the process of these mechanisms. This chapter reviews the heat transfer process, the Fourier heat conduction model, the numerical solution to the governing equation of the heat conduction model and the various temperature models for determining solar radiation, air temperature, water temperature, and foundation temperature. Figure 6.1 shows a schematic presentation of the heat transfer process in concrete arch dams.

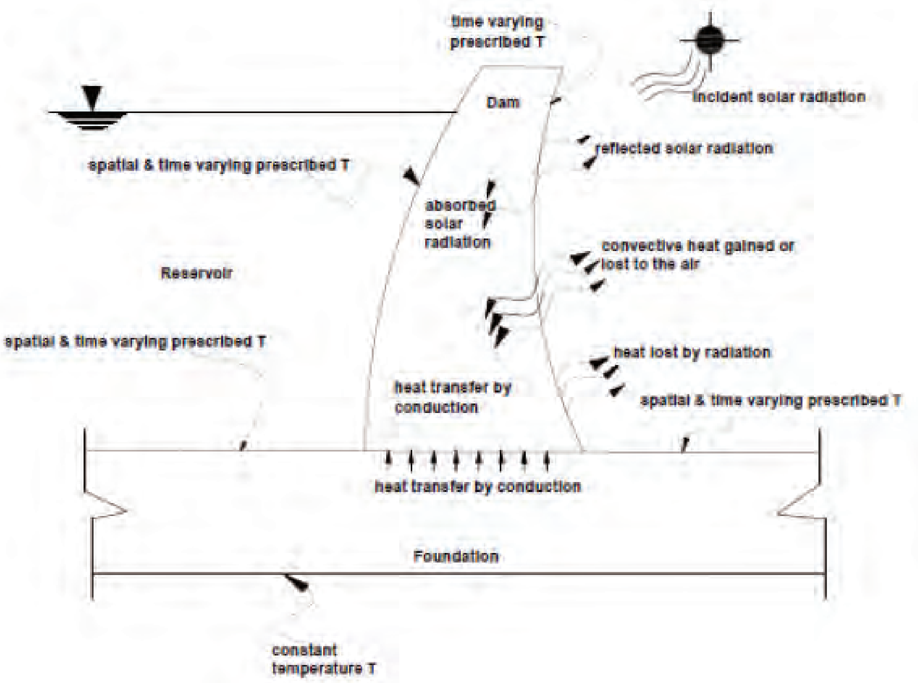

Figure 6.1: Solar radiation, convection and conduction in a typical concrete arch dam.

6.1. Heat Transfer in concrete arch dams

Heat transfer, also referred as heat conduction, is highly dependent on the thermal properties of concrete and is considered a fundamental problem involving the solution to partial differential equations for scalar quantities (Eckert et al., 1996). It involves contact conduction and contact resistance. Contact conduction is generally associated with operational arch dams and is influenced by external heating sources such as air temperature, reservoir temperature, foundation temperature and solar radiation. Contact resistance is associated with dams under construction and influenced by internal heating sources such as concrete closure temperatures. In finite element temperature analysis, mathematical temperature models are used to model the external and internal heating sources. The models are not accurate and require measured data to verify the results of analysis (Federal Energy Regulatory Commission, 1999). They assume a uniform and isotropic distribution of thermal properties on the entire body of the dam (Feng, Jian and Jinting, 2010). Because a lot of assumptions, it is helpful to perform analysis on existing dams that have undergone monitoring in order to validate the models.

6.1.1. Fourier heat conduction model

Heat transfer in concrete arch dams system is assumed to be governed by the three dimensional Fourier heat conduction model given as follows:

$$\frac{\partial^2 T}{\partial x^2}+\frac{\partial^2 T}{\partial y^2}+\frac{\partial^2 T}{\partial z^2}+\frac{Q}{k}=\frac{1}{D_m}\frac{\partial T}{\partial t} \quad , \qquad D_m=\frac{k}{\rho c} \tag{6.1}$$

$$\Delta^2 T+\frac{Q}{k}=\frac{1}{D_m}\frac{\partial T}{\partial t} \tag{6.2}$$

Where, T (℃) is the 3D temperature field; $Q\ (kJ/m^3h)$ is the rate of heat generation per unit volume; Δ is the Laplace operator for temperature. The quotient parameters for D_m (concrete) are $\rho(kg/m^3)$ density, $c\ (kJ/Kg℃)$ specific heat and $\kappa\ (W/m℃)$ heat conduction coefficient.

The model considers spatial variation in the incident rays of the sun at any location on the surface of the concrete arch dam at a certain instance. It focuses on heat transfer in three principal directions of the datum axes, following the sophisticated geometry of arch dams.

6.1.2. FEM boundary conditions for heat conduction model

For every finite element model, certain boundary conditions have to be applied at the domain interface. In arch dams, this interface is defined by the thermal contact boundary. This is further classified into two sets of boundary conditions; essential boundary and natural boundary. The essential boundary condition defines temperature applied in the system (air, reservoir and foundation temperatures) while the natural boundary conditions describe the fluxes applied in the system (convection, solar radiation, and solar irradiation).

Essential boundary condition

The essential condition, also referred to as initial boundary conditions, for the solution to Equation (6.1) is defined by the temperature in the integration domain at a specific instant that is adopted as the time origin (Agullo, Aguado, & Mirambell, 1991):

$$T(x,y,z,t) = T_{initial}(x,y,z,t) = \bar{T} \qquad 6.3$$

where $\bar{T}$ is a prescribed initial temperature on the surface on the dam.

Natural boundary conditions

The natural boundary conditions, also referred to as Neumann boundary conditions, for the solution to Equation (6.1) mathematically represent the different mechanisms of heat transfer. These conditions are considered separately for the downstream and upstream phase.

Downstream face

In the downstream face, the condition of applied flux is used. It represents the heat transfer by three different mechanisms; convection, solar-radiation and solar-irradiation (Agullo, Aguado and Mirambell, 1996). The models for these mechanisms are discussed in the following sections.

$$k\frac{\partial T}{\partial n}(x,y,z,t) + q(x,y,z,t) = \bar{q} \qquad 6.4$$

where k is the conductivity tensor; T is the temperature of the surface at instant t; q is the thermal energy transferred across the downstream face. $\bar{q}$ is the heat flux in the concrete arch dam.

The thermal energy transferred across the downstream face (q), is expressed as a sum of the energies due to convection (q_c), solar radiation (q_s) and the solar irradiation (q_r):

$$q = q_c(x,y,z,t) + q_s(x,y,z,t) + q_r(x,y,z,t) \qquad 6.5$$

The components of Equation (6.5) are expressed through three laws of heat transfer.

The heat loss or gained as a result of convection is explained using Newton's law of cooling:

$$q_c(x,y,z,t) = h_c \cdot [\, T(x,y,z,t) - T_a(t) \,] \qquad 6.6$$

where h_c is the convection coefficient of heat transfer that is a function of velocity, V (m/s), (see Equation (6.33)); T is the temperature of the surface at instant t and T_a is the air temperature at time t.

The solar radiation is explained through a proportionality law of solar radiation:

$$q_s(x,y,z,t) = a \cdot I_h(x,y,z,t) \qquad 6.7$$

where, a is absorptivity of concrete material; I_h is the total incident solar radiation at time t (see Equation (6.24)).

The heat transferred due to thermal solar irradiation is expressed through the Stephan-Boltzmann law:

$$q_r(x,y,z,t) = h_r \cdot [\ T(x,y,z,t) - T_a(t)\ ] \qquad 6.8$$

where h_r is the solar radiation coefficient of heat transfer which is a function of surface temperatures of the dam, expressed as a near-linear form:

$$h_r(x,y,z,t) = e \cdot C_s \cdot \{\ [\ (T+T^*)^2 + (T_a(t) + T^*\ )^2\ ] \cdot\ T + T_a(t) + 2T^*\ \} \qquad 6.9$$

Upstream face

On the upstream face, the boundary condition is defined by the water temperature model developed by Bafong (1997). It is imposed as periodic temperature loading, implying that the upstream temperature is known at all areas on the concrete surface at any time t.

$$T(x,y,z,t) = T_u(x,y,z,t) \qquad 6.10$$

Bafong's (1997) temperature model is discussed in the following sections. In a full dam, the boundary condition is applied entirely in the upstream face whereas in an exposed reservoir, the imposed flux shown in Equation (3.6) is used (Agullo, Aguado and Mirambell, 1996).

6.1.3. Numerical solution to the heat conduction model

The method of solution is based on an explicit finite element method that uses an iteration scheme which simplifies the order of partial derivatives from second order to first order. The solution is computed at the nodes of the domain. The computational solution involves use of element shape functions with a quadratic or cubic order. The solution is conducted in sequential steps; strong form, then weak form.

6.1.4. Idealised temperature contact boundaries of a typical arch dam

Temperature modelling of concrete arch dams requires identification of thermal contact boundaries that influence their mechanical behaviour. This section briefly discusses how the FEM boundary conditions are identified in a typical concrete arch dam that is in operation. The thermal contact boundaries are idealistically presented by the concrete-water boundary, concrete-air boundary, wall-foundation boundary and the foundation boundary. Figure 2.5 show a schematic presentation of idealised temperature contact boundaries through a section of a typical concrete arch dam.

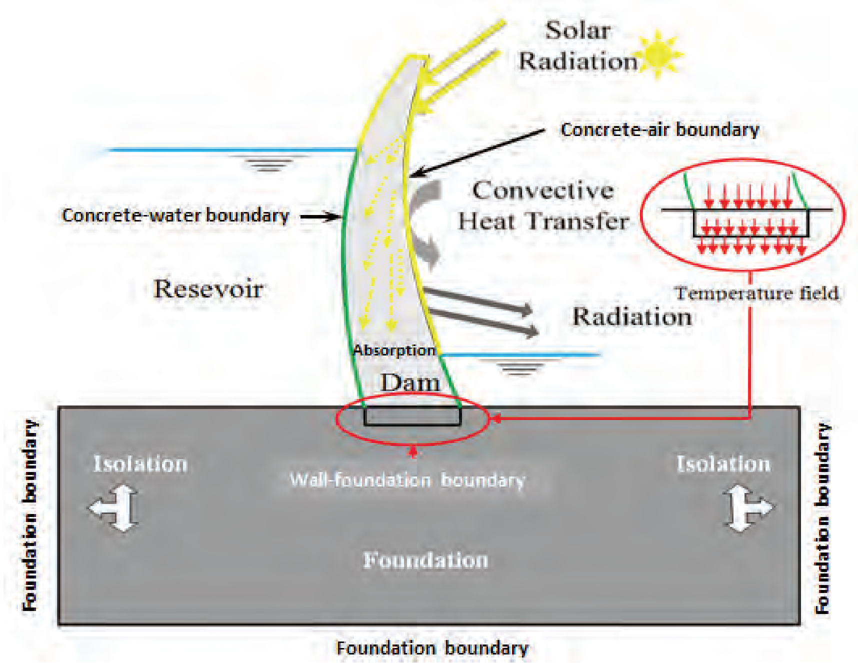

Figure 6.2: Idealised temperature contact boundaries of a typical arch dam in operation.

Concrete-water boundary

This is the contact between the upstream concrete surface and reservoir. The temperature in this boundary can be established with temperature models or experimentally. The former is done using Bafong's (1997) periodic temperature model and the latter by placing thermometers in the upstream surface (Agullo, Aguado, & Mirambell, 1991). In very cold areas the water temperature is considered to be 3℃ because the surface is usually frozen (S. Malla, 1999).

Concreter-air boundary

This is the interface between the concrete surface and the thin fluid medium of surrounding air. This medium causes natural cooling on the structure, which occurs through heat transfer (Bereau of reclamation, 1977). Heat gain and loss varies periodically in the structure, due to change in season. In summer, a large portion of the dam is exposed to sun due to a lowered reservoir level, while in winter the inverse occurs. The geometry of concrete arch dams also contributes to the variation of heat loss and heat gain in this boundary. In regard to the above conditions, the upstream and downstream face experience different temperature field patterns, because of the different shares in temperature fields (Ghaemian & Sheibany, 2006).

Foundation (adiabatic) boundary

Arch dams are hyper-elastic 3D shells with edges restricted by bedrock and the base of the foundation is usually located at large depths into the ground to minimize chances of seepage (Zhang, Liu and Zhou, 2008). This limits the effect of water temperature on the foundation temperature. The foundation boundary, also refereed as the adiabatic boundary, is therefore modelled using earth temperatures which assume zero thermal flux at large depths (Milano and Leonardo da Vinci, 2008). The size of the foundation makes it a thermodynamically isolated system and the thermo-dynamic processes occur without heat gain or heat loss (Ghaemian & Sheibany, 2006). From this, we gather that the foundation temperature has a small influence on the thermo-mechanical behaviour of arch dams, and it can be excluded in the finite element model. If it is modelled, it is defined using constant temperature or variable temperature models. Meri(2011) carried out an investigation on both models and reported that both have negligible effect on the thermal response of the dam at a distance from the wall-foundation interface.

Wall-foundation boundary

Temperature variations in arch dams induce high stresses in the arch wall. These stresses are transferred to the foundation by means of thrust action. Because of the difference in thermo-mechanical properties of both structural components, the wall-foundation boundary is critical to evaluate. Dressler et al. (2003) discovered that the wall-foundation boundary introduces flexibility at the base of the wall and provides addition damping mechanism through material damping and energy radiation. A typical representation of a wall-foundation interface in a finite element dam model is shown in Figure 6.3.

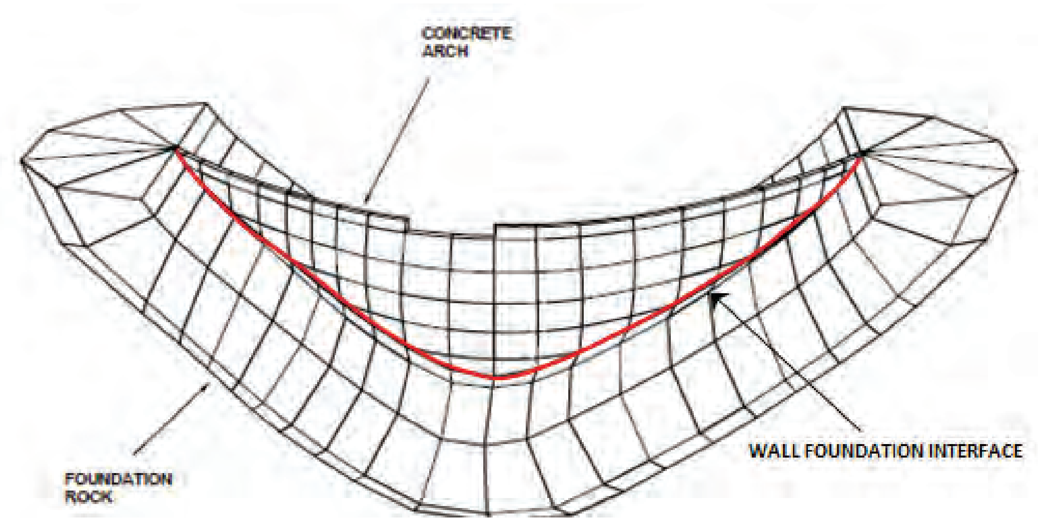

Figure 6.3: Typical finite element dam model, sourced from (Dressler, et al., 2003).

Solar radiation model

Solar radiation refers to the energy transfer by electromagnetic waves with varying wavelengths between the sun and site of concrete dams (Janna, 1986). The concrete surface emits radiant energy but the net heat flow of heat is controlled by the net heat from high to low temperature regions. Solar radiation reaching the earth has 43% attributed to visible light (solar energy), 5% to ultra-violet rays (UV) and 52% to infrared light (EPA, 2008). Figure 6.4: shows a normalised solar radiation intensity graph.

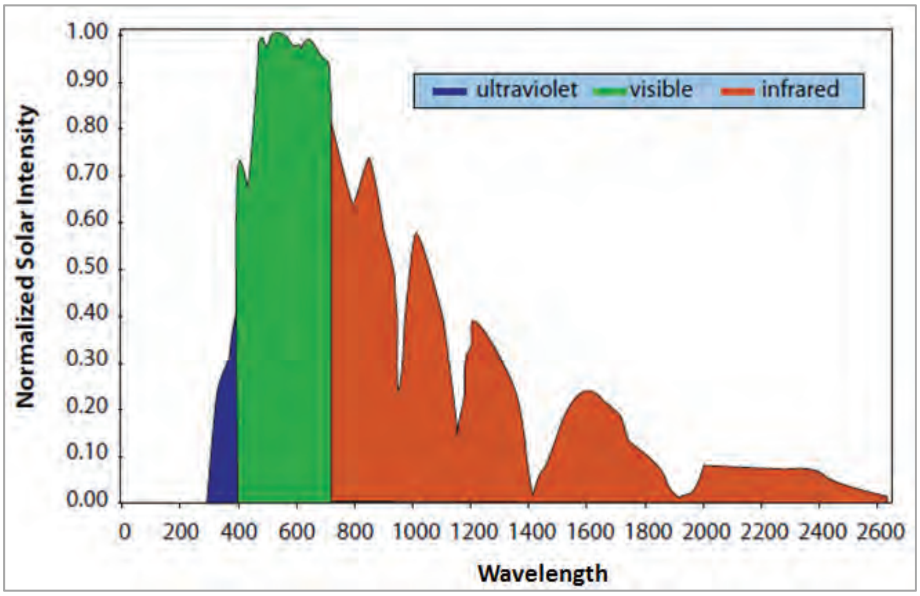

Figure 6.4: Solar energy reaching the earth against wavelength reaching the earth's surface, sourced from (EPA, 2008).

Thermal analysis of concrete arch dams focuses on the solar energy component, because most of it reaches the surface due to its high intensity. It is necessary to note that solar energy is controlled by the opaqueness of the concrete surface. Also, the resultant solar energy is influenced by the radiant properties of concrete namely emissivity, reflectivity, absorptivity and transmissivity. The net action of these properties determines how much heat is gained in the concrete dam.

6.1.5. Radiant properties of concrete

Emissivity

This is the relative ability of exposed surfaces to emit radiant energy. The opacity of concrete arch dams allows absorption and emission of solar energy. The emitted radiant energy is released to the environment.

Reflectivity

Solar reflectance, also referred to as albedo, is a ratio of the reflected solar radiation to the total amount of solar radiation that falls on a particular concrete surface, known as the incident solar radiation. It is measured on a scale from 0, for perfect absorbers, to 1, for perfect reflectors (ACPA, 2002). It prevents high absorption of solar radiation which is converted into heat causing the surface temperatures to become higher than air temperature and infrared radiation to be re-emitted to the environment (Sweeney, West and O'Connor, 2010).

As concrete ages it tends to change its opaqueness to a dark colour because dirt and wear, therefore most older concretes have solar reflectance in the range of 0.20 to 0.30 (ACPA, 2002). Use of white cements and slag cements can influence a concrete’s solar reflectance largely. Concrete that has been exposed to environmental action for a prolonged period of approximately 50 years is classified under aged grey Portland-cement concrete with a solar reflectance of approximately 0.30 (ACPA, 2002). Solar reflectance values for different concrete types are obtainable in Table 6.1.

Table 6.1: Solar reflectance values (albedos) of various cement concrete types, adapted from (ACPA, 2002).

Concrete Surface Type	Solar Reflectance
New grey portland-cement concrete	0.35-0.40
Aged (weathered) grey portland-cement concrete	0.20-0.30
New white portland-cement concrete	0.70-0.80
Aged (weathered) white portland-cement concrete	0.40-0.60

Absorptivity

This property refers to the fraction of incident radiant energy absorbed by the concrete surface (Janna, 1986).

Transmissivity

This property refers to the fraction of incident radiant energy that penetrates through a layer that is close to the surface on the exposed part of a concrete dam.

6.1.6. Variability in radiation and sunshine duration

Solar radiation in concrete arch dams is largely influenced by spatial and temporary variability in global irradiance (direct radiation), diffuse irradiance (diffuse radiation), horizontal direct irradiance (reflected radiation) and sunshine duration (Power and Mills, 2005). Surfaces of irradiance (surfaces on which solar radiation is directed) are the downstream face and often the upstream face, depending on the water level in relation to seasons of the year. The geometry of arch dams plays a role in the amount of irradiance that reaches these surfaces. Usually the angle of incidence of the sun's rays determines this. The variability of these conditions causes a non-linear thermal loading on the global structure. The equivalent solar irradiance in concrete dams is approximated by a summation of global irradiance (H_0), direct irradiance (H_b) and diffuse irradiance (H_d). All three components are approximated using experimental data, or otherwise, through numerical models that incorporate factors for varying dam geometries and site terrain.

Power and Mills (2005) performed experimental work to determine spatial and temporal variability in global, diffuse and horizontal direct irradiance and sunshine duration at eight stations in South Africa and two stations in Namibia for a time series range between 21 and 41 years. Their experimental work also included a study in the Western Cape Province, Cape Town. The total solar irradiance at the investigated locations was associated with the duration of sunshine and cloud cover (Power and Mills, 2005). This considers the fact that high amount of cloud cover leads to a decrease in sunshine duration and gives rise to diffuse irradiance and a decrease in global and direct irradiance. Conversely, less cloud cover would prolong the sunshine duration, thereby giving an increase in global and direct irradiance and a decrease in diffuse irradiance.

6.1.7. Solar radiation model for exposed concrete dams

Measurements of solar irradiance are not always readily available for most dams, especially concrete arch dams. It is necessary to be familiar with solar radiation models for computing irradiance on various kinds of concrete dams. Concrete arch dams have a tilted curved surface and evaluation of irradiance is done through hourly and daily time varying models. It can be estimated from the average daily global radiation using a solar radiation model developed by Liu and Jordan, (1963), also expressed mathematically by Klien (1977). Agullo, Aguado, and Mirambell (1996) also used a similar approach in analysing several arch dams in Spain namely; Baserca, Lauset and Almendra Arch Dams, and Mequinenza Gravity Dam. The model allows evaluation of global irradiance (H_0), direct irradiance (H_b) and diffuse irradiance (H_d) including incident solar rays.

The relation between H_0 and H_d is expressed as follows:

$$H_d = H_0 \cdot \left(1.390 - 4.027\, K_T + 5.531\, {K_T}^2 - 3.108\, {K_T}^3\right) \qquad 6.11$$

Where K_T is the index of the average montly cloudiness defined by the ratio between the daily global solar radiation (H_0) and the monthly average extra-terrestrial solar radiation (H_e) i.e. $K_T = \frac{H_0}{H_e}$

With:

$$H_e = \frac{24}{\pi} r^2 \cdot I_{SC}(cos\delta \cdot cos\varphi \cdot sinh_s + \ h_s \cdot sin\delta \cdot cos\varphi) \qquad 6.12$$

$$r^2 = 1 + 0.003\, cos\left(\frac{360\ Z}{365}\right) \text{ for } 1 \leq Z \leq 365\ days\ (86400\,\text{secs}) \qquad 6.13$$

I_{SC} ($4870.8\ \text{KJ}\,\text{h}^{-1}\text{m}^{-2}$) is the solar constant; δ is the solar declination; φ is the latitude of location; h_s (rads) is the absolute value of hourly angle corresponding to sunset.

In the calculation of the declination δ, a representative day is normally chosen, when the extra-terrestrial radiation is closest to the value of the average daily extra-terrestrial radiation of a given month. In Table 6.2, after Coronas et al. (1982), solar declinations with a corresponding representative day of every month are presented. The declination values are computed using Equation (6.14), by Cooper (1969), also recommended by Liu and Jordan (1963).

$$\delta = 23.5 \sin\left[360\ \left(\frac{284 + \text{n}}{365}\right)\right] \qquad 6.14$$

where $n = \text{jd} - 2451545$, and jd is the Julian Day.

Table 6.2: Middle days and their solar declination for Canada (Agullo, Aguado and Mirambell, 1996)

Month	Middle day	Degrees (°)
January	17	-20.7
February	15	-12.6
March	16	-1.70
April	15	9.80
May	15	18.9
June	10	23.0
July	17	21.2
August	17	13.4
September	16	2.60
October	16	-8.90
November	15	-18.5
December	11	-23.0

The hourly angle (h_s) equivalent to sunset is obtained from:

$$cosh_s = tan\varphi \cdot tan\delta \qquad 6.15$$

The negative value of h_s is the hourly angle that corresponds to sunrise.

With computation of sunset and sunrise hourly angles, the duration of the solar day (TSV) can be determined. This duration is the time between two consecutive passes of the sun over the longitude of the location. The relation between the solar day TSV(hours) and the hourly angle (°) is specified by:

$$h = 15(TSV - 12) \qquad 6.16$$

The beginning (TSV_i) and end (TSV_f) of a solar day as well as the duration (TSV_0), are defined using Equation (6.17)-(6.19), correspondingly.

$$TSV_i = 10 - \frac{1}{15} arc\cos(-tan\varphi \,.\, tan\delta) \qquad 6.17$$

$$TSV_f = 12 + \frac{1}{15} arc\cos(-tan\varphi \,.\, tan\delta) \qquad 6.18$$

$$TSV_0 = \frac{2}{15} arc\cos(-tan\varphi \,.\, tan\delta) \qquad 6.19$$

The above relations depend mainly on the site of the dam (φ) and the day of the year (δ). This allows computation of the interval of solar radiation for a given arch dam. Beyond this interval, the incident solar radiation is taken as zero.

The direct irradiance (H_b) is computed as the difference between the daily global irradiance (H_0) and the diffuse irradiance (H_d) in Equation (6.20), as follows:

$$H_b = H_0 - H_d \tag{6.20}$$

Equation 6.20 can be expressed in hourly radiation corresponding to the interval between sunrise and sunset on site of the dam. This is obtained by factors that are principally dependent on the hour and duration of the day.

$$H_{h,0} = r_t \cdot \; H_0 \tag{6.21}$$

$$H_{h,d} = r_d \cdot \; H_d \tag{6.22}$$

With:

$$r_t(h, h_s) = \frac{\pi}{24} \cdot (a + b \cdot \cos h) \cdot \frac{\cos h - \cos h_s}{sin\; h_s - \; h_s \cdot \cos h_s}$$

$$r_{d)} = \frac{\pi}{24} \cdot \frac{\cos h - \cos h_s}{sin\; h_s - \; h_s \cdot \cos h_s}$$

where $a = 0.4090 + 0.5016 \sin(h_s - 1.047)$ and $b = 0.6609 + 0.4767 \sin(h_s - 1.047)$.

With reference to Equation 6.20, the direct hourly radiation ($H_{h,b}$) can be written as a difference between the hourly global solar radiation ($H_{h,0}$) and the hourly diffuse solar radiation ($H_{h,d}$).

$$H_{h,b} = H_{h,0} - H_{h,d} \tag{6.23}$$

By considering the direct and diffuse component of solar radiation, the incident radiation on the faces of the arch dam (I_h) can be calculated as a sum of the associated hourly direct ($I_{h,b}$), diffuse ($I_{h,d}$) and reflected ($I_{h,r}$) components.

$$I_h = I_{h,b} + I_{h,d} + I_{h,r} \tag{6.24}$$

The direct component of Equation (3.32) is evaluated as follows:

$$I_{h,b} = R_b \cdot H_{h,b} \tag{6.25}$$

With:

$$R_b = \frac{\cos \theta}{\cos \psi}$$

$$\cos \theta = \sin \delta \sin \varphi \cos S - \sin \delta \cos \varphi \sin S \cos \gamma + \cos \delta \cos \varphi \cos h$$
$$+ \cos \delta \sin \varphi \sin S \cos \gamma \cos h + \cos \delta \sin S \sin \gamma \sin h$$

and

$$\cos \psi = \sin \varphi \sin \delta + \cos \varphi \cos \delta \cos h$$

Where, the zenith angle (ψ) depends on the solar declination (δ), latitude (φ) and hourly angle latitude (h); the incident angle of the sunbeam (θ) depends on two more additional parameter to the zenith angle, the inclination on the face of the dam (S) and the azimuth of the surface (γ).

The diffuse component of Equation (6.24) on the surface of the dam is computed as follows:

$$I_{h,d} = \frac{1 + \cos S}{2} \cdot H_{h,d} \qquad 6.26$$

The reflected component of Equation (6.24) on the surface of the dam is computed as a fraction of the global radiation incident on the horizontal plane.

$$I_{h,r} = p \cdot \frac{1 + \cos S}{2} \cdot \left(H_{h,d} + H_{h,b}\right) \qquad 6.27$$

Where p is the average coefficient of reflection from the surroundings of the inclined surface. The reflection coefficients for different surroundings are presented in Table 6.3.

Table 6.3: Reflection coefficient for different types of surroundings on site of a dam.

Type of surrounding	**p(%)**
Recent Snow	80-90
Old Snow	60-70
Cultivated ground	
Without vegetation	10-15
Dry grass	28-32
Lawn and wooded	15-30
Sandy Soil	15-25
Cement, concrete	55
White sand	25-40
Water	
Summer	5
Winter	18

6.1.8. Solar absorptivity model

An operational dam receives a substantial amount of radiant energy in its downstream face. This causes the concrete surface temperature to elevate higher than the air temperature. During the heat transfer process, some energy is absorbed into the dam and some is reflected away. This model identifies the amount of solar energy absorbed by the concrete arch dam, which is given by:

$$q_a = aI \qquad 6.28$$

where a is the solar absorptivity of the concrete surface; I is the total amount daily solar energy reaching the surface, calculated as a sum of the associated daily direct (I_b), diffuse (I_d) and reflected (I_r) component of incident radiation, similarly defined as Equation (6.24). Solar absorptivity is obtained by taking a difference between 1 and the solar reflectance values in Table 6.1.

6.1.9. Solar irradiation model

The surface of a concrete arch dam releases radiant heat, known as thermal radiation, as a result of temperature differences between the surface and the surrounding air. This radiation is measured by the Stefan-Boltzmann law:

$$q_r = eC_s(T^4 - T_a^4) \qquad 6.29$$

Where e represents the emissivity of the concrete surface. It is dependent on the colour of the surface, measured in a range of 0 to 1 for ideal radiators (i.e. black surfaces); C_s is a proportionality constant called the Stefan-Boltzmann constant given as $5.669\, x\, 10^{-8}\, W \cdot m^{-2}$; $T(K)$ is the temperature on Γ_q boundaries; $T_a(K)$ is the ambient temperature.

It should be noted that heat loss by radiation is not expected to be significant within the range of temperature differences between the air and the concrete surface. With this in mind, Equation (6.29) can then be written in a more user friendly form (Leger, Venturelli and Bhattacharjee, 1993).

$$q_r = h_r(T - T_a) \qquad 6.30$$

Where h_r is defined as:

$$h_r = eC_s(T^2 + T_a^2)(T + T_a) \qquad 6.31$$

6.1.10. Convection model

This model describes the exchange of heat by convection as a result of temperature differences between Γ_q boundaries and ambient temperature. The heat lost or gained to the surrounding air is given by Newton's law of cooling:

$$q_c = h_c(T - T_a) \qquad 6.32$$

In which h_c $(W \cdot m^{-2} \cdot K^{-1})$ is the coefficient of convection, also a function of wind speed V $(m \cdot s^{-1})$; T (K) is the temperature on Γ_q boundaries; T_a (K) is the ambient (air) temperature.

The surface temperature of a concrete dam subject to convection heat transfer will normally follow closely the air temperature variation, and the amount of lag between the concrete surface and air temperature is dependent on the coefficient of convection. If for any case, a large convection coefficient is used (e.g. $h_c = 10^m, m \geq 10$), the surface temperature will follow the air temperature exactly (Polivka and Wilson, 1976).

The convection coefficient for heat transfer analysis is treated as an input data with an alternative that it can vary throughout the year. As stated above, it is a function of wind velocity (*V*) and computed using various models. In this study, the formula (Duffie and Beckman (1980) is used, since previous study considers it relatively accurate. The formula is given by:

$$h_c = 3V + 2.8 \qquad 6.33$$

6.1.11. Water temperature model

The concrete-water boundary in the wet upstream face of concrete dams is evaluated using a water temperature model derived by Bafong (1997). It approximates the water temperature for arch dams of varying depths while incorporating seasonal and annual variations of temperature, through monthly averages. This generally means the formulation is a function of depth (y) and time (t). Also, it assumes that the concrete temperature is equal to the water temperature. This assumption is based on the idea of a small difference observed between the concrete temperature variation and water temperature fluctuations at the concrete-water interface (Agullo, Aguado and Mirambell, 1996).

Bafong's (1997) water temperature model is expressed as:

$$T_u(y,t) = T_{um}(y) + A_u(y)\cos\big(\omega(t - t_0 - \xi)\big)\ , \qquad T(y,t) \geq 4℃ \qquad 6.34$$

with:

$$T_{um}(y) = C + (b - C)e^{-\frac{y}{25}} \quad , \ C = \frac{T_b - bg}{1-g}\ , \ g = e^{-\frac{H}{25}}\ , \ A_u(y) = A_0 e^{-0.018y}$$

$$\xi = 65.4 - 39.42e^{-0.085y}\ , \ \omega = \frac{2\pi}{365}$$

where y (m) is the water depth; t (days) is the time; $T_{um}(y)$ is the annual mean temperature of water in the reservoir at depth y; T_b is the bottom water temperature; b is the annual mean temperature at the surface of the reservoir; $A_u(y)$ is the amplitude of annual variation of water temperature; $T_u(y)$ is the water temperature at depth y and time t; t_0 is the day which the ambient air temperature is maximum; A_0 is the amplitude of annual variation of water temperature at the surface of reservoir and H is the depth of reservoir.

6.1.12. Air temperature model

Air temperatures are normally obtained from weather stations located close to site of the dam. In finite element modelling of concrete arch dams, mean annual air temperature models are used to predict the concrete-air boundary temperatures. Agullo, Aguado and Mirambell, (1996) derived a bi-sinusoidal function that models environmental temperature variations during the day. Farrokh and Mohsen, (2006) also used this mathematical model in their finite element analysis of Karaj concrete arch dam in Iran. The model is compatible for concrete arch dams. In gravity dams, the formulation remains the same but evaluation of the constants uses a different approach. The constants are dependent on recorded annual environmental temperature. Accuracy of the model can be improved by a longer time series range of data. Figure 6.5 illustrates the sinusoidal pattern of the formulation. This function is expressed analytically as:

$$T_a = A \cdot \sin\left(2\pi \cdot \frac{t - b_1}{2b_2}\right) + B \qquad 6.35$$

with:

$$A = \frac{T_{max} - T_{min}}{2}, B = \frac{T_{max} + T_{min}}{2}, b_1 = \frac{h_{max} + h_{min}}{2}, b_2 = h_{max} + h_{min}$$

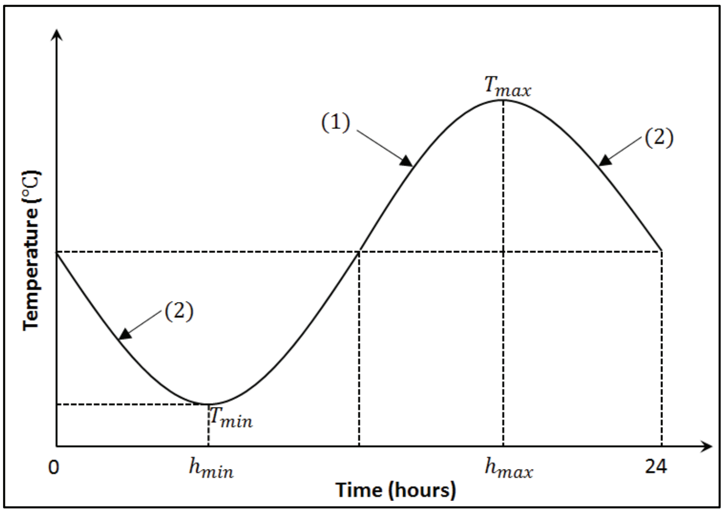

Figure 6.5: Sinusoidal representation of daily average air temperature, sourced from (Agullo, Aguado and Mirambell, 1996)

where T_{max} is the maximum daily temperature and h_{max} is the corresponding time; T_{min} is the minimum daily temperature; and h_{min} is the corresponding time.

6.1.13. Foundation temperature model

The foundation temperature is predicted using periodic variation of the ground temperature with depth. El-Din (1999) developed the foundation temperature model, and based it on the energy balance equation at the ground surface and the assumption that the temperature variation at the ground surface is in the form of a sine-wave or a Fourier series. Solution to his model is in two forms; sine-wave approximation and Fourier series approximation. Both approximations relate sufficient foundation temperatures. Finite element modelling packages are usually more adaptive to the latter form.

Like concrete, we need a heat conduction equation that describes heat flow in the ground. El-Din (1999) considered heat flow to occur in the direction normal to the earth's surface. The one dimensional, unsteady heat conduction equation is expressed as follows:

$$\frac{\partial^2 T_g}{\partial z^2} = \frac{1}{D_{gm}} \frac{\partial T_g}{\partial t} \qquad 6.36$$

Since the ground is assumed to be a semi-infinite homogeneous solid with constant thermal properties, Equation (6.36) can be solved when the boundary condition at surface is known. The boundary condition used is the energy balance equation at the ground surface that is expressed as follows:

$$-k\left(\frac{\partial T_g(z,t)}{\partial z}\right)_{z=0} = h(T_{atm} - T_s) + a_s\overline{H} - e_s\Delta R - LE \qquad 6.37$$

In which k is the ground thermal conductivity; h is the coefficient of convection; T_{atm} is the atmospheric temperature; T_s is the ground surface temperature; a_s is the surface absorptivity of solar radiation; I is the total amount of solar energy reaching the surface; D_{gm} is the ground diffusivity; e_s represents the emissivity of the surface *LE* is the latent heat flux from the ground surface due to evaporation. Penman (1963) developed the expression for LE as:

$$LE = 0.0168fh[B(1-r) - A(rT_{atm} - T_s)] \qquad 6.38$$

In which $A = 103\ Pa\ K^{-1}$ and $B = 609\ Pa$, for ground temperature in a range of $263\ K \leq T_g \leq 303\ K$; *f* is a fraction which depends mainly on the ground cover and on the moisture content of the ground. The *f* values for possible soil types in which dams are sited shown in Table 6.4.

Table 6.4: Fractions of evaporation of the ground for different types of soil.

Type of soil	f
Bare soils	
Saturated	1
Moist	0.6-0.8
Dry	0.4-0.5
Arid	0.1-0.2
Grass covered soils	
Saturated	0.7
Moist	0.4-0.6
Dry	0.3-0.4
Arid	0.05-0.1

Equation (6.37) can be rearranged to the expression below:

$$-k\left(\frac{\partial T_g(z,t)}{\partial z}\right)_{z=0} = h'(T_{se} - T_s) \qquad 6.39$$

In which

$$h' = (1 + 0.0168fA)h \qquad 6.40a$$

$$T_{se} = \left[(1 + 0.0168fA\,r)hT_{atm} + a_s\overline{H} - e_s\Delta R - 0.0168fBh(1-r)\right]/h' \qquad 6.40b$$

T_{se} is called the sol-air evaporation temperature. When $f = 0$, it becomes the well-known sol-air temperature, T_{sa} (i.e. total heat-gain in the ground from air and solar radiation).

As highlighted, the ground temperature approximation considers two forms. In the finite element model of this study the Fourier series approximation for ground temperature is considered. The solution to heat conduction model, Equation (3.44), is then expressed as:

$$T_g(z,t) = T_0 + \sum_{n=1}^{\infty} e^{-za_s\, n^{\frac{1}{2}}}\left[A_n \sin\left(n\omega t - za_s\, n^{\frac{1}{2}}\right) + B_n \cos\left(n\omega t - za_s\, n^{\frac{1}{2}}\right)\right] \quad 6.41$$

In which the coefficients A_n and B_n are given by:

$$A_n = \frac{4}{P}\int_0^P T_g(0,t)\sin(n\omega t)\, dt \quad , \qquad B_n = \frac{4}{P}\int_0^P T_g(0,t)\cos(n\omega t)\, dt$$

Where $\alpha = \left(\frac{\omega}{2D_{gm}}\right)$; $\omega = \frac{2\pi}{P}$, the angular frequency; D_{gm} is the ground diffusivity and P is the period of the cycle.

The sol-air evaporation temperature (Equation (3.48b)) can also be expressed as a Fourier series:

$$T_{se} = T_{se,0} + \sum_{n=1}^{\infty}\left[A_n \cos(n\omega t) + B_n \sin(n\omega t)\right] \quad 6.42$$

Substituting Equations) (3.49) and (3.50) into Equation (3.44) gives the solution to the ground temperature conduction equation:

$$T_g(z,t) = T_{se,0} + \sum_{n=1}^{\infty} U_n e^{-za_s\, n^{\frac{1}{2}}}\cos\left(n\omega t - za_s\, n^{\frac{1}{2}} - \sigma_n - \beta_n\right) \quad 6.43$$

In which U_n, $\sigma_n$and β_n are given by:

$$U_n = C_n\left[\left(1 + \mu\, n^{\frac{1}{2}}\right)^2 + \mu^2\, n\right]^{-\frac{1}{2}} ,C_n = ({A_n}^2 + {B_n}^2)^{\frac{1}{2}} ,\sigma_n = tan^{-1}\left(\frac{a_n}{b_n}\right)$$

$$\beta_n = tan^{-1}\left(\frac{\mu\, n^{\frac{1}{2}}}{1 + \mu\, n^{\frac{1}{2}}}\right)$$

The depth at which the temperature fluctuations are damped is called the damping depth. El-Dim (1988) developed the following mathematical relation for specifying this depth:

$$\left|\frac{T_g(\bar{z},t) - T_0}{T_0}\right| < \delta \quad 6.44$$

where $\bar{z}$ is the damping depth and δ is a small increment ($\delta = 0.001$).

6.2. Summary

Following the review of temperature modelling of concrete dams, it is clear that substantial work has been carried out on the static behaviour of concrete dams under thermal loading. However, there are no technical reports on the effect of thermal loading on the dynamic properties of arch dams.

7. STRUCTURAL HEALTH MONITORING OF ROODE ELSBERG DAM

SHM of Roode Elsberg Dam is in the context of an integrated dam management system in which instrumented health monitoring data is used in conjunction with visual inspections and numerical models, thereby providing a more holistic approach to safety assessment of dams. In this project finite element modelling, ambient vibration testing and static displacement measurements are used to assess the structural performance of Roode Elsberg Dam.

7.1. Description of dam

Roode Elsberg Dam (Figure 7.1) is located on the Sanddrift River about 9 km west of De Doorns and 30 km from Worcester. The dam is the lower of two storage dams constructed on the Sanddrift River (Figure 7.2). The two dams supply irrigation water to the surrounding vineyards. Roode Elsberg Dam is a double curvature concrete arch dam with a centrally located spillway. The dam has a gross capacity of 8.21 million m^3. The height to lowest foundation point is 72m and the length of the crest is 274m. Two galleries have been provided, one following foundation level and a horizontal instrumentation gallery. Figure 7.2 shows a typical cross-section through the dam.

Figure 7.1: Roode Elsberg Dam

Figure 7.2: Location of dam

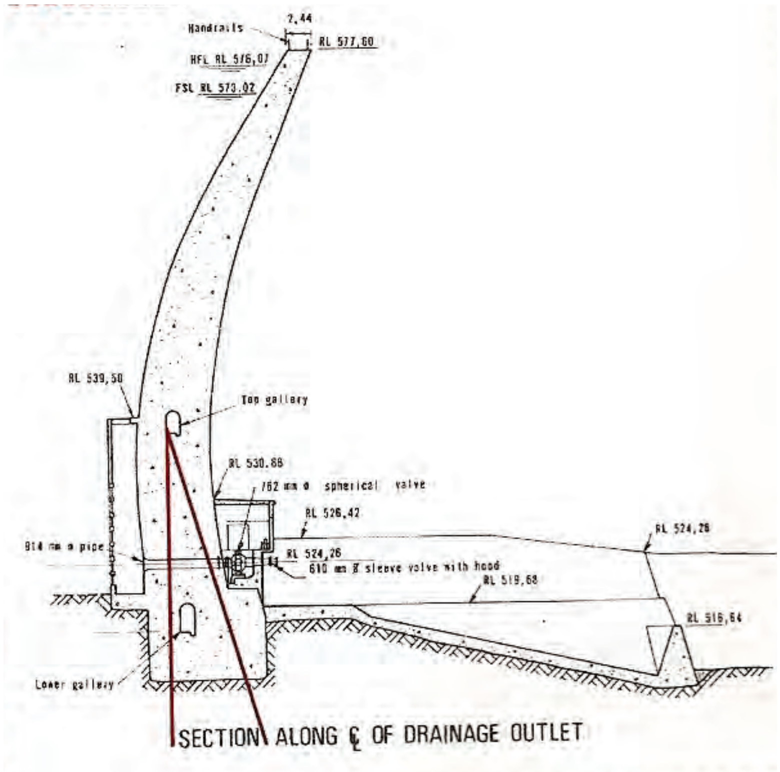

Figure 7.3: Typical cross-section of Roode Elsberg Dam

7.2. Development of the Finite Element Model of Roode Elsberg Dam

The finite element (FE) model of Roode Elsberg Dam was created using Abaqus CAE.

7.2.1. Dam geometry

All the necessary information regarding the geometry of the Roode Elsberg dam's superstructure was extracted from the design drawings 43936 and 43938. Roode Elsberg dam is a one-centred arch dam which means that all the lines of centres of the arches lie on the same reference plane. A local coordinate system was defined in Abaqus, for the arch definition of the dam where the origin was fixed at a point along the line of intersection of the reference plane and the plane that contains the bottom most part of the arch.

As described in the drawings, all the arch units from the crest down to the reduced level of 545.6m are of uniform thickness. This is reflected in that for all levels above 545.6m, the loci for the line of centres of both the extrados and the intrados coincide. The two loci differ for all arch units lower than this level which translates to varying thickness for these arch units. The extent of the arch units on both sides of the reference plane is defined by the subtended angles between the reference plane of the dam and the cushion line at various levels. The subtended angles are measured at different levels along the line of centres of the arch units' meridians. This information was input into Abaqus CAE in the part module to produce the arch as shown in Figure 7.4.

The canyon in which Roode Elsberg dam is built did not allowed for a construction of a symmetric dam hence the inclusion of the pulvino in the dam design and structure. The pulvino was also created in Abaqus. The construction instructions given in the design drawing 43936 were used as guidelines in defining the geometry of the cushion. It was mentioned that from the reduced level of 515.1m to the crest of the dam, the cushion line was to be carried horizontally with the same projection of 3.05m until meeting the solid rock line.

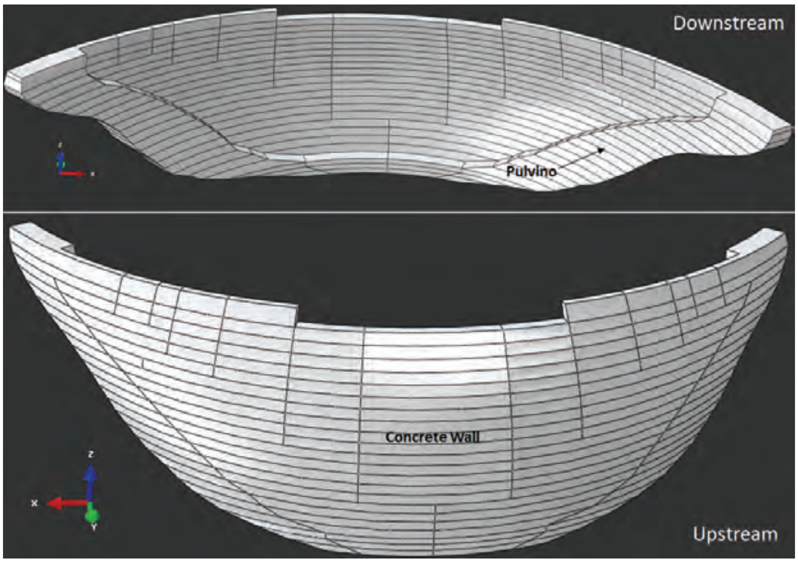

Figure 7.4: The dam arch as drawn according to the design drawings

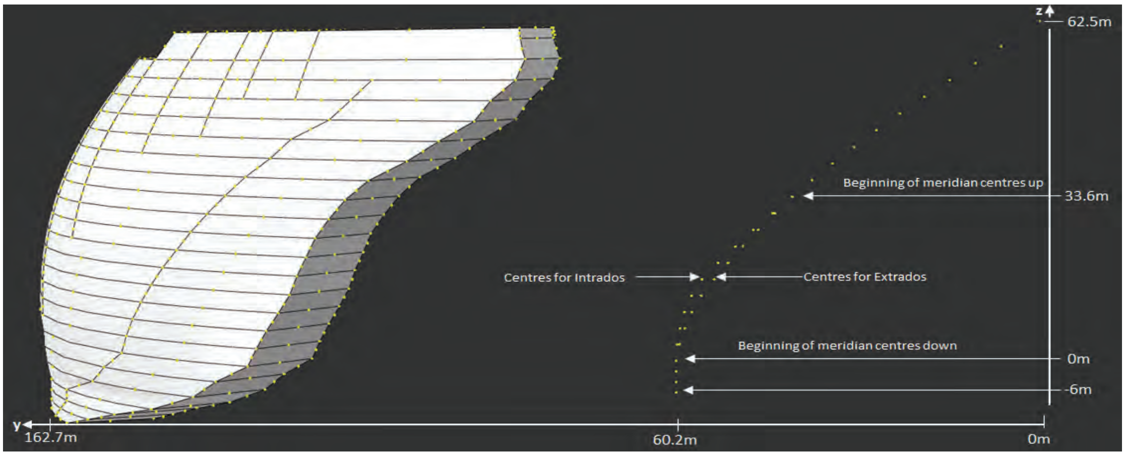

Figure 7.5: The profile of the position of centres of the meridian, intrados and extrados.

7.2.2. Foundation geometry

The geometry of the foundation was based on the guidelines provided by the Arch Dam Design Manual (1994) which mentions that for a ratio of the foundation's deformation modulus to the dam's elastic modulus of about 1, the minimum radius of the semi-circular foundation can be chosen to be equivalent to the dam wall height as a starting point to a parametric study in which the foundation size is increased until such increase has no effect on the static stresses, natural frequencies and mode shapes of the system. The rectangular foundation of depth equal to the dam height was chosen as the starting point in the validation of the Roode Elsberg arch dam model.

The foundation, the cushion and the arch were created as different parts in Abaqus. All these components of the solid arch dam system could have still been created as one part in Abaqus but for the convenience of greater flexibility and ease in future analysis and executions, they were instead created as three different parts. For example, in order to enable the foundation size to be changed with ease and further enable manageable meshing of the foundation, it is better to have the foundation as a distinct part from the rest of the dam components. If however the components had been created as one part in Abaqus, they would have had to be separated by partitions.

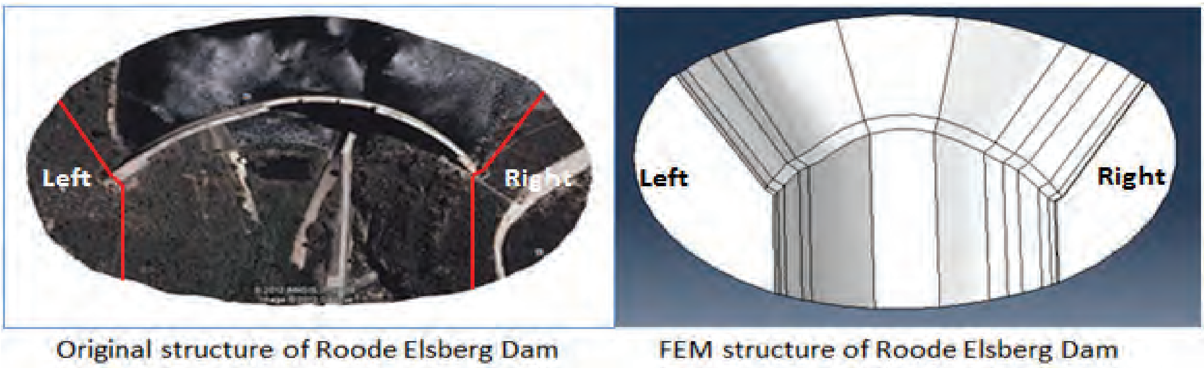

Figure 7.6: The initial foundation model of the Roode Elsberg dam, upstream view. The different rock type foundations as proposed by O'Connor (1985) are also shown.

7.2.3. Element Types

With regard to element type selection, firstly the choice of the elements' shape to be used is made in the mesh controls command. A choice of hexahedral elements was made for both the solid foundation and pulvino parts and the dam-wall arch was meshed with a hexahedral dominated mesh with some wedge elements.

Secondly, there was the choice of the order of the elements to be used in the modelling. The degrees of freedom such as displacements, rotations and temperature are calculated on the nodes in Finite Element analysis procedures. At any other point in the element, the degrees of freedom are calculated by interpolating from the nodes. Usually, the interpolating order is determined by the number of nodes in an element (Dassault Systems Simulia Corp., 2010).

The wall system was meshed using double layered C3D20RT elements with an approximate global size of 6.7. Figure 7.7 shows a geometrical representation of the nodes used for meshing the wall system. The wall system was meshed with 1612 elements consisting of 9203 nodes. Because of the foundation complexity, C3D10MT elements were used. These elements helped in reducing the calculation time and memory consumption. The foundation system was meshed with 34196 elements consisting of 51315 nodes.

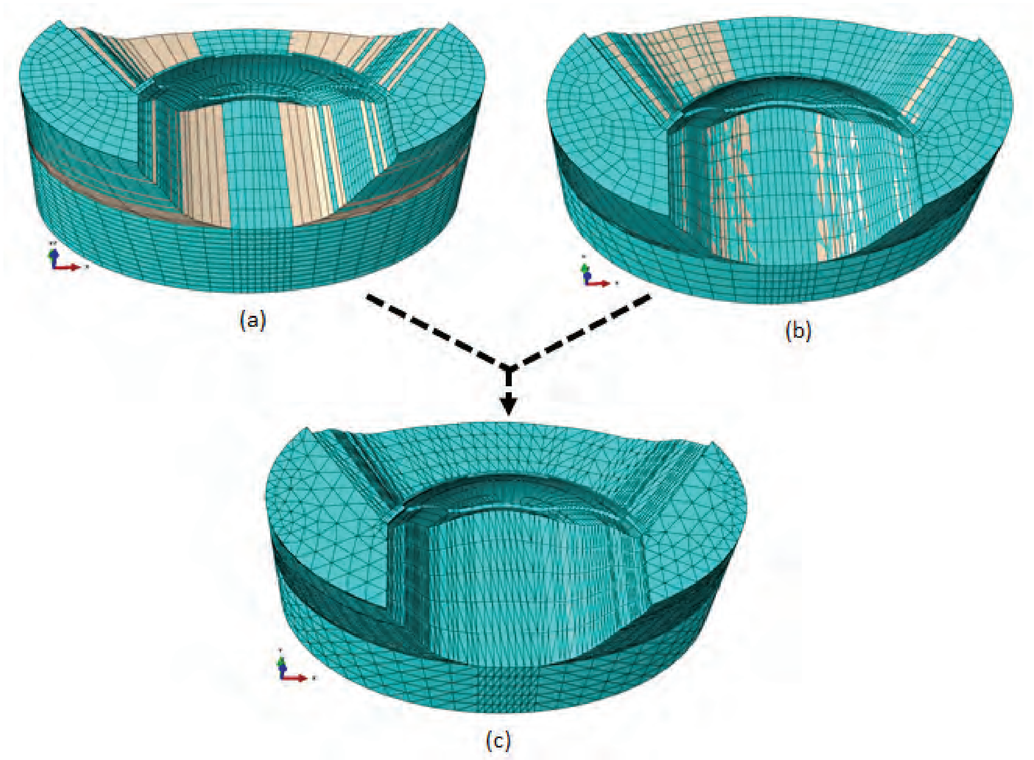

Figure 7.7: Mesh optimisation for finite element dam model; (a) Only C3D20RT elements with single-layered wall elements, (b) only C3D20RT elements with double-layered wall elements and, (c) C3D20RT double-layered element (wall system) and C3D10MT elements (foundation system).

7.2.4. Material properties

The Dam Wall concrete

For the initial stages of the analysis, linear behaviour, isotropy and homogeneity were assumed for the dam wall concrete. With these material behaviours assumed, only a few material properties for the dam concrete had to be estimated and input into Abaqus' Property module for the initial analysis. These are the sustained dynamic modulus of elasticity, the dynamic Poisson's ratio and the unit weight of the concrete. In order to estimate the current dynamic modulus of the dam concrete, first the 28 day static elastic modulus had to be estimated.

The static elastic modulus of concrete was determined from the correlation between concrete's 28 day mean strength and the static elastic modulus mentioned in Fulton's Concrete Technology (2009). The type of aggregate in the concrete was used as the variable which determines the concrete elastic modulus in the correlation graphs. It was therefore essential that a good assumption is made of which aggregate was used in the Roode Elsberg dam concrete. It was deduced that the local table mountain quartzitic could have been used as it was readily available. The working drawings indicated that the desired 28 day strength of the dam wall concrete was 29MPa, for which the correlation was done in the correlation graphs to give a 28 day static elastic modulus of 31GPa. An extract, from working drawings, of the design data for the Roode Elsberg, is shown in Table 7.1.

Table 7.1: Extract from the design drawings of Roode Elsberg Dam.

Property and Symbol	SI Units	Concrete Wall	Rock foundation		
			Left	Bedrock	Right
Mechanical properties					
Thermal expansion, α	$1/\mathrm{K} \times 10^{-6}$	12	8.05	8.05	8.05
Modulus of elasticity, E	$\mathrm{Pa} \times 10^{9}$	31.0	25.0	25.0	23.0 /20.0
Density	$\mathrm{kg/m^3}$	2400	2500	2500	2500
Poisson's ratio		0.22	0.25	0.25	0.25

There is however a difference between a 28 day static elastic modulus and a long term sustained static elastic modulus. The latter includes the effects of creep. According to the effective modulus creep theory; the sustained static elastic modulus is lower than the 28 day static elastic modulus. Fulton (2009) was referred to in this case for the guidelines on how to convert the 28 days static elastic modulus to the sustained static elastic modulus and then to the dynamic modulus. The relevant equations used to account for creep and dynamic behaviour are given as equation 7.1 and equation 7.2 respectively where E_c is the 28 day static elastic modulus, E'_c is the sustained static elastic modulus, E_d is the dynamic modulus and φ is the creep factor. A creep factor of 0.35 was chosen as advised in the Engineering guidelines for the evaluation of hydropower projects (1999). Using these equations, a dynamic modulus of 40GP was selected.

$$\boldsymbol{E'_C = \frac{E_c}{1+\varphi}} \qquad 7.1$$

$$E'_C = 1.25E_d - 19 \quad 7.2$$

The choice of the first trial of the Poisson's ratio for the concrete to be used in the analysis was based on the guidelines provided in the Arch Dam Design Manual (1994), which states that for dynamic analysis of arch dams a Poisson's ratio of 0.22 can be assumed. The density of 2400 kg/m^3 for the dam wall was used in this study as it was previously assumed in the design of the dam. That is according to the extract from the design drawings in Table 7.1.

The foundation material

In the early stages of the analysis, the foundation was assumed to obey linear behaviour. From the design data in Table 7.1, it can be observed that the foundation rock is of Table Mountain quartzitic sandstone type. According to Alexander & Mindess (2001), samples of this type of sandstone can have a modulus of elasticity with a wide range of values with a mean of about 60GPa. On being reduced to the afore-mentioned deformation modulus, in order to account for the faults and joints in the massive foundation rock, this value can be expected to be a lot lower than 60GPa.

According to the jacking tests done on the foundation rock (O'Connor, 1985), the foundation rock on the left abutment clearly has very different elastic deformation properties from the right abutment. It is however not very clear exactly where the boundary that separates the softer rock from the harder one can be described. O'Connor (1985) decided on the boundary as shown in Figure 7.7. Rock 1 had a deformation modulus of 29.5GPa in the two perpendicular horizontal directions and 6.9GPa in the vertical direction while Rock 2 had a deformation modulus of 2.3GPa in the perpendicular horizontal directions and 3.1GPa in the vertical direction.

7.3. Theoretical frequency extraction

7.3.1. Application of the Westergaard Method

Initially, it was decided that the added mass was to be added on the wetted upstream nodes of the orphan meshes as nodal point mass.

If only the original Westergaard method is applied, the magnitude of each nodal point mass depends on the water depth, height of the node above the base and the tributary area assigned to that particular node. Several models will be used, each for a certain water level in the dam and the Westergaard added masses will be the difference between all these models.

The application of the original Westergaard method using the point mass approach in Abaqus is only possible through the use of the orphan mesh. However, the use of an orphan mesh would in future make the combined analysis of both thermal and ambient dynamic behaviour very difficult. This is because, partitioning, which is a very indispensable tool for such an analysis, is limited in orphan meshes.

It was hence decided that an application which introduces the added mass as a change in density of the structure will instead be applied. Over the area on which the added mass will be applied, there is likely to be a change of the parameter that is used to calculate the added mass e.g. the height. This calls for the use of the integration mathematical technique or a use of a parameter that can be considered representative for the whole area, e.g. the average height instead of integrating from one height to the other.

If however integration is used, it is advisable that the dam wall is partitioned. Once partitions are made then each added mass can be added on its respective partition. It has to be ensured that in each partition any of the parameters that is used to calculate the added mass does not vary very much otherwise complicated integration might need to be done. The dam wall was hence partitioned as shown in Figure 7.8. Note that all the cell partitions have at least one horizontal partition to facilitate easy application of the added mass which varies with height.

The conversion of nodal masses into masses that are applied on the surface was carried out by dividing the nodal masses into either four or two depending on the position of a node. For the nodes at the dam wall edge and those that are at a water level, their nodal masses would be divided by two, while elsewhere the nodal masses would be divided by four to be distributed to the adjacent surfaces.

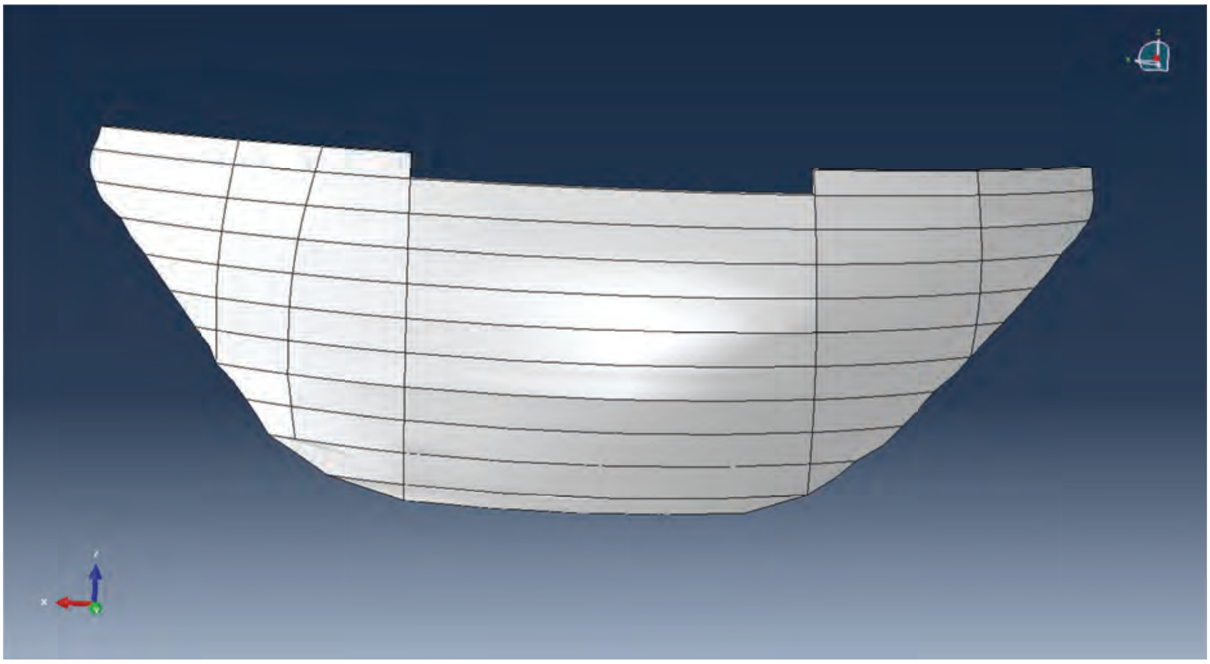

Figure 7.8: The dam wall part with its cell partitions.

7.3.2. Natural frequencies extraction

Subspace iteration method

A small set of base vectors is created, thus defining a subspace. This subspace is then transformed, by iteration and Ritz analysis, into the space containing the lowest few eigenvectors of the overall system. The advantage of the subspace method is that the extraction of the eigenvalues is in a reduced space, resulting in rapid convergence to the eigenvectors in full space (Dassault Systems Simulia Corp., 2010).

However, the choice of starting vectors is also important because if these are chosen such that they span the space of the eigenvectors as completely as possible, rapid convergence can be achieved. The number of base vectors carried in the iterations is also of importance since if more vectors are used, the number of required iterations is reduced, but each iteration takes longer. The default value used in Abaqus has been found to effective and optimum (Bathe, 1996).

Lanczos iteration method

Theoretically, the basic steps of the Lanczos method transform the generalized eigenproblem in equation 7.3 into a standard form with a tri-diagonal coefficient matrix. The applied transformation for every Lanczos run is stated in equation 7.4.

$$[\boldsymbol{K}]\{\boldsymbol{\Phi}\} = \omega^2[\boldsymbol{M}^*]\{\boldsymbol{\Phi}\} \tag{7.3}$$

$$[\boldsymbol{M}^*]([\boldsymbol{K}] - \sigma[\boldsymbol{M}^*])^{-\mathbf{1}}[\boldsymbol{M}^*]\{\boldsymbol{\Phi}\} = \theta[\boldsymbol{M}^*]\{\boldsymbol{\Phi}\} \tag{7.4}$$

M*and ***K*** are the structure's mass and stiffness matrices respectively. If, however the fluid-structure interaction is considered using the added mass concept, then ***M**** represents both the mass of the structure and the added water mass. ω is the undamped natural frequency of the structure and $\boldsymbol{\Phi}$ is the corresponding mode shape. σ is the shift, θ is the eigenvalue of the transformed equation and these two variables are related to ω by equation 7.5. This transformation allows rapid convergence to the desired eigenvalues. The same eigenvectors apply to equation 5.3 as in the transformed problem in equation 7.4.

$$\omega^2 = \frac{1}{\theta} + \sigma \tag{7.5}$$

The Lanczos method is generally faster when a large number of eigenmodes is required for a system with many degrees of freedom and account for initial stresses in the structure. (Dassault Systems Simulia Corp., 2010). Hence it was chosen for the analysis of Roode Elsberg Dam.

7.3.3. Pre-calibration Results

Table 7.1 shows the first six natural frequencies of the dam obtained using the geometric and material properties described above.

Table 7.1: First six natural frequencies for a full dam.

Mode Number	FEM (Hz)
Mode 1	2.32
Mode 2	2.59
Mode 3	3.71
Mode 4	4.37
Mode 5	5.39
Mode 6	5.70

The results of the analytical frequency extraction set the scene for comparing measured dynamic properties and theoretical values and hence start of the model calibration process.

7.4. Ambient vibration testing

Ambient vibration measurements on Roode Elsberg Dam have been periodically carried out as part of this project since April 2010. Some of the results will be presented for the purpose of illustrating modelling calibration. Three dimensional measurements (vertical, radial and tangential directions) were carried out at the crest level of the dam locations 2-9 (Figure 7.9). Each position represents the centre of a block.

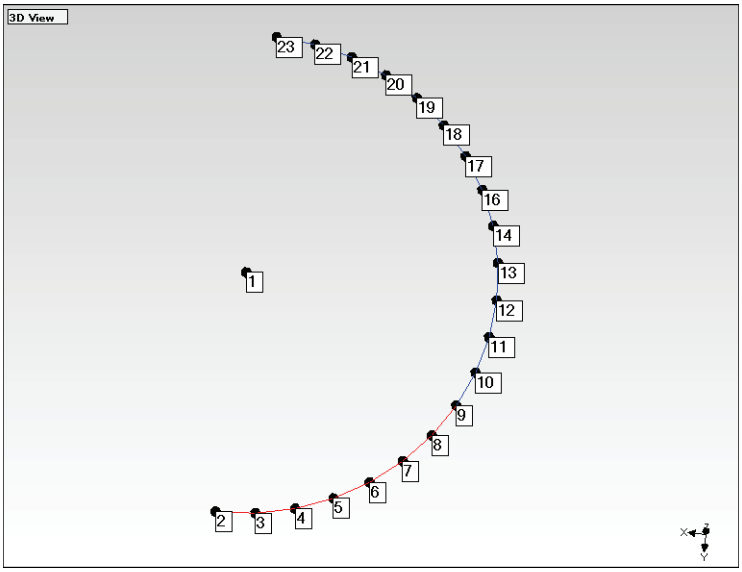

Figure 7.9: Measurement locations: Roode Elsberg Dam

7.4.1. Instrumentation used

Roving force balance accelerometers with a resolution down to 1µg and intrinsic noise of 7 µg (0-10 Hz) and 70 µg (10-500 Hz) and a set of three seismic piezoelectric accelerometers were used as reference (Figure 7.10). The force balance accelerometers have a nominal sensitivity of 6V/g while the piezoelectric accelerometers have a nominal sensitivity of 1V/g. Data acquisition was via the National Instruments 8 channel dynamic signal analyser (NI PCI 4472B). All 8 inputs are simultaneously sampled with a 24bit resolution at 1000 Hz. Power supply was provided by a portable generator.

Figure 7.10: Typical measurement set-up at Roode Elsberg Dam.

Figure 7.11 shows a typical time history measured on the dam crest. Output-only frequency response functions were obtained using MEScope software ® through the frequency domain rational polynomial function. Figure 7.12 shows the typical frequency response spectrum of Roode Elsberg Dam approximately 20% full. The first dominant frequency is about 3.50 Hz. Figure 7.13 also shows the typical frequency response function of Roode Elsberg Dam approximately 30% full. The first dominant frequency occurs at 3.37 Hz indicating that the natural frequency of the dam decreased with increasing water volume. Clearly, there is a general decrease of the natural frequency with decrease in water level. The first sixteen measured natural frequencies of the dam are given in Table 7.2. The largest changes in frequency occur in the first seven modes. Thus it is reasonable to use these frequencies as reference natural frequencies for long term measurements. Note however that mode 4 remained almost unchanged. Nine modes are clustered between 9 Hz and 12 Hz. Although changes in this range are observable, it would be quite easy to misinterpret the observed changes.

Mode shapes of Roode Elsberg Dam could not be extracted due to inaccessibility of spillway portion of the dam.

Table 7.2: Roode Elsberg dam natural frequencies

Mode number	April 2010	Dec 2010	% change
1	3.50	3.37	3.71
2	3.97	3.65	8.06
3	4.84	4.74	2.07
4	6.06	6.03	0.50
5	7.68	7.49	2.47
6	8.62	8.29	3.83
7	9.31	9.14	1.83
8	9.79	9.75	0.41
9	9.97	9.97	0.00
10	10.23	10.2	0.29
11	10.53	10.53	0.00
12	10.82	10.82	0.00
13	11.19	11.16	0.27
14	11.42	11.39	0.26
15	11.83	11.83	0.00
16	12.51	12.44	0.56

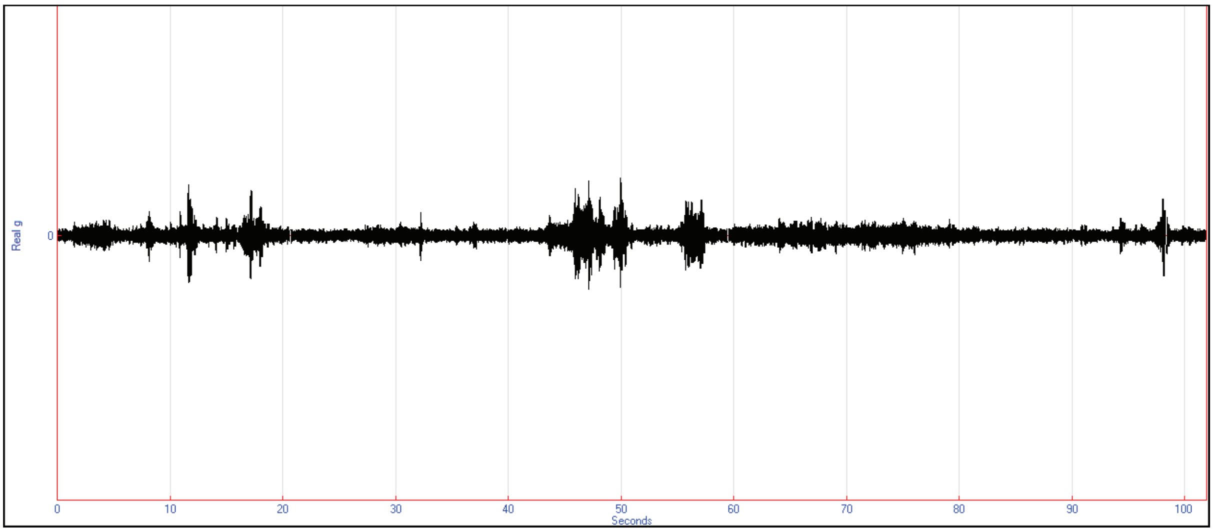

Figure 7.11: Typical time history

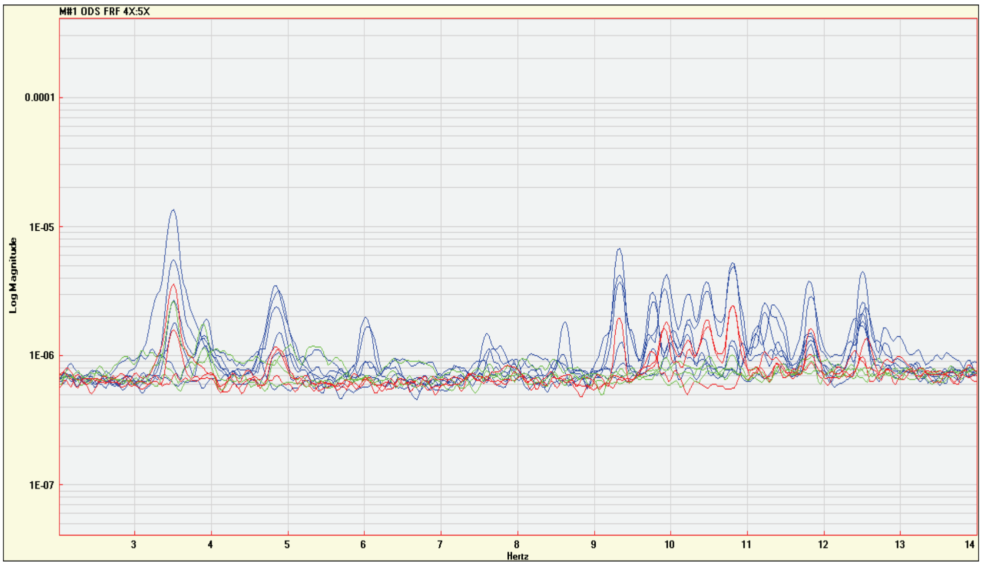

Figure 7.12: Roode Elsberg Dam Frequency Response Function: 20% full

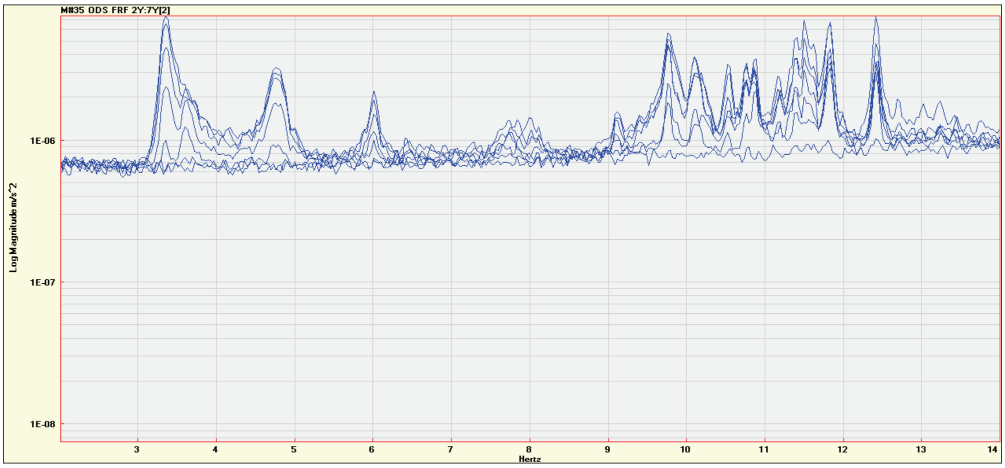

Figure 7.13: Roode Elsberg Dam Frequency Response Function: 30% full

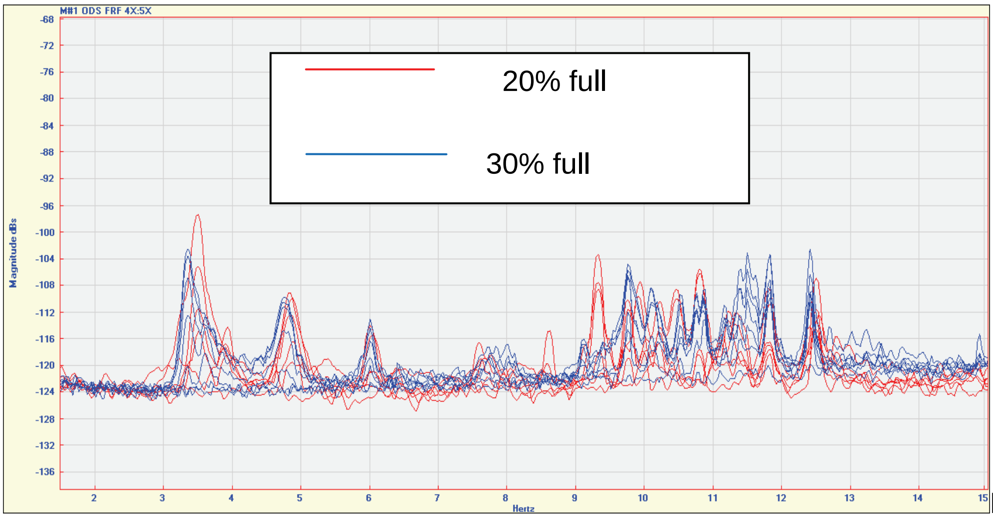

Figure 7.14: Roode Elsberg Dam Frequency Response Function: Overlaid

7.5. Temperature modelling

7.5.1. Thermal and mechanical properties of Roode Elsberg Dam

The concrete properties were extracted from the design data provided by the Department of Water Affairs. The foundation data was extracted from geological sources of the area near Worcester. The material properties include specific heat c, thermal conductivity k, convection coefficient h, coefficient of thermal expansion α, modulus of elasticity E, density ρ, poisson's ratio ν, solar absorptivity a, and emissivity e. Table 7.3 presents a summary of these properties.

Table 7.3: Thermal material properties for the concrete wall and rock foundation.

Property and Symbol	SI Units	Concrete Wall	Rock foundation		
			Left	Bedrock	Right
Thermal properties					
Specific heat, c	$\mathrm{J/(kg\,.\,K)}$	912	840	840	840
Thermal conductivity, k	$\mathrm{W/(m\,K)}$	2.00	2.2	2.2	2.2
Convection coefficient, h		23.2	n/a	n/a	n/a
Emissivity, e		0.88	n/a	n/a	n/a
Solar absorptivity, a		0.65	n/a	n/a	n/a

7.5.2. Application of thermal boundary conditions

Concrete-air interface

This is the boundary between the concrete surface heat conditions and the surrounding ambient temperature. The thermal gradients on the concrete surface result from solar radiation. The exchange of heat conditions between the concrete surface and the surrounding environment occurs through three heat transfer mechanisms; conduction, convection, and radiation. Heat transfer laws are applied when defining boundary conditions and they use the thermal material constants discussed in section 6.1.

Air temperatures

The air temperature data used in this study was acquired from temperature records gathered by the South African Weather Services (SAWS) for Worcester, Western Cape. The data is recorded daily covering a design period of 15 years (i.e. from 1955 to 2010). The daily temperatures were averaged for minimum and maximum values for each month of a particular year. A design template capturing all this information was generated and presented as illustrated in Figure 7.15. The air temperature was applied using approximate Fourier series coefficients and an annual circular frequency, in the field module of ABAQUS.

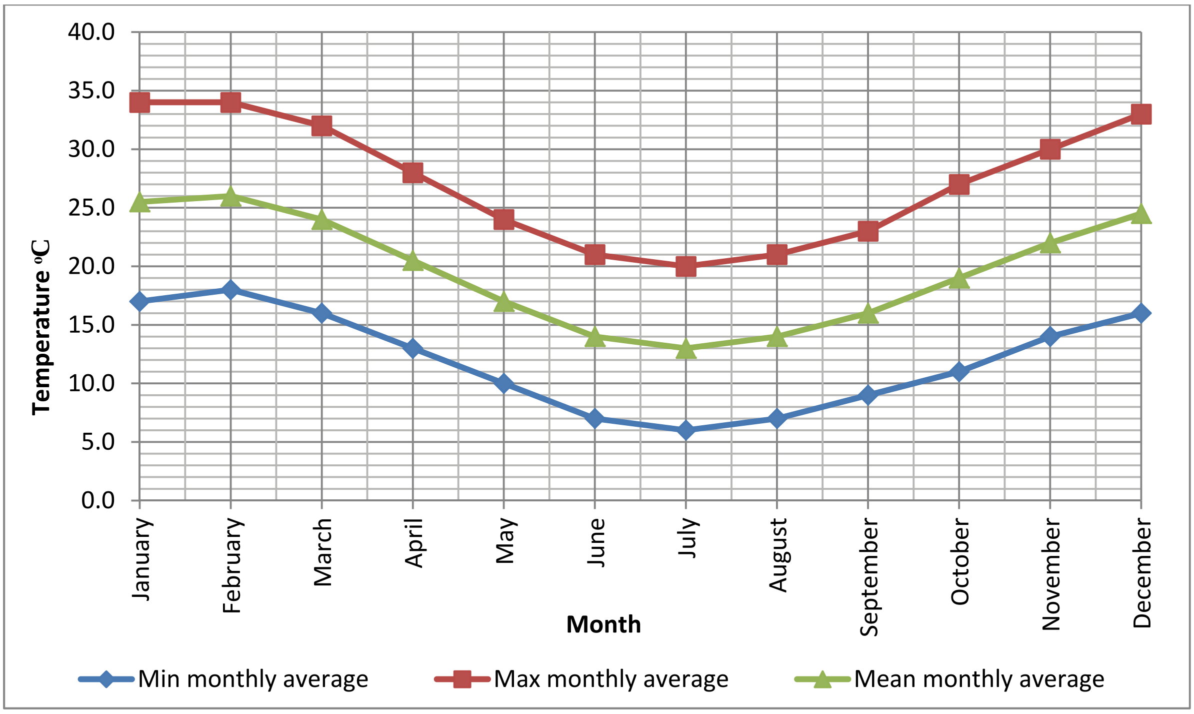

Figure 7.15: Average maximum/minimum monthly temperature data for Worcester, Western Cape, SA.

This boundary condition was also modelled using the amount of wind interacting with the concrete surface at Worcester, Western Cape. The equation proposed by Duffie and Beckman (1980) was used to account for wind speed conditions.

$$h_c = 3V + 2.8 \tag{7.6}$$

An average annual wind speed of $V = 4\, m/s$ was used for calculating the heat transfer coefficient ($h_c = 14.8\ \mathrm{W.m^{-2}\ K^{-1}}$).

Concrete-radiation interface

Incident solar radiation was chosen based on orientation and geometry of the Roode Elsberg Dam. Solar radiation acting in the downstream face varies in intensity due the curvature of the dam and trajectory of the sun. Three incident solar radiation components were calculate to take account of the different energy intensities. The first radiation component was classified as the extra shaded part that receives low energy. The second radiation component was classified as partly shaded that receives medium energy while the third component received total radiation as the sun moved from the east to the west. A representation of the different solar radiation intensities is shown in Figure 7.16.

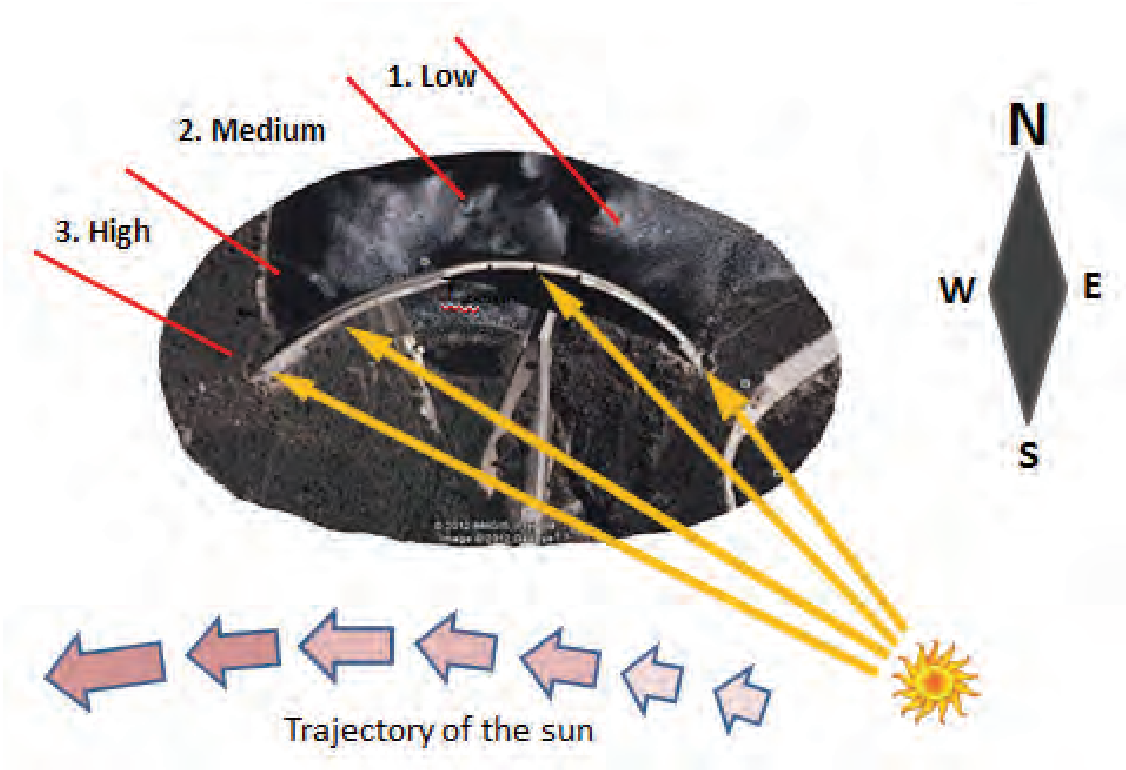

Figure 7.16: Incident solar radiation on the concrete surface.

The total solar energy (I) reaching the concrete surface was approximated through a summation of direct (I_b), diffuse (I_d) and reflected (I_r) components of solar radiation that were obtained by Power and Mills (2005) for the Cape Town area.

Concrete-water boundary

This is the contact between the upstream concrete surface and reservoir. The temperature in this boundary can be established with temperature models or experimentally. In this study the model proposed by Bafong (1997) is used.

$$T_w(y_w, t) = T_m(y) + A_u(y)\cos\omega(t - t_o - \xi) \qquad 7.7$$

t is time in days; y_w is the water depth; T_m is the annual mean temperature of water obtained as $T_m = c_o + (b - c_o)e^{-0.04y_w}$;$c_o = \frac{T_b - bg}{1-g}$;$g = e^{-0.004H}$, T_b is the water temperature at the bottom; b is the annual mean water temperature at the surface of the reservoir; H is the depth of the reservoir; $A_u y_w$ is the amplitude of annual variation of water temperature given by:

$A_u(y_w) = A_o e^{-0.018y_w}$, where A_o is the amplitude of annual variation of water temperature at the surface of the reservoir; t_o is the time of maximum air temperature; ξ is the phase difference between the maximum temperatures of water and air.

Three cases that were investigated are as follows:

1. Full reservoir

The upstream face was assumed to be entirely covered by water. This was associated with the wettest season of the year, winter. In the static thermal analysis of a chosen typical year, a day with the lowest concrete and air temperature conditions was selected to compute static stresses, displacements, dynamic frequencies and mode shapes.

2. Half-full reservoir

The upstream face was assumed half-full in the upstream face. Half the dam was exposed to air temperature and solar radiation. This level was assumed to be associated with medium temperature conditions of a typical year of analysis, spring season. The same procedure of analysis as explained for the first case applies here.

3. Quarter-full reservoir

The upstream face was assumed quarter-full in the upstream face. A three quarter area of the dam was exposed to air temperature and solar radiation. This level was assumed to be associated with maximum temperature conditions of a typical year of analysis, summer season. The same procedure of analysis as explained for the first case applies here.

Convergence of heat transfer analysis

A convergence analysis was first performed in the model to determine a time step where complete steady-state convergence was attained within the dam body. Figure 7.17 shows the time histories of mean annual air temperature and mean annual concrete temperature. The mean concrete temperature was evaluated at three sections in the dam body (top, middle and bottom section) using a representative node in each section. The time histories were obtained by implementing an un-scaled steady-state step followed by a 4 year transient-state step with day increments. Convergence was obtained in the second year of analyses. The critical thermal states for concrete were then read off shown in Figure 7.17. For obtaining a good approximation of average temperature in the concrete wall, convergence was estimated at 2.5 years. A typical year for seasonal temperature variation was consequently selected between 2.5 and 3.5 years of the complete time history. Table 7.4 shows the selected days for the chosen typical year scaled over 1460 days of transient analyses.

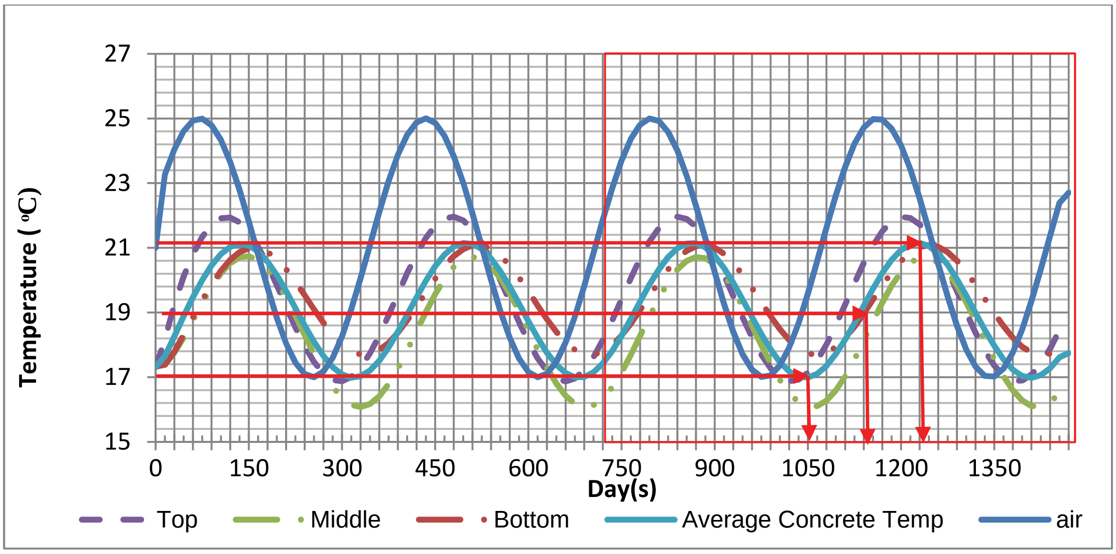

Figure 7.17: Convergence of mathematical solution.

Table 7.4: Critical temperature states for structural analysis on Roode Elsberg dam.

Reservoir level	End increments for critical temperatures over a 4 years period		
	Minimum (days)	Median (days)	Maximum (days)
Full dam	1050	1140	1230
Half-full dam	1050	1140	1230
Quarter-full dam	1035	1125	1215

7.5.3. Transient temperature response of dam

A 365 daily thermal distribution was chosen after the year of convergence for the heat transfer analysis, to represent a typical yearly response of the dam body. This yearly response includes the maximum, average and minimum temperature states that are responsible for computation of critical thermal stresses and displacements. The yearly end increments for temperature are shown in Table 7.5 for three water levels considered. These were selected from the yearly transient temperature response. Such a typical response is shown in Figure 7.18, which illustrates the mean air temperature and average thermal response for a half-full dam evaluated through temperatures for the top, middle and bottom sections of the concrete wall. The top, middle and bottom sections for evaluation of this response are relatively in phase. The air temperature has a time lag of 35 ± 10 days in relation to the average concrete temperature for the investigated water levels. This time lag is a result of thermal inertia, which is described by the time taken for the dam to attain average concrete temperature from which the air temperature is occurring.

Table 7.5: Annual average concrete temperatures for the three investigated water levels.

Reservoir level	Temperatures at critical temperature end increments		
	Minimum (°C)	Median (°C)	Maximum (°C)
Full dam	17.0	19.0	21.0
Half-full dam	17.5	20.0	22.0
Quarter-full dam	18.0	20.5	23.0

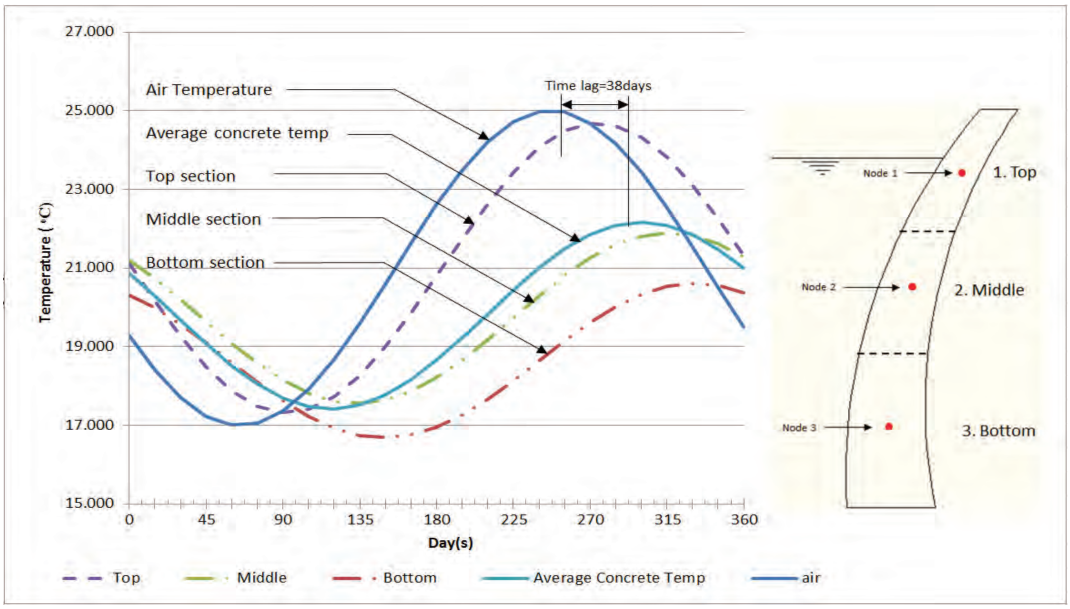

Figure 7.18: Yearly average thermal response of a half-full dam.

7.6. Finite element model calibration

7.6.1. Added mass calibration

The added mass was estimated using the generalised Westergaard method which allows added mass to be applied to curved dam walls. Table 5.1 is a comparison of measured natural frequencies and calculated natural frequencies for the case when the dam was full. There is a significant difference between the measured values and theoretical values. Assuming that the geometry of the wall and the geometry of the foundation are within acceptable error bounds the difference between measured values and the generalised Westergaard method results from inaccurate estimation of the added mass.

Table 7.6: Comparisons between the analytical frequencies found using the Original Westergaard method with field ambient testing for a full dam.

Mode Number	FEM with Original Westergaard Masses Results	Ambient Vibration Testing Results	Percentage Error
Mode 1	2.32	3.07	24
Mode 2	2.59	3.59	28
Mode 3	3.71	4.11	10
Mode 4	4.37	4.49	3
Mode 5	5.39	5.64	4
Mode 6	5.70	6.41	11

A closer look at the site layout of Roode Elsberg Dam shows that the reservoir is not symmetrical with the dam wall (Figure 7.19). Thus adjustments should be made to the Westergaard method to account for the effects of lack of symmetry between water body and the dam wall. Clearly this lack of symmetry would affect the estimation of the parameter 'b' in equation 2.5. Kuo (1982) noted that dams of diverging reservoir walls experience less dynamic pressures than the same sized prismatic dams under same ambient conditions. The effects of asymmetric and diverging reservoir are likely to be even more significant for Roode Elsberg dam due to a presence of a kink just upstream of the dam wall which noticeably divides the water body into two parts.

Figure 7.19: An aerial photograph of Roode Elsberg Dam (Courtesy of Google maps, 2005).

Kou (1982) proposed the curves shown in Figure 7.20 for estimating the pressure on the dam wall and thus added for dams with diverging reservoirs. θ is the angle between the line of symmetry of the dam and the line passing through the reservoir. The angle θ is close to 40^o for Roode Elsberg Dam. Based on Figure 7.20, the added mass estimated following assumption of symmetry, should be reduced by more than 50%. It was hence decided that the added mass be scaled by a factor using a trial-and-error until a good correlation was found between the analytical and the experimental results. The results of the trial and error are summarised in Figure 7.21.

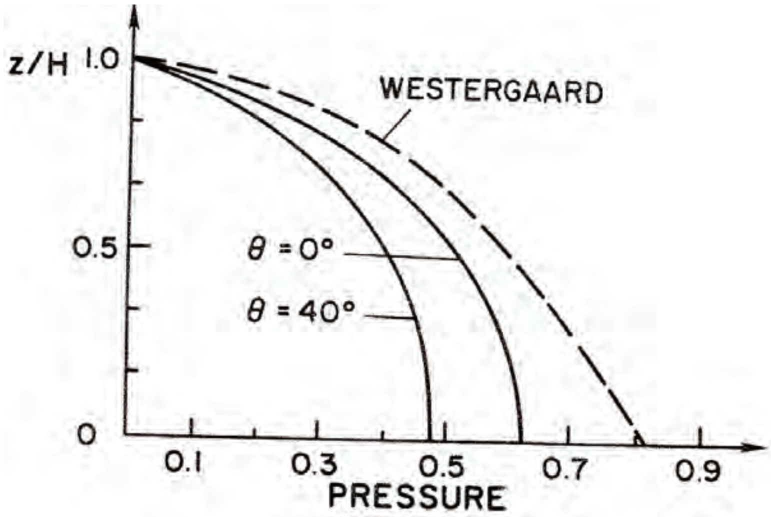

Figure 7.20: Pressure distributions at crown section of a cylindrical dam, showing the finite element fluid results compared to the Westergaard added mass ones. The reservoir wall diverging angle was varied from 0° to 40° for

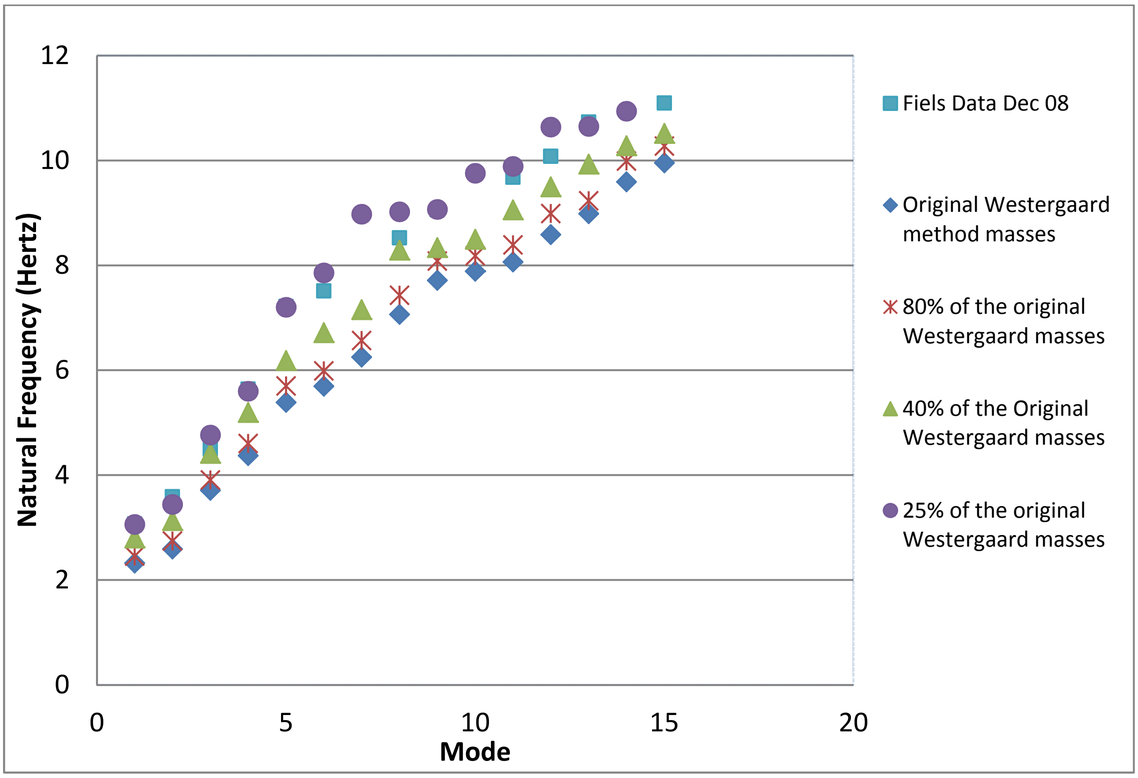

Figure 7.21: Comparisons of the natural frequencies when the different percentages of the Original Westergaard masses are applied.

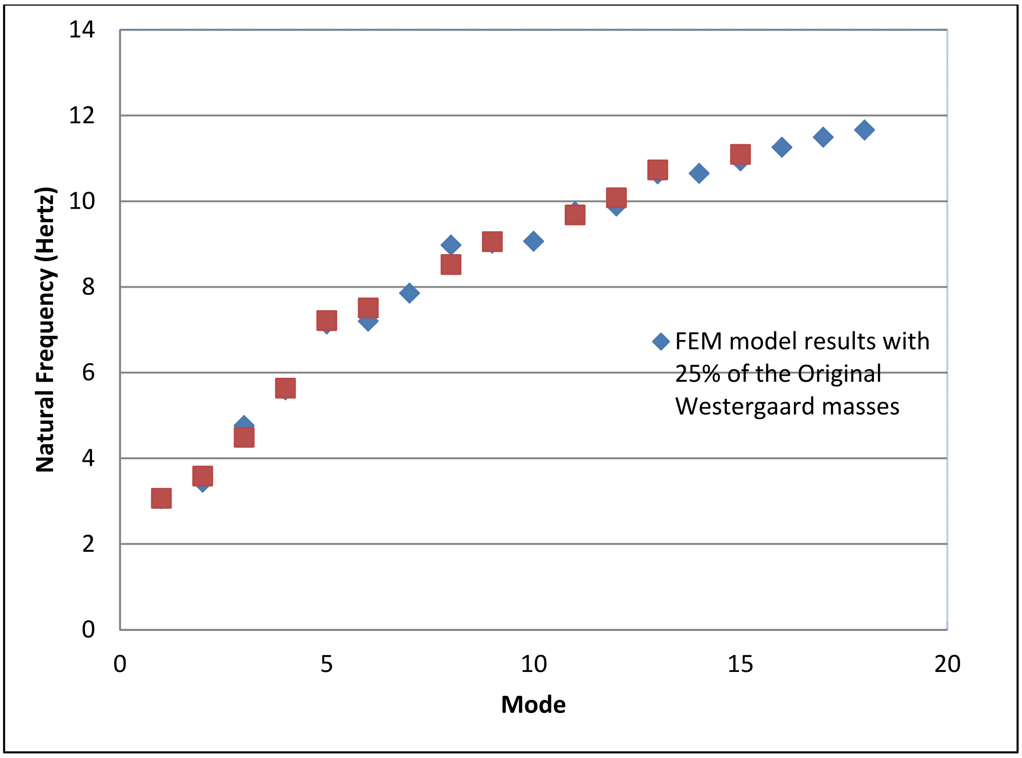

Figure 7.22: Comparisons of the natural frequencies when the different percentages of the Original Westergaard masses are applied.

The best match between the measured values and the theoretical values occurs when the original Westergaard masses for a full dam model are factored by a factor 0.25 (Figure 7.21 and Figure 7.22). This model was taken as the calibrated model, with added mass approximately 25% of the mass estimated assuming that the reservoir is not divergent. This calibrated model was used to investigate the variation of natural frequencies with the water level. The expected behaviour of the natural frequencies which increase with decreasing water level up to a certain water level is observable. The comparison of measured natural frequencies at lower water levels shows that while the variation of natural frequency is for both cases, there is a slight difference between calculated and measured values indicating the influence of other parameters such as temperature on measured natural frequency.

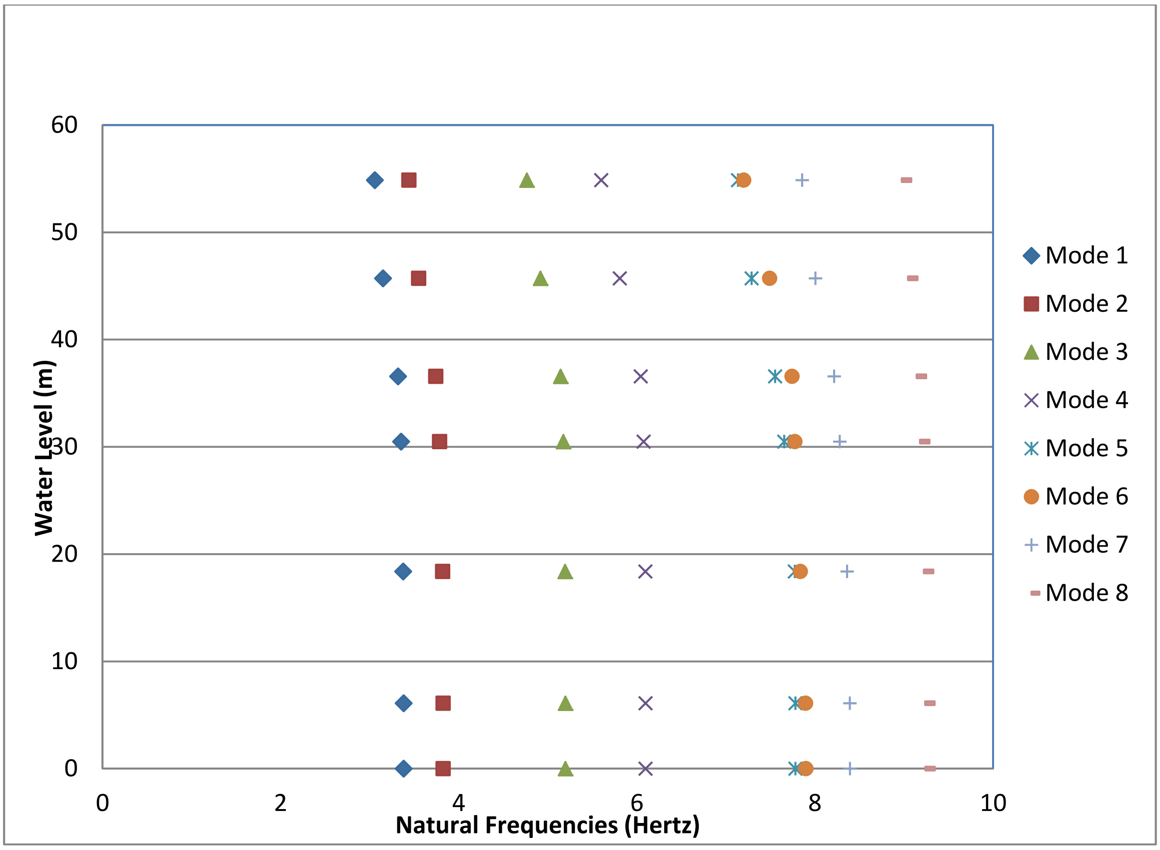

Figure 7.23: Variations of the natural frequencies with water level in the dam model of Roode Elsberg Dam.

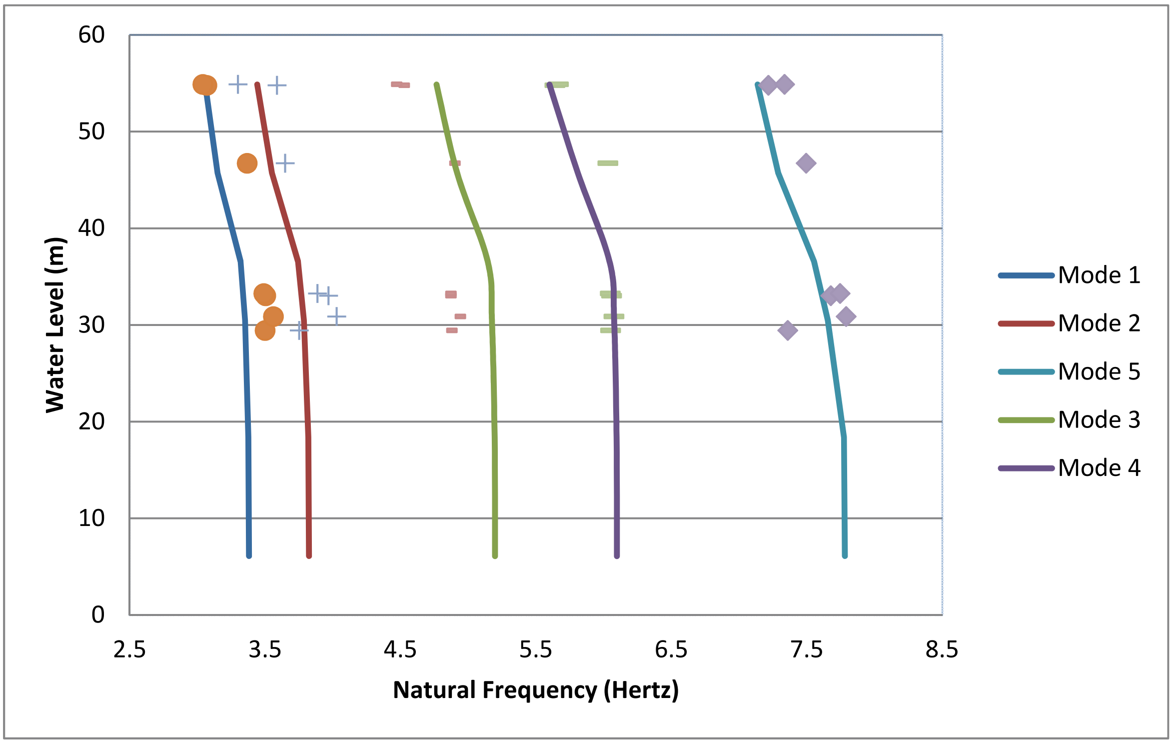

Figure 7.24: Variations of the natural frequencies with water level of Roode Elsberg Dam.

7.6.2. Effect of seasonal temperature on the dynamic characteristics

Natural frequencies for temperature analysis

Using the design information captured from the drawings of Roode Elsberg Dam including relevant modelling theory, the dynamic concrete modulus was estimated at $40\,GPa$ and the foundation properties remained as specified in Table 7.3. The first eighteen modes were considered in checking the effect of seasonal temperature variation on the dynamic properties on arch dams, notably Roode Elsberg Dam. This objective was reported for a non-loaded dam, and three cases of a thermally loaded dam namely full, half-full and quarter-full reservoir.

Table 7.7: Comparison of FE natural frequencies for the investigated reservoir levels.

Mode Number	FEM frequencies for no loading	FEM frequencies for full reservoir	FEM frequencies for half-full reservoir	FEM frequencies for quarter-full reservoir
Mode 1	3.4962	3.5208	3.5206	3.5205
Mode 2	3.6819	3.9405	3.9407	3.9409
Mode 3	3.9491	5.2444	5.2443	5.2443
Mode 4	5.2020	6.2515	6.2504	6.2505
Mode 5	5.2281	7.8023	7.8022	7.8023
Mode 6	5.9629	7.8806	7.8797	7.8799
Mode 7	6.3174	8.0456	8.0458	8.0457
Mode 8	6.4928	8.2488	8.2489	8.2489
Mode 9	6.8223	8.5026	8.5026	8.5026
Mode 10	6.9812	8.7091	8.7091	8.7091
Mode 11	7.6245	8.8819	8.8819	8.8819
Mode 12	7.9475	9.1768	9.1766	9.1767
Mode 13	8.0494	9.3214	9.3213	9.3213
Mode 14	8.5266	9.9215	9.9216	9.9216
Mode 15	8.6801	9.9395	9.9392	9.9392
Mode 16	8.7765	10.0999	10.0999	10.0999
Mode 17	9.0979	10.4519	10.4517	10.4518
Mode 18	9.2691	10.5780	10.5780	10.5780

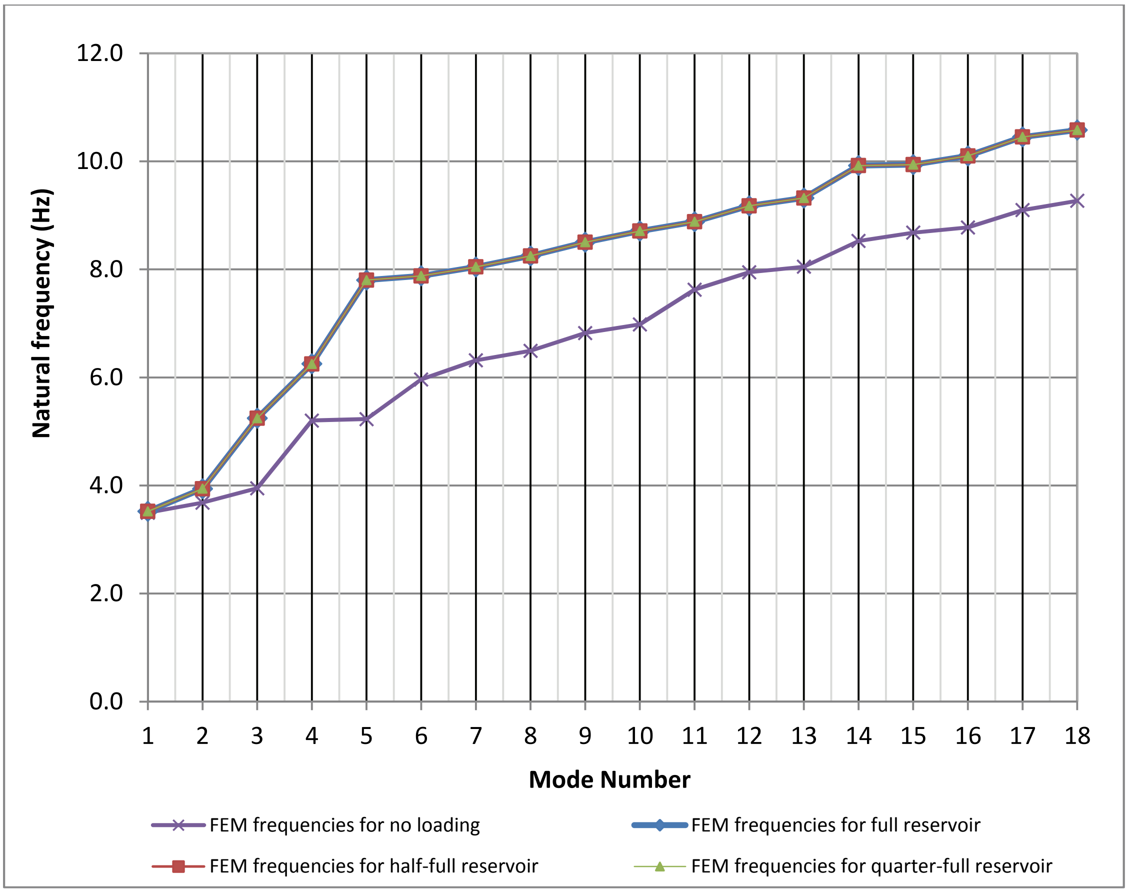

Figure 7.25: Graphical presentation of variation of dynamic properties with seasonal temperature variation.

In Table 7.7, the natural frequencies were presented to the nearest fourth decimal place because low sensitivity was observed with seasonal temperature variation. Change in the natural frequencies was only observed to the third and fourth decimal. However it was observed that dynamic properties of arch dams are affected by temperature loading. In Figure 7.25, significant difference in natural frequencies from modes 2 to 18 is observed for the non-loaded and thermally loaded dam.

Since seasonal temperature variation showed little effect on the natural frequencies, the first six FEM natural frequencies were chosen for a quarter-full reservoir and compared with results obtained though ambient vibration testing (AVT). The AVT natural frequencies were obtained in December 2010 for Roode Elsberg at 20% full. Assuming that the dam was almost empty and entirely exposed to air and solar radiation, the AVT results would therefore be slightly similar to the FEM results. Table 7.8 show a close correlation in the natural frequencies. From this assessment we confirm that the finite element model generates sufficient natural frequencies for temperature analysis.

Table 7.8: Comparison between AVT and FEM natural frequencies.

Mode Number	AVT Frequencies for 20% Full dam in December 2010	FEM frequencies for quarter-full reservoir	Error (%)
Mode 1	3.50	3.52	1
Mode 2	3.97	3.94	-1
Mode 3	4.84	5.24	8
Mode 4	6.06	6.25	3
Mode 5	7.68	7.80	2
Mode 6	8.62	7.88	-9

Following thermal analysis of Roode Elsberg Dam the following observations were made;

The dynamic behaviour of the dam is significantly different between the unstressed and stressed condition. However, there is practically no impact on the dam's natural frequencies due to seasonal temperature variations. Thus it can be concluded that while temperature variations do not seem to impact the natural frequencies of Roode Elsberg Dam, it is critical to perform a thermal analysis before any dynamic analysis

7.6.3. Validation of finite element model through static displacement data

The finite element model had to be initially validated for static analysis due to solar radiation, air, water and foundation temperatures. This was done by a comparison of FEM displacements produced by the combined action of thermal and hydrostatic loads, with empirical data obtained over the period of operation of the dam. The base date for the finite element model was chosen for the dam at full reservoir level, which corresponds to the winter season. It was chosen in similar respect as the base date for Roode Elsberg Dam (i.e. the winter season).

The validation process involved two processes; (i) investigating the effect of foundation stiffness properties on static analysis, which was mainly for interpolating for foundation stiffness properties that would produce minimal variation in the difference in crest displacement (Δu) produced by the full and quarter-full reservoir and, (ii) using the model with appropriated model stiffness to compare its displacement data with experimental data as means of completing the validation process of the model for static analysis.

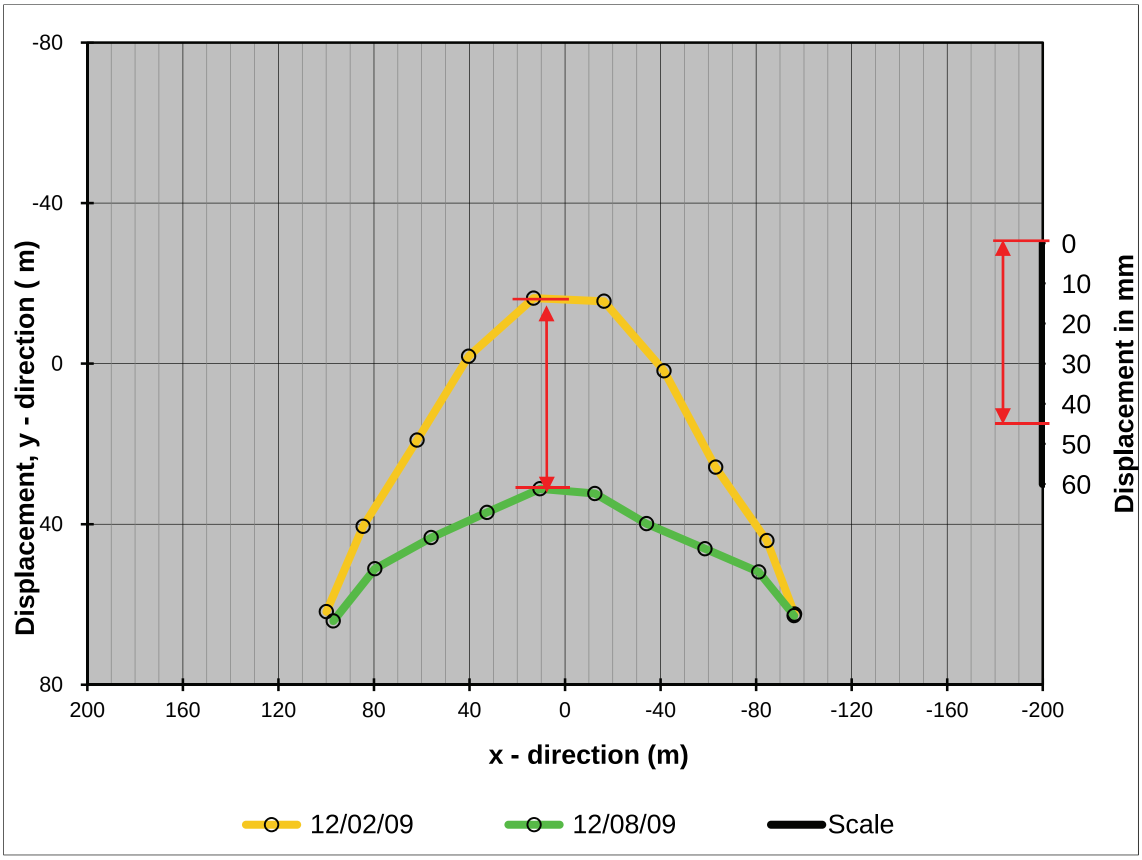

Figure 7.26: Crest displacement for Roode Elsberg dam, obtained from the Department of Water Affairs, recorded 12-02-2009 (summer) and 12-08-2009 (winter).

In Figure 7.26, the difference in the empirical crest displacement (Δu_{exp}) for the extreme water level conditions, notably full (i.e. in winter) and quarter-full (i.e. in summer), is approximately 46 mm.

7.6.4. Effect of foundation stiffness properties on static behaviour

A full field investigation to provide an extensive definition of the variation of modulus of the deformation is costly and may not be necessary (FERC, 1999). Foundation field investigations for modelling can be done using parameter sensitivity studies that account for any uncertainties in assumed foundation properties for a dam. Two types of foundations are considered in the parameter sensitivity studies namely soft ($E_f/E_c < 1$) and hard foundation ($E_f/E_c > 1$), where E_f is an effective modulus of deformation for the foundation and E_c is modulus of elasticity of the mass concrete. Eight cases of foundation moduli were studied and reported for their respective crest displacements of full and quarter-full dam under thermal and hydrostatic loading. The elasticity modulus of the concrete material was taken $E_c = 31GPa$ since of displacements arch dam form a component of static analysis. The criterion of this investigation was obtaining a foundation modulus that would yield minimal sensitivity in the difference in crest displacements (Δu_{FEM}) of the assessed water levels. Table 7.9 shows the investigated cases of the foundation, where case 4 represents the assumed modelling foundation modulus of Roode Elsberg Dam (see Table 7.3).

Table 7.9: Foundation moduli considered in the validation of the model for static analysis.

Studied cases	Foundation description	Foundation modulus, Ef(GPa)	Ef/Ec (Ec=31 GPa)	Δ Displacement (mm) Quarter-Full
Case 1	soft	6	0.2	41.0
Case 2	soft	15	0.5	38.5
Case 3	soft	20	0.6	37.8
Case 4	soft	23	0.7	37.8
Case 5	soft	25	0.8	37.8
Case 6	hard	31	1.0	37.8
Case 7	hard	40	1.3	37.7
Case 8	hard	46.5	1.5	37.7

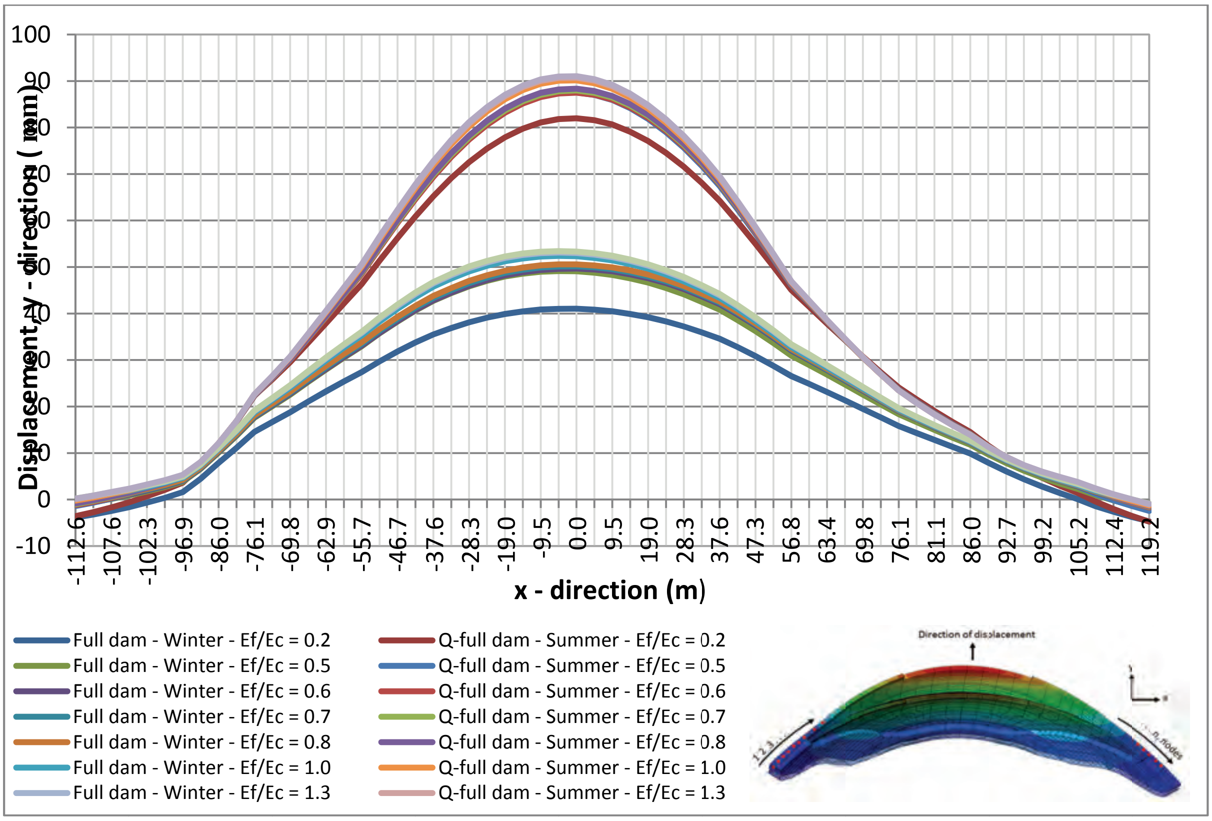

Figure 7.27: Crest thermal and hydrostatic displacements for varying foundation modulus of concrete arch dams.

In Figure 7.27, it is noted that the crest displacements are very sensitive to variation in foundation modulus. However, low sensitivity is observed in the difference in crest displacement with change in foundation modulus. More upstream displacements are observed for a hard foundation modulus as compared to soft foundation. U.S. Army Corps of Engineers (1994); FERC (1999) also highlight similar observations on the displacement with change in foundation modulus. The appropriate choice of foundation modulus was chosen by considering a foundation scenario that produced substantial upstream deflections but minimal sensitivity in the delta displacement. In Table 7.9, cases 3-6 proved to satisfy this criterion. Subsequently, case 4 was verified as a suitable foundation modulus for the finite element model. The finite element model for Roode Elsberg dam could not be further refined to give crest displacements (Δu_{FEM}) that match with experimental crest displacements ($\Delta u_{exp} = 46\ \mathrm{mm}$). The finite element model was deemed capable of predicting sufficient static response of the dam using the assumed foundation modulus in Table 7.10 (i.e. case 4).

7.7. Static temperature and stress analyses

The static analysis comprises the temperature distribution, thermal stress distribution and thermal displacements for the three reservoir conditions namely full dam, half-full dam and quarter full dam.

Here focus is mainly on the temperature and stresses observed over a typical year as highlighted in the preceding sections. Table 7.11 shows representative days associated with the critical average concrete temperatures experienced by the dam over the selected year of analysis. The full dam is associated with winter conditions (minimum day temperatures), because of high rainfall during that period. The half-full dam is associated with spring conditions (medium day temperature) while the quarter-full dam analysis is associated with summer conditions (maximum day temperature). The winter season is assumed as one with the winter season. Table 7.10 is a modified version of Table 7.4 scaled over 365 days of transient state analyses.

Table 7.10: Annual critical temperature states for evaluation of critical thermal stresses.

Reservoir level	Yearly critical temperature field		
	Minimum (days)	Median (days)	Maximum (days)
Full dam	120	210	300
Half-full dam	120	210	300
Quarter-full dam	105	195	285

The upstream and downstream surface temperatures will appear as constants even though they are modelled as periodic boundary conditions. The internal temperature profile follows certain behaviour depending on the water level being investigated.

Because most concern is drawn on the upstream face, the water temperature is expected to decrease with depth. The modelling strategy correlates with the theoretical interpretation of this for all the studied water levels. The nodes of analyses are then chosen longitudinally on the upstream face. To accommodate the layers that are near this surface, the single upstream longitudinal elements are considered. Each element comprises three transverse nodes that are at the upstream surface (A_i), at quarter distance from the upstream surface (B_i) and at half distance from the upstream surface (C_i). This selection of nodes assumes that the upstream thermal cracks cannot propagate all the way to reach the middle section or else the dam would have failed by then. Figure 7.28 shows the type of node selection chosen for this study. All three types of longitudinal nodes are read from the dam-foundation interface to the spillway level.

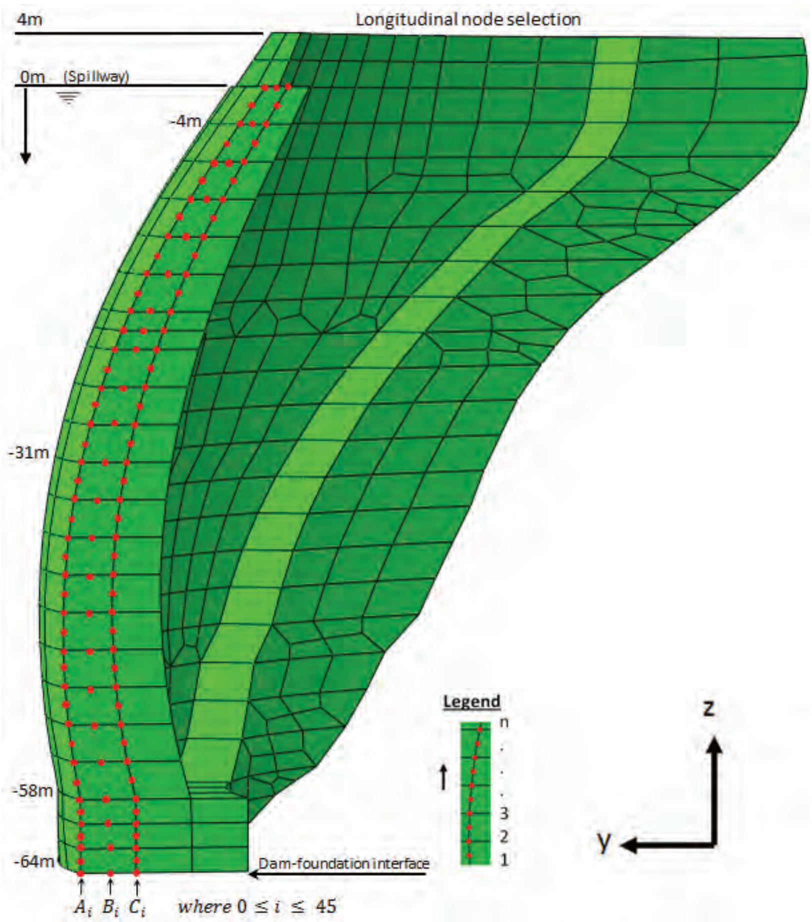

Figure 7.28: Longitudinal nodes for temperature and stress graphs.

7.7.1. Full dam analysis

In full-reservoir analyses the maximum temperature gradient between the upstream and downstream face is approximately 9℃. This is due to the difference in the upstream water temperature and the downstream air temperature and solar radiation.

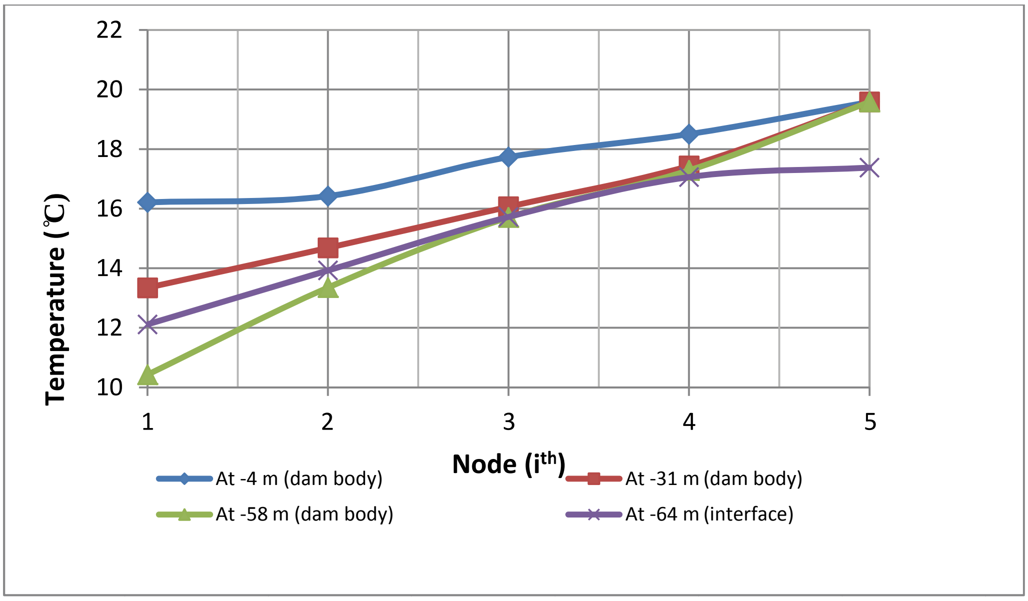

Figure 7.29: Temperature gradient between the upstream and downstream face of the dam at full reservoir level for selected transverse nodes.

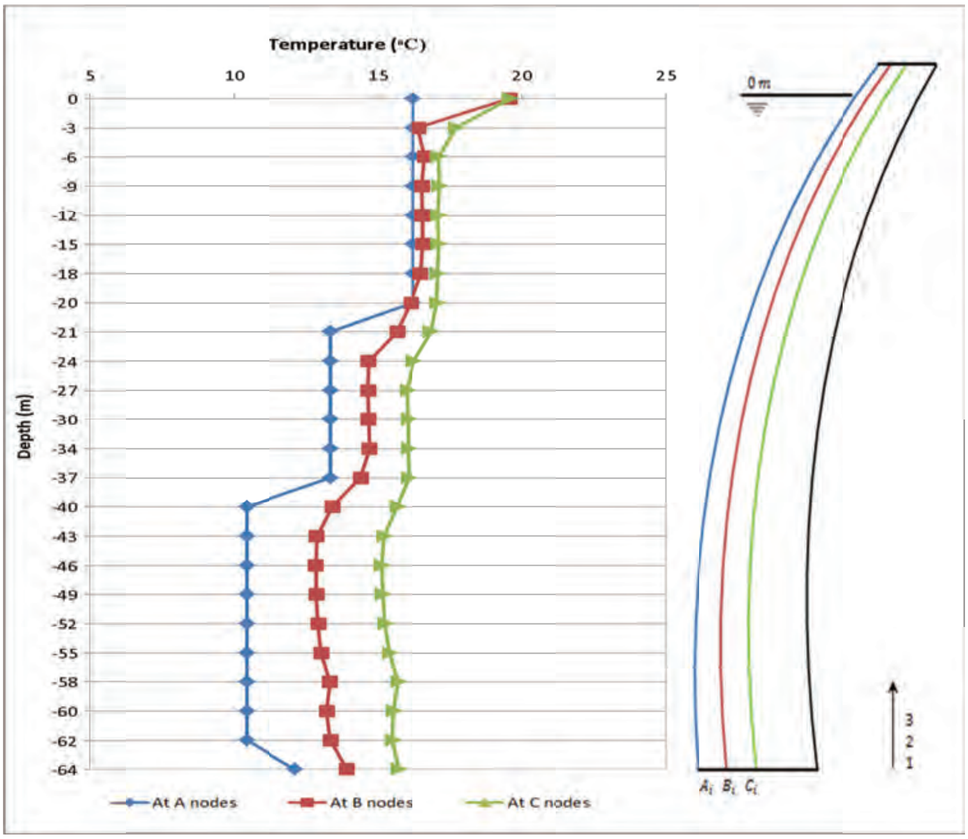

Figure 7.30: Temperature distribution for the first three upstream longitudinal nodes of the full dam.

In Figure 7.30 the highest temperature is observed at the spillway level with a value of 19.6℃. Near the dam-foundation interface, temperature decreases rapidly from -64 m to -62 m for all the longitudinal nodes.

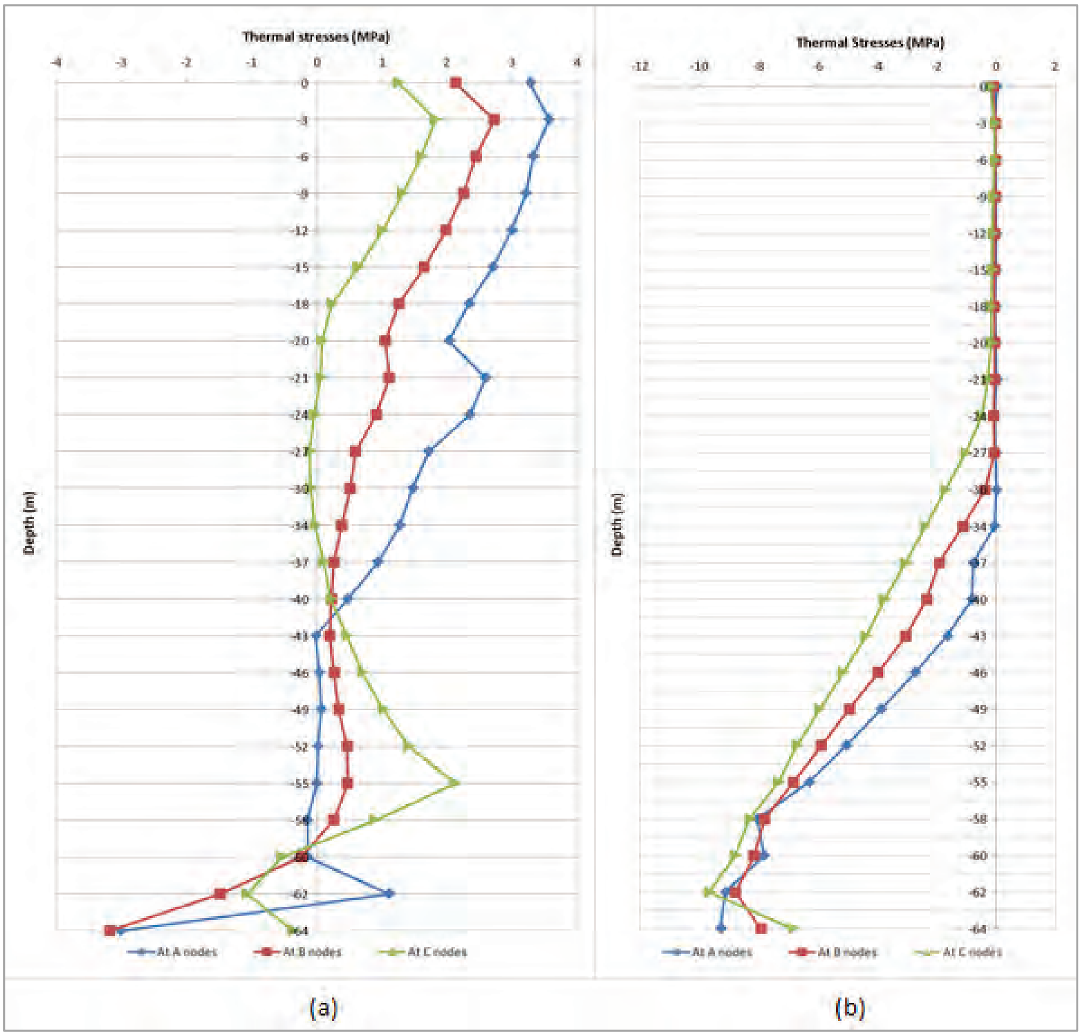

Figure 7.31: Longitudinal (a) maximum principal (tensile) stresses and (b) minimum principal (compressive) stresses for the first three upstream nodes of a full dam.

In Figure 7.31 (a), the largest thermal tensile principal stress is approximately $3.6\ MPa$ and occurs in upstream face near the crest, observed for A_i nodes while the largest thermal compressive stress is approximately 10.5MPa and occurs near the foundation level (Figure 7.31 (b)).

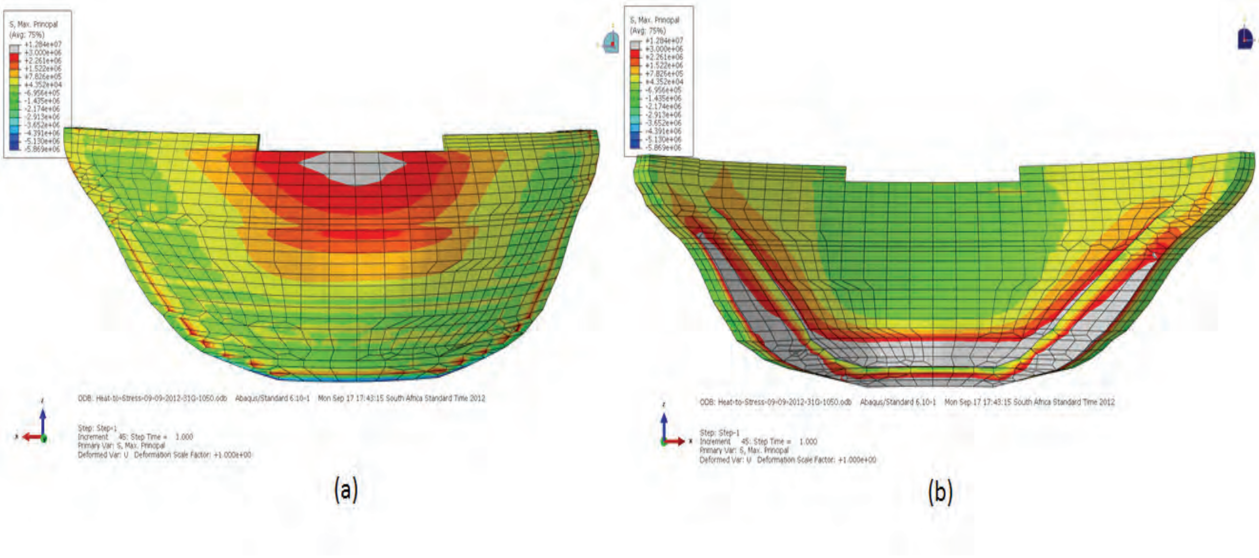

Figure 7.32: Maximum principal (tensile) stress distribution; (a) upstream and (b) downstream for a full reservoir.

Figure 7.33 shows the distribution of tensile thermal stresses on the downstream and upstream faces of the dam. The maximum stresses occur in the grey and red shaded areas. The maximum thermal tensile stresses on the upstream face occur near the crest while the maximum thermal tensile stresses on the downstream face occur around the wall-foundation interface.

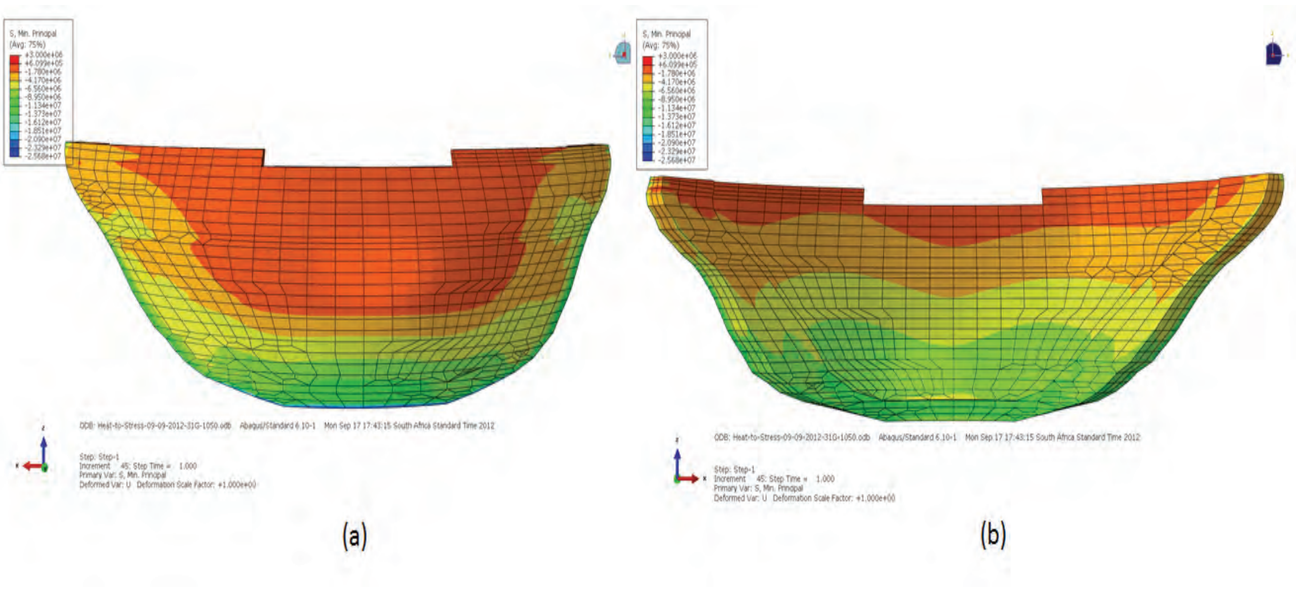

Figure 7.33: Minimum principal (compressive) stress distribution; (a) upstream and (b) downstream of a full reservoir.

In Figure 7.33, the largest thermal compressive principal stresses occur on the upstream face around the wall-foundation interface.

7.7.2. Half-full dam analysis

In half-full dam analysis, the water temperature is applied for the lower half of the dam, while the upper portion and downstream face remain exposed to air temperature and solar radiation. This analysis is associated with spring temperature conditions. The maximum temperature gradient between the upstream and downstream face is approximately 8℃, observed for selected critical elevations in the dam.

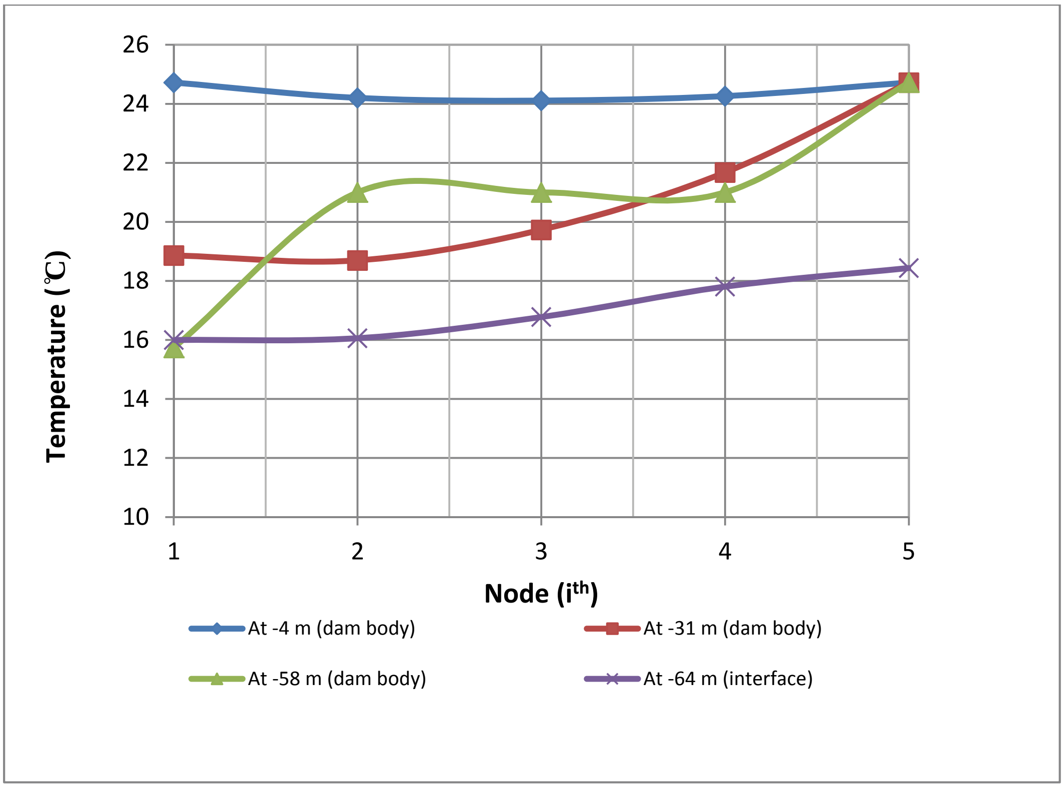

Figure 7.34: Temperature gradient between the upstream and downstream face for half-full dam at selected elevations in the dam.

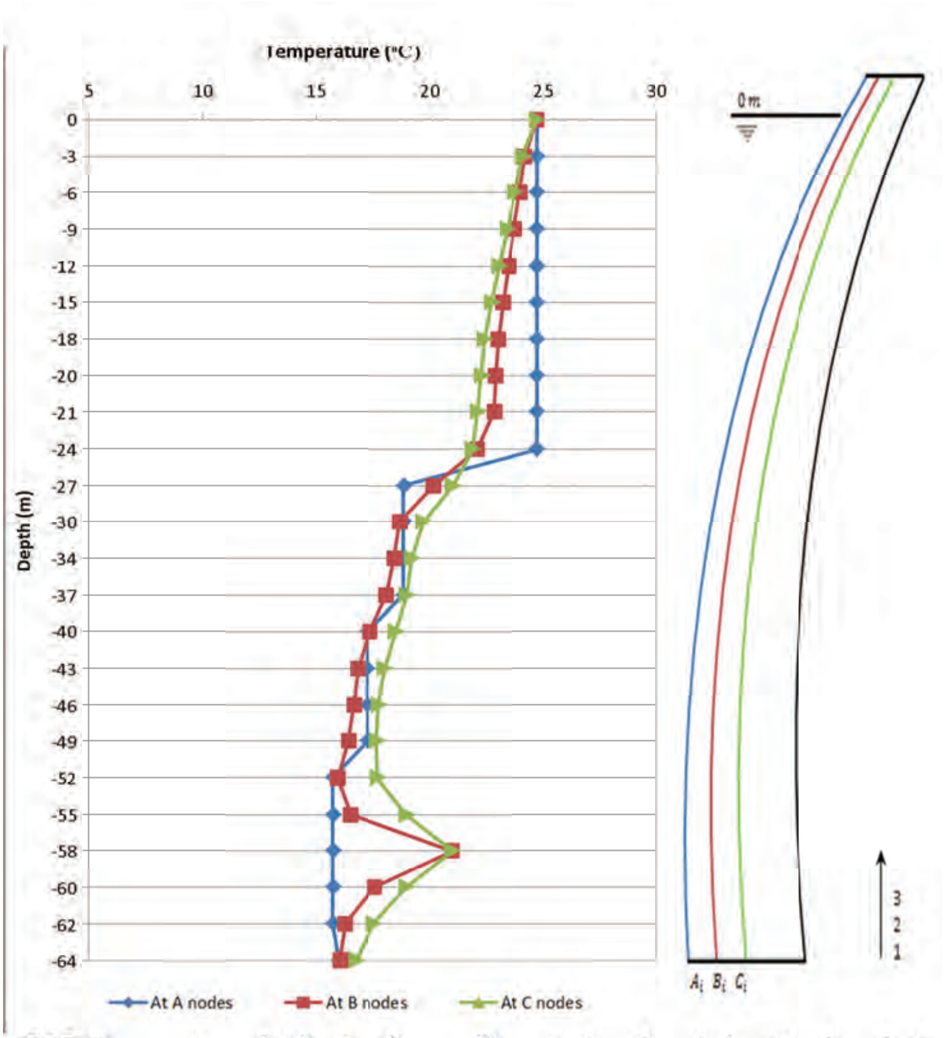

Figure 7.35: Temperature distribution from spillway to dam-foundation interface for half-full dam.

In Figure 7.35, the highest temperature is observed in mostly the exposed upstream face, seen from A_i nodes. Unlike full dam analysis, a rapid increase is observed from -64 m to -62 m for the studied longitudinal nodes.

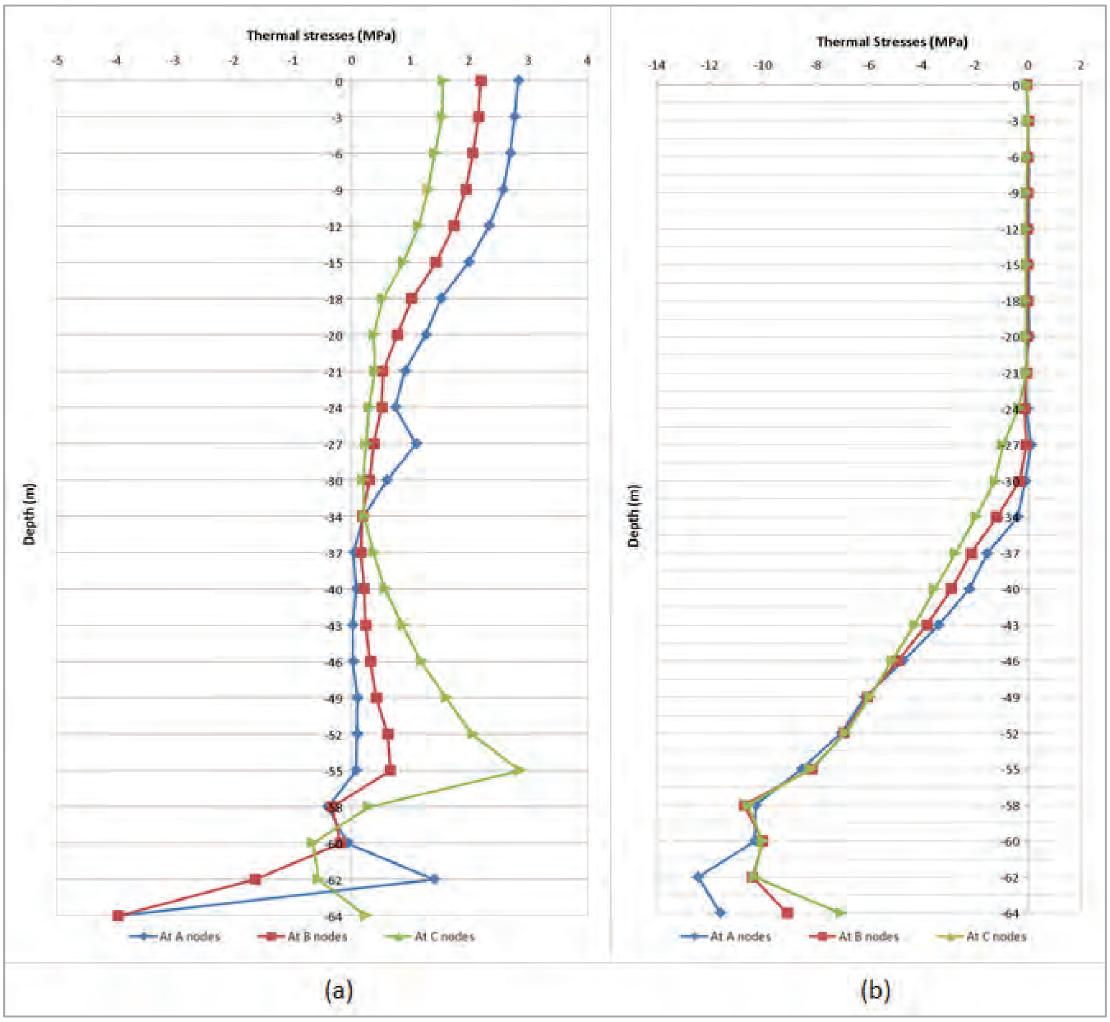

Figure 7.36: Longitudinal (a) maximum principal (tensile) stresses and (b) minimum principal (compressive) stresses for the first three upstream nodes of a half-full dam.

In half-full dam analysis half of the upstream face of the dam wall is exposed to high ambient season temperatures. Figure 7.36 shows that the tensile thermal stresses are reduced [maximum 2.8MPa compared to maximum 3.6MPa] while the compressive thermal stresses become higher compared to the case when the dam is full [maximum -12.8MPa compared to -10.5MPa]. This happens because the dam expands further while subjected under high restraint, thus resulting in a high amount of compressive stresses, usually near the supports.

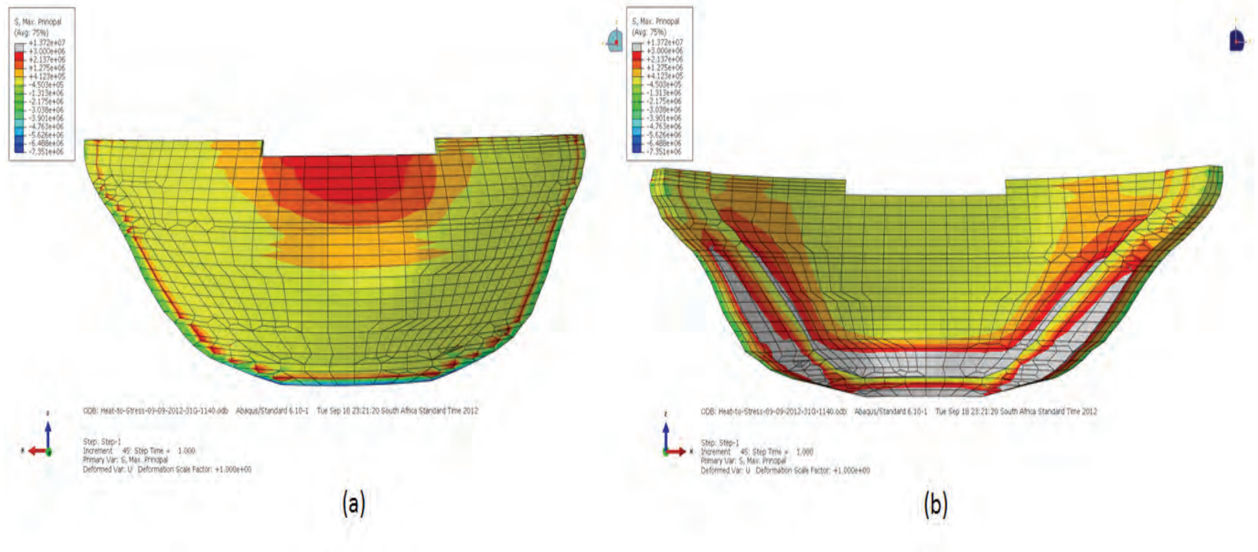

Figure 7.37: Maximum principal (tensile) stress distribution; (a) upstream and (b) downstream of a half-full reservoir.

The stress distribution is similar to full-dam analysis, with high thermal tensile stresses occurring near the crest on the upstream face and near the wall-foundation interface on the upstream face.

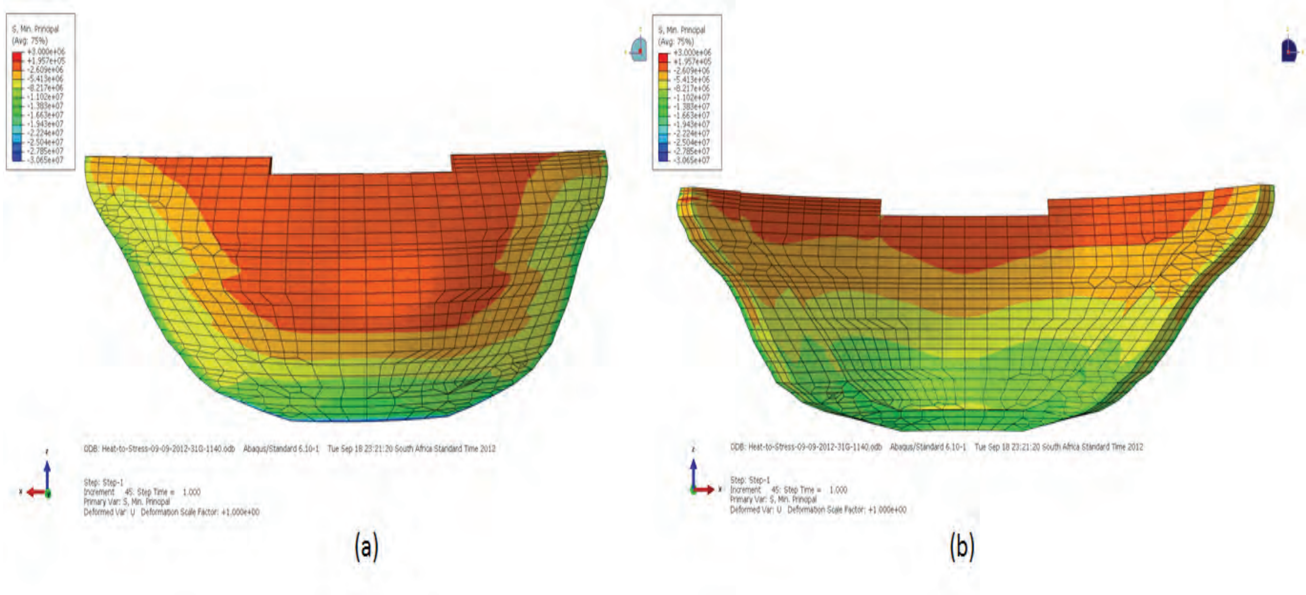

Figure 7.38: Minimum principal (compressive) stress distribution; (a) upstream and (b) downstream of a half-full reservoir.

The distribution of compressive thermal stress is similar to the case when the dam is full, with maximum compressive stresses occurring on the upstream side of the wall around the foundation level (Figure 7.36).

7.7.3. Quarter-full dam analysis

In quarter-full dam analysis the dam is subjected to summer temperature conditions. The quarter lower portion is exposed to water temperature loading while the remaining portion remains exposed to air temperature and solar radiation. The largest temperature gradient between the upstream and downstream face is approximately 5℃, observed for selected critical elevations in the dam.

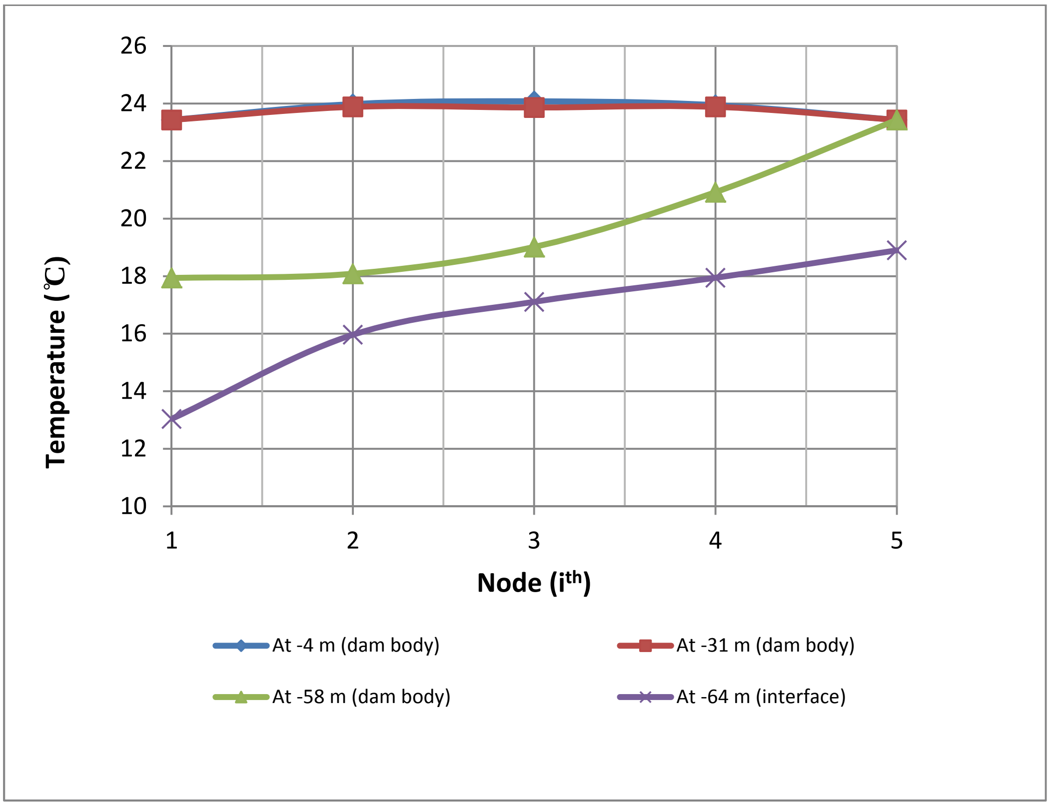

Figure 7.39: Transversal temperature distribution in the dam for a quarter-full reservoir in summer season.

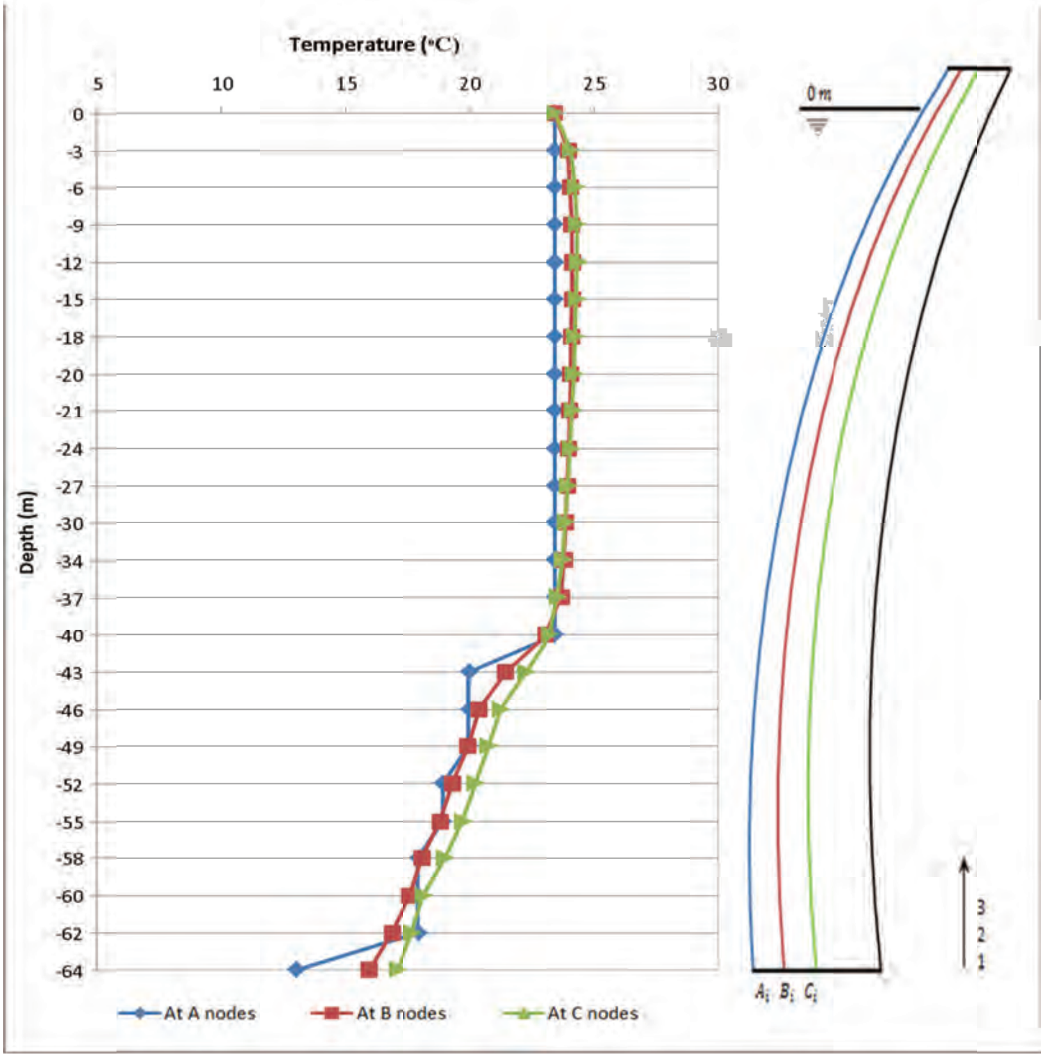

Figure 7.40: Temperature distribution from spillway to dam-foundation interface for quarter-full reservoir.

In Figure 7.40, the highest temperature is observed interior concrete layers of the upstream face, seen from B_i and C_i nodes. Similarly to half-full dam analysis, a rapid temperature increase is observed from the dam-foundation interface (-64 m) to nodes that are two metres higher (-62 m) in the set of longitudinal nodes.

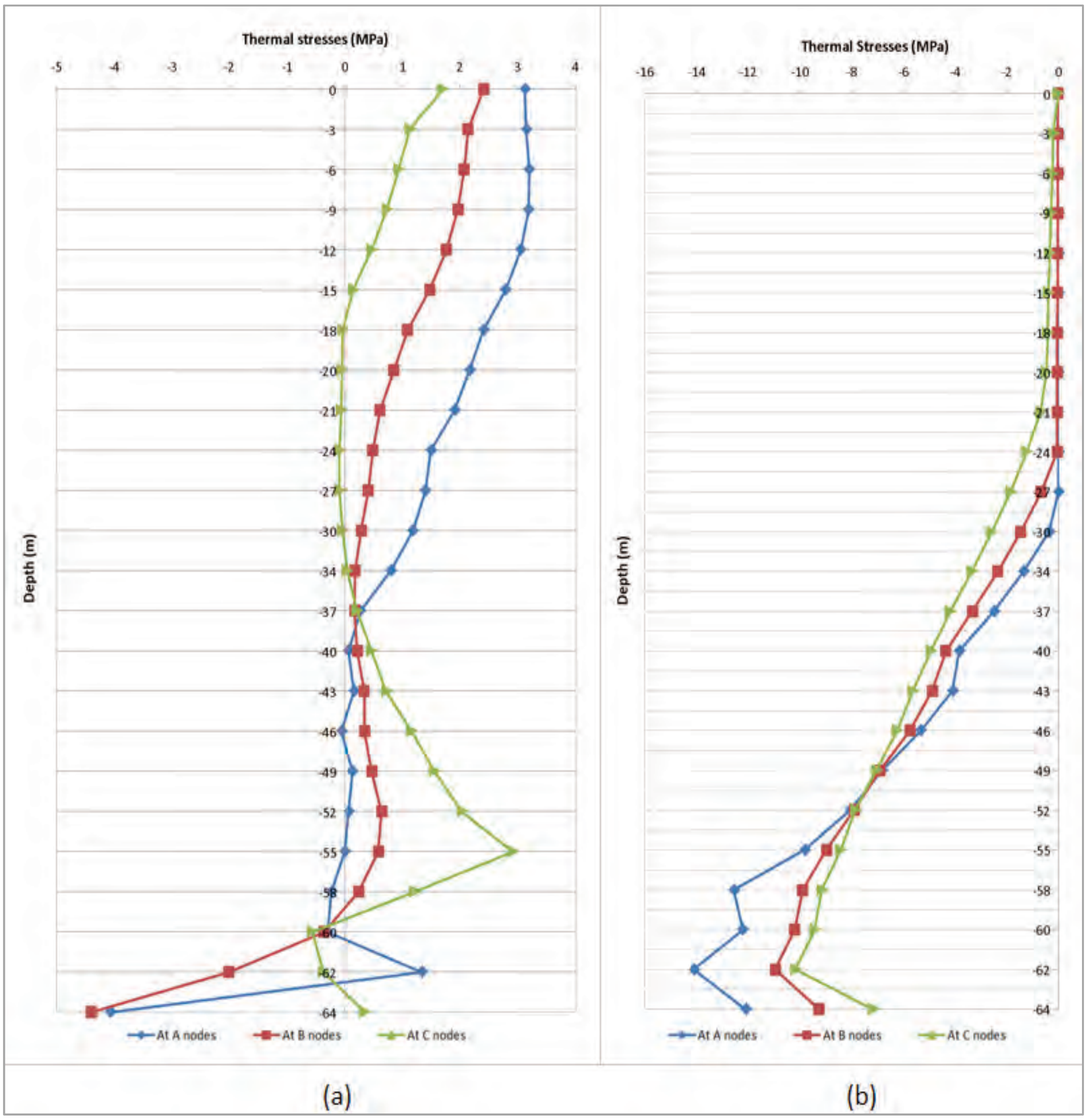

Figure 7.41: Longitudinal (a) maximum principal (tensile) stresses and (b) minimum principal (compressive) stresses for the first three upstream nodes of a quarter-full dam.

Because most part of the upstream face is exposed to high season temperature, lesser tensile stresses and larger compressive stresses are expected for the selected concrete layers as compared to half-full dam analysis. In Figure 7.41 it is observed that a substantial portion of upstream face is subjected high thermal tensile stresses compared to both the full and half cases. See also Figure 7.42 and Figure 7.43.

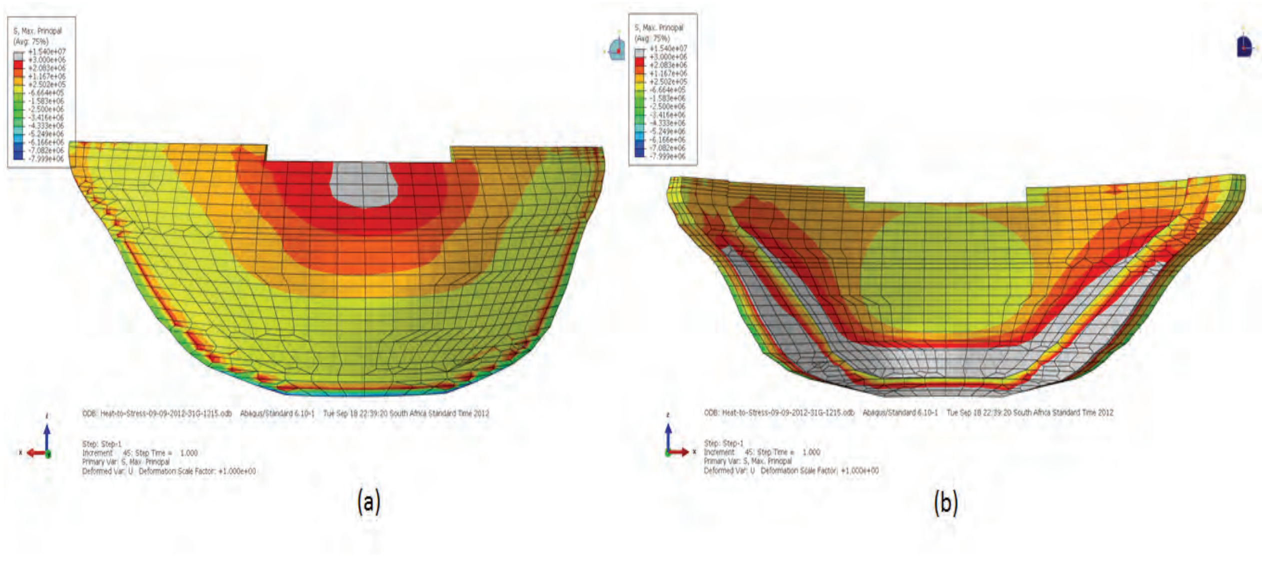

Figure 7.42: Maximum principal stress distribution; (a) upstream and (b) downstream of a quarter-full reservoir.

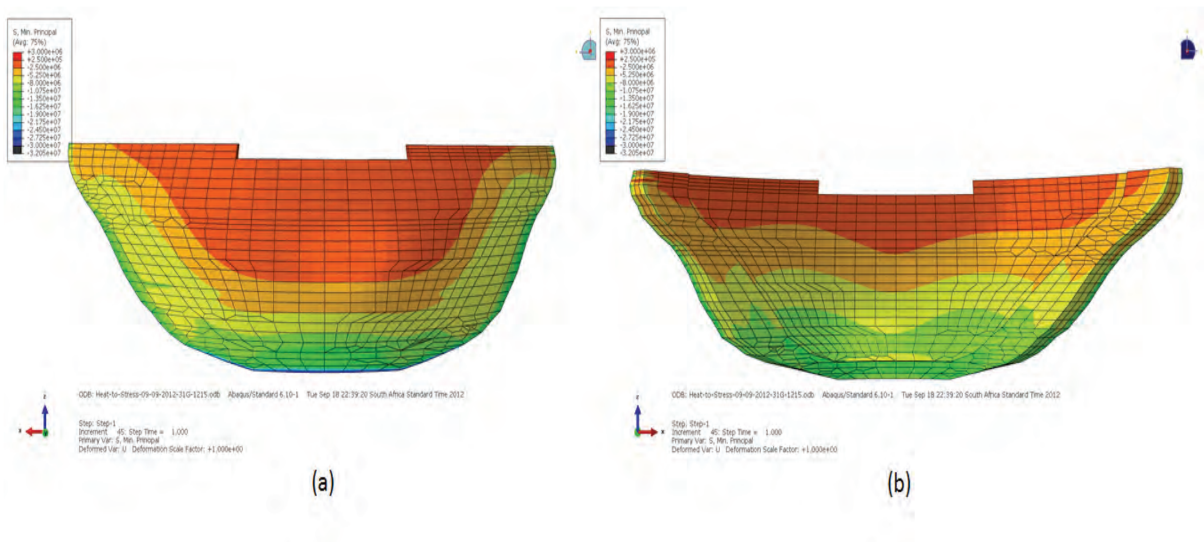

Figure 7.43: Minimum principal stress distribution; (a) upstream and (b) downstream of a quarter-full reservoir.

7.8. Static thermal displacements

Relative displacements due to seasonal temperature variations were computed using the realistic foundation properties given in Table 7.3. Figure 7.46 shows the relative seasonal crest displacements for three cases considered. Higher thermal displacements are observed for the cases when the dam is half full and quarter full. The maximum displacement between the critical seasons was 14.3 mm. The maximum observed displacement of the dam is approximately 44mm. Figure 7.46 and thus seasonal temperature variations contribute about one third of the overall deformation of Roode Elsberg Dam.

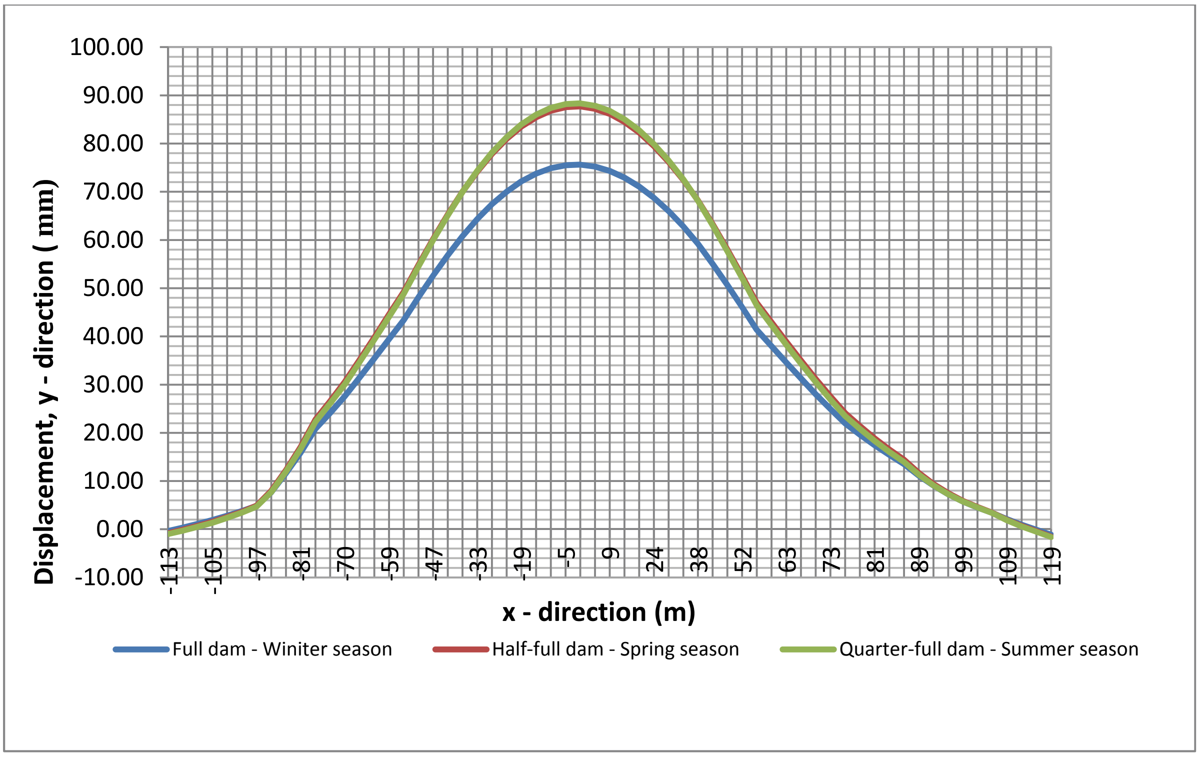

Figure 7.44: FEM crest displacements evaluated for three water level cases.

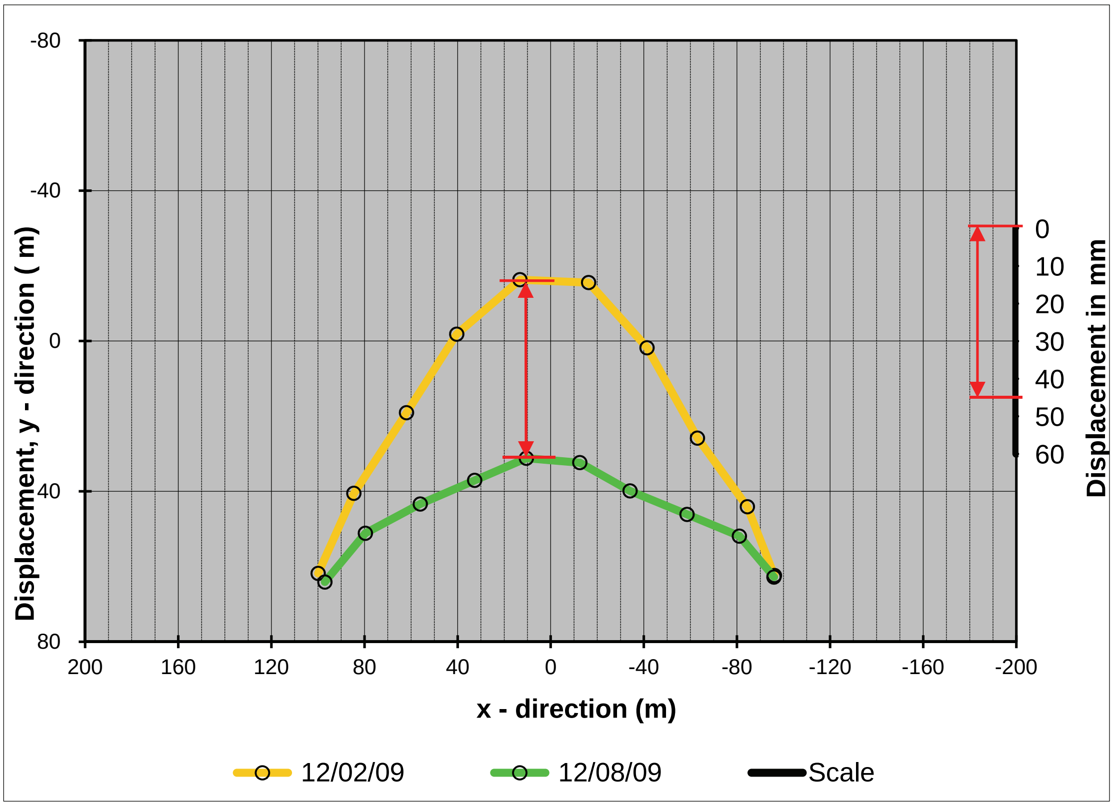

Figure 7.45: Crest displacement for Roode Elsberg dam, obtained from the Department of Water Affairs, recorded 12-02-2009 (summer) and 12-08-2009 (winter).

The analysis shows that seasonal temperature variations have a significant contribution to internal stresses and hence overall deformation of the dam. Recall that frequency analysis showed that natural frequencies are not sensitive to temperature variations. The present result indicates that curvatures obtained from mode shapes of the dam could be used to detect seasonal variations in dam behaviour.

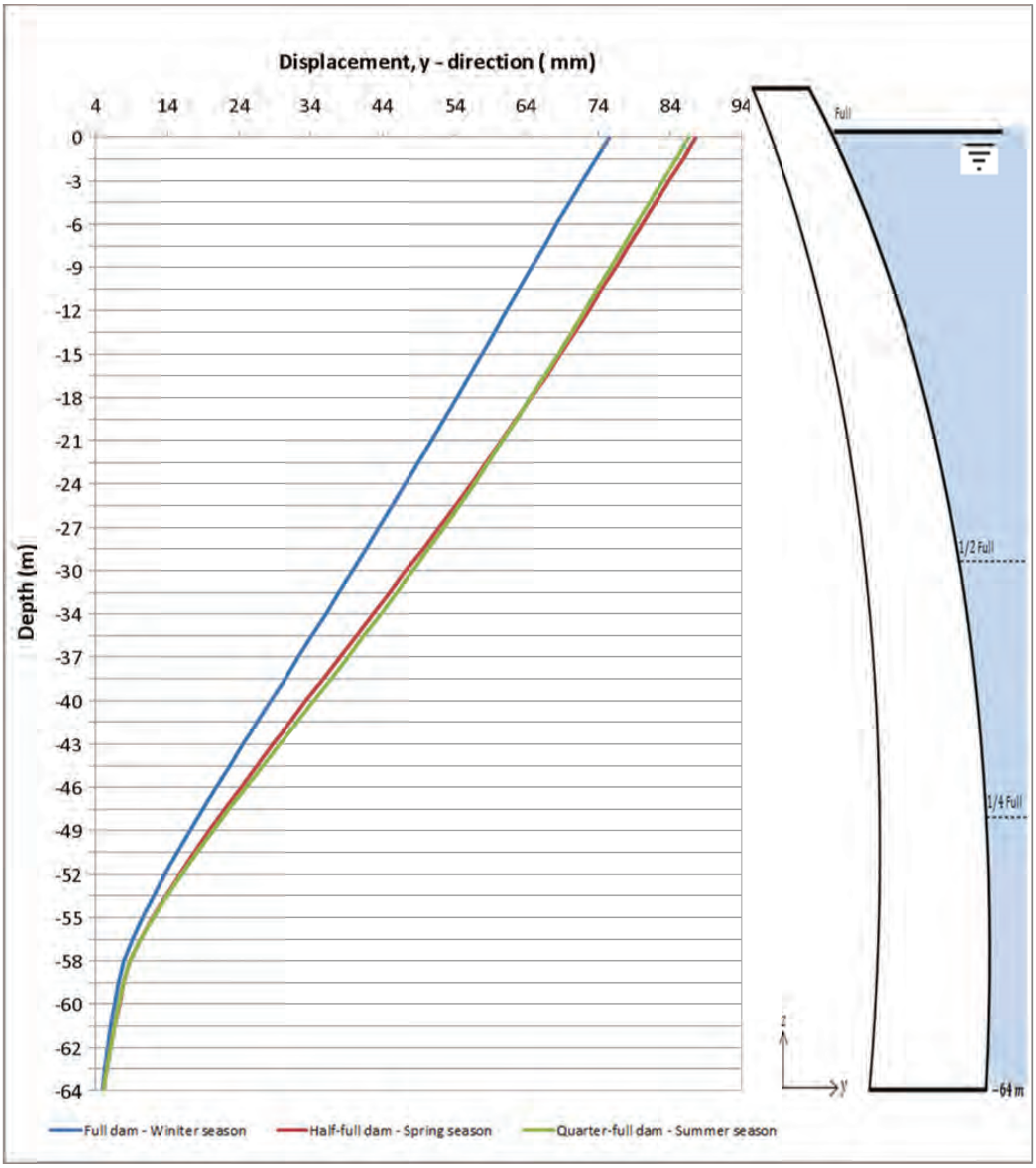

Figure 7.46: FEM longitudinal displacements evaluated for three water level cases.

8. CONCLUDING REMARKS

Dynamic testing can offer insight into the behaviour of dams and the calibration of dam structural models. A major drawback has been the need to measure excitation forces during testing in order to extract modal parameters (natural frequencies, damping ratios, modal mass, etc.) from measurements. The development of the so called output only techniques (ambient vibration testing, operational modal analysis) for extracting modal parameters has expanded the applications of dynamic testing. In ambient vibration testing, dynamic properties are measured under a structure's operating conditions. Thus ambient vibration testing lends itself well to dynamic testing of large civil structures such as dams which would require heavy excitation equipment. This project has demonstrated the suitability of ambient vibration testing for dams. Combining ambient vibration testing with static monitoring offers a very powerful tool for dam safety assessment.

This work has demonstrated how ambient vibration testing can be used to address key finite element modelling issues namely;

i) The foundation size and properties were optimised to minimise computational error.
ii) The Westergaard methods over-estimates the mass of water if the skewness of the reservoir is not taken into account. The added mass had to be reduced by as much as 75% to match the measured dynamic properties and theoretical values.

A unique aspect of the thermal analysis performed for Roode Elsberg Dam is the application of temperature field for appropriate reservoir levels, leading to a realistic thermal loading on the dam. Thus the thermal response obtained is realistic within the limitations of computational modelling of the dam. The results of thermal analysis show that seasonal temperature variations contribute significantly to the deformation of Roode Elsberg Dam. Temperature induced deformations increase with decreasing reservoir level.

Following thermo-mechanical analysis and dynamic analysis of Roode Elsberg dam it is concluded that an initial temperature and thermal stress analysis should be performed before the determination of dynamic characteristics. This ensures that initial stress in the dam is included in the analysis. While thermal and stress analysis are essential prior to the determination of dynamic properties, seasonal temperature variations show little influence on dynamic properties. This is a key point interface between dynamic and static monitoring. While natural frequencies are not sensitive to temperature variations, curvature which can be estimated from static measurements is sensitive to temperature changes.

9. RECOMMENDATIONS

Following this work on structural health monitoring of dams it has become clear that a number of technical issues need to be resolved in two broad areas, viz. finite element modelling and model updating and general monitoring and surveillance.

In finite element modelling the following challenges need to be resolved;

i) Accurate estimation of the added mass

The so called Westergaard method is the most commonly used approach to account for additional mass due to water load for dynamic analysis of dams. This approach is preferred for its simplicity and ease of application. However the method in its current form does not account for certain reservoir geometries. In particular the technique is not directly applicable to divergent and/or skewed reservoirs. Roode Elsberg dam has such a reservoir.

ii) Accounting for initial stresses in dam wall

Temperature studies carried out so far indicate that the behaviour of Roode Elsberg is strongly dependent on seasonal temperature changes. Depending on boundary conditions, initial stresses due to temperature and the hydrostatic load can produce a stiffening effect of the dam wall and thus influence the dynamic properties of the dam.

In dam surveillance and monitoring the following are key research problems;

iii) Extraction of dynamic properties from measured data

A number of methods have been developed for extracting dynamic properties from ambient vibration measurements. While these methods worked well for flexible structures such a tall buildings and bridges, challenges exist with stiff structures such as dams. Appropriate pre-processing of data is necessary. Experience gained with ambient vibration testing show that a combination of methods is necessary to extract dynamic properties from data. This is not a trivial process and requires substantial development of procedures for integrating various methods. Since dynamic properties are central to finite element model calibration, it is essential to obtain dynamic properties as accurately as possible.

Integrating dynamic properties with static measurements for dam safety assessment

It has been shown that dynamic properties change with the change in the loading environment. These properties can thus be used for continuous monitoring of dams in conjunction with static parameters. Dynamic characteristics have the advantage that they can easily be related to the stiffness and mass of the dam wall.

10. REFERENCES

Aktan, A.E., Farhey, D.N., V., Helmicki, A.J., Brown, D.L., Hunt, V.J., Lee, K.L., Levi, A. (1996), “Structural Identification for Condition Assessment: Experimental Arts”, Journal of Structural Engineering, American Society of Civil Engineers, Vol. 123, No.12, pp. 1674-1684.

Andersen P, R. Brincker, M. Goursat, L. Mevel, Automated modal parameter estimation for operational modal analysis of large systems, in: Proceedings of the 2nd International Operational Modal Analysis Conference, vol. 1, Copenhagen, Denmark, 2007, pp. 299-308.

Andersen P. 1997. Identification of Civil engineering structures using Vector ARMAR Model, Ph.D. Thesis, Aalborg University, Denmark, 1997.

Antoni J and Chauhan, 2011. An alternating least square based Blind Source Separation Algorithm for Operation Modal Analysis. Conference Proceedings of the Society for Experimental Mechanics Series, 2011, Volume 6, 179-187, DOI: 10.1007/978-1-4419-9299-4_15

Asmussen J.C. 1997. Modal Analysis based on the Random Decrement technique – Application to civil engineering structures, PhD Thesis, Department of Building Technology and Structural Engineering, Aalborg University, Aalborg, Denmark

Aznarez, J., Maeso, O., & Dominnguez, J. (2006). BE analysis of bottom sediments in dynamic fluid structure interaction problems. Engineering analysis with Boundary elements , 124-136.

Batel M, 2002. Operational Modal Analysis – another way of doing modal testing. *Sound and Vibration, 2002*

Bathe, K. (1996). Finite Element Procedures. New Jersey: Prentice-Hall.

Bayraktar, A., Sevim, B., & Altunisik, C. A. (2011). Finite element model updating effects on non-linear seismic response of arch dam-reservoir-foundation systems. Finite elements in analysis and design , 85-97.

Bendat, J. and Piersiol, A., 1993. Random Data, Analysis and Measurement Procedures, John Wiley 7 Son, New York, USA.

Bianchi M and Bremen R. 2000. Health monitoring of arch dams recent developments. International Workshop on the present and future in health monitoring. Germany September, 3-6, 2000.

Bouaanani, N., & Miquel, B. (2010). A new formulation and error analysis for vibrating dam-reservoir systems with upstream transmitting boundary conditions. Journal of sound and vibration , 1924-1953.

Brebbia, C. A., Tottenham, H., Warburton, G., Wilson, J., & Wilson, R. (1975). Vibrations of Engineering Structures. Southampton: Computational Mechanics.

Brincker R, and Andersen P.2006. Understanding Stochastic Subspace Identification. In *Proceedings of the 24th International Modal Analysis Conference (IMAC)*, St. Louis, Missouri USA, 2006.

Brincker R., P. Andersen, N.J. 2007. Jacobsen, Automated frequency domain decomposition for operational modal analysis, in: *Proceedings of the 25th SEM International Modal Analysis Conference*, Orlando, FL, USA, 2007.

Brincker R., Ventura C., and Andersen P. 2001. Damping Estimation by Frequency Domain Decomposition. *Proceedings of the 19th International Modal Analysis Conference (IMAC),* San Antonio, Texas USA 2001.

Brincker R., Ventura C.E. & Andersen P. 2003. Why Output-Only Modal Testing is a Desirable Tool for a Wide Range of Practical Applications, *Proceedings of the 21st International Modal Analysis Conference (IMAC)*, Kissimmee, Florida, USA

Brincker, R 1995. Note about the Random Decrement Technique, Aalborg University

Brincker, R, Krenk, S, Kirkegaard, P and Rytter, A. 1992. Identification of the dynamic properties from correlation function estimates. Bygningsstatiske Meddelelser, Danish Society for Structural Science and Engineering, Vol. 63, No 1,pp 1-38.

Brincker, R.; Zhang, L.; and Anderson, P. 2000. Modal identification from ambient responses using frequency domain decomposition. *Proceeding of the 18th International Modal Analysis Conference (IMAC-XVIII).*Kissimme, Florida USA, 2000.

Brownjohn J.M.W., P. Carden, 2007. Tracking the effects of changing environmental conditions on the modal parameters of Tamar bridge, in: *Proceedings of the 3rd International Conference on Structural Health Monitoring of Intelligent Infrastructure*, Vancouver, Canada, 2007

Brownjohn, J. M. W. 1990. Dynamic investigation of Hermitage Dam, Jamaica. Report UBCE-EE-90-13 University of Bristol Department of Civil Engineering.

Brownjohn, J.M.W. Severn, R.T., and Taylor C.A 1986. Ambient vibration survey of Contra dam. Research Report University of Bristol Department of Civil Engineering on dams. *Proceedings, Institution of Civil Engineers*, Part 2, Vol 69 ICE London, UK, 1980.

Burman, A., Maity, D., & Sreedeep, S. (2010). Iterative analysis of concrete dam-nonlinear foundation interaction. International Journal of Engineering, Science and Technology , 85-99.

Cauberghe B, 2004. Applied frequency-domain system identification in the field of experimental and operational modal analysis. PhD thesis, Department of Mechanical Engineering, Vrije Universiteit Brussel, Belgium, avrg.vub.ac.be, 2004.

Chopra, K. A. (1967). Hydrodynamic pressure on dams during earthquakes. ASCE Journal of Mechanical Engineering Division , 205-223.

Chuhan, Z., Jianwen, P., & Jinting, W. (2009). Influence of seismic input mechanisms and radiation damping on arch dam response. Soil Dynamics and Earthquake Engineering , 1282-1293.

Clough, P. W., & Tocher, J. L. (1964). Analysis of Thin Arch Dams by the Finite Element Method. International Symposium (pp. 107-122). Southampton: Pergamon Press.

Cole, H.A 1967. On line Analysis of Random Vibrations, AIAA Paper No.68-288

Cunha A. 2005. Keynote Lecture, From Input-Output to Output-Only Modal Identification of Civil Engineering Structures, *Proceedings First International Operational Modal Analysis Conference, IOMAC 1*, Copenhagen, Denmark, 2005

Daniell, W. E., & Taylor, C. A. (1999). Effective ambient vibration testing for validating numerical models of concrete dams. Earthquake engineering and structural dynamics , 1327-1344.

Danielle, W.E and Taylor, C.A. 1999. Effective ambient vibration testing for validating numerical models of concrete dams. Earthquake Engineering. Structural Dynamics. 28(11):1327-1344.

Darbre G.R and Proulx J. 2002. Short Communication: Continuous ambient-vibration monitoring of the arch dam of Mauvoisin. Earthquake Engineering and Structural Dynamics 31(2):475-480.

Darbre G.R, De Smet CAM, Kraemer C. 2000. Natural frequencies measured from ambient vibration response of the arch dam of Mauvoisin. Earthquake Engineering and Structural Dynamics 29(5):577-58.

Darbre, G. R. (2000). State of practice in earthquake analysis of dams. Zurich.

Darbre, G. R., de Smet, C. A., & Kraemer, C. (2000). Natural frequencies measured from ambient vibration response of the arch dam of Mauvoisin. Earthquake engineering and structural dynamics , 577-586.

Dassault Systems Simulia Corp. (2010). Abaqus/CAE User's Manual. Providence: Dassault Systems.

Davey, R. A., Walker, J., & Ho, K. V. (2006). Seismic Assessment and Remediation of the Aviemore Dam Spillway and Sluice Gates.

Deinum et al., 1982. Vibration tests on Emmoson arch dam, Switzerland. Earthquake Engineering and Structural dynamics, 10(3): 996

DETR 2001 List of Panel Engineers: Reservoirs Act 1975. Department of the Environment, Transportation and the Regions. www.dtatabases.detr.gov.uk/reservoir.

Devriendt C., Guillaume P, 2006. Operational Modal Analysis in the Presence of Unknown Arbitrary Loads Using Transmissibility Measurements, *Proceedings of the 13th International Congress on Sound and Vibration* (ICSV13); July 2006; Vienna, Austria.

Devriendt C., Guillaume P, De Sitter G, 2005. Identification of modal parameters from transmissibility measurements with multiple loads*, Proceedings of the 12th International Congress on Sound and Vibration* (ICSV12); July 2005; Lisbon, Portugal.

Devriendt C., T. De Troyer, G. De Sitter, P. Guillaume, 2008. Automated operational modal analysis using transmissibility functions, in: *Proceedings of the International Conference on Noise and Vibration Engineering* ISMA 2008, Leuven, Belgium, 2008.

Dowling, M. J. (1987, September 17). Nonlinier seismic analysis of arch dams. Thesis . Pasadena, California, United States of America: California Institute of Technology.

Du, X., Zhang, Y., & Zhang, B. (2007). Nonlinier seismic response analysis of arch dam-foundation systems-part 1dam-foundation rock interaction. Bull Earthquake Engineering (5), 105-119.

Duron Z H and Hall J F. (1988). Experimental and finite element studies of the forced vibration response of Morrow Point dam. Earthquake Engineering and Structural dynamics, 16(7):1021-1039.

Ellis B.R, Jeary A.P and Litter J.D, 1983. Vibration testing of Contra dam. Building Research Establishment report.

Ellis et al., 2010. Dynamic characterization of a large multiple arch dam. Proceedings of the 30th Annual USSD conference, Sacramento, California, April 12-16, 2010.

Federal Energy Regulatory Committee. (1999). Engineering guidelines for the evaluation of hydropower projects: Arch Dams. Washington DC: Division of Dam Safety and Regulations.

Fenves, G., & Chopra, A. K. (1985). Effects of reservoir bottom absorption and dam-water-foundation rock interaction on frequency response functions for concrete gravity dams. Earthquake engineering and structural dynamics , 13-31.

Fok, K. A., & Chopra, A. (1987). Water compressibility in earthquake response of arch dams. Journal of Structural Engineering , 958-975.

Fok, K. L., & Chopra, A. (1986). Earthquake analysis of arch dams including dam-water interaction, reservoir boundary absorption and foundation flexibility. Earthquake Engineering and Structural Dynamics , 155=184.

Fok, K. L., & Chopra, A. (1986). Earthquake analysis of arch dams including dam-water interaction, reservoir boundary absorption and foundation flexibility. Earthquake Engineering and Structural Dynamics , 155-184.

Gade et al., 2005. Frequency domain techniques for operational modal analysis. *Proceeding of 1st IOMAC conference, 2005, Copenhagen, Denmark.*

Ghanaat, Y. (1993). Theoretical Manual for Analysis of Arch Dams. Washington DC: U.S. Army Corps of Engineers.

Ghanaat, Y. (1993). Theoretical Manual for Analysis of Arch Dams. Washington DC: U.S. Army Corps of Engineers.

Gogoi, I., & Maity, D. (2010). A novel procedure for determination of hydrodynamic pressure along upstream face of dams due to earthquakes. Computers and Structures .

Gouttebroze S. and Lardiès J. 2001. On using the wavelet transform in modal analysis, *Mechanics Research Communications*, 28(5), pp. 561-569.

Guillaume P, Devriendt C., and. De Sitter G Identification of Modal Parameters from Transmissibility Measurements; *Proceedings of the 1st International Operational Modal Analysis Conference*, April 2005; Copenhagen, Denmark.

Guillaume P., Verboven P., Vanlanduit S., Van der Auweraer H. & Peeters B. (2003). A polyreference implementation of the least-square complex frequency domain estimator. *Proceeding of IMAC XXI*. Kissimmee, FL, USA.

Hall, J. F. (1996). Efficient nonlinear seismic analysis of arch dams. California: California Institute of Technology.

Han J., Ren W and Xu X. 2005. Wavelet-based modal parameter identification through operational measurements, *Proceedings of the 1st International Operational Modal Analysis Conference*, Copenhagen, Denmark

Heylen W, S. Lammens, P. Sas, Modal Analysis Theory and Testing, Katholieke Universiteit Leuven, Leuven, Belgium, 2002.

Huang, C. (2001). Structural identification from ambient vibration measurement using the multivariable ar model. Journal of sound and vibration , 337-359.

Huang, C.S.2001. Structural identification from ambient vibration measurements using the multivariate AR model. J. Sound Vib. Vol. 241, pp 337-359.

Ibrahim S.R. and Mikulcik E.C. 1977. A Method for the Direct Identification of Vibration Parameters from the Free Response. *The Shock and Vibration Bulletin* No. 47.

Jacobsen, N.L, 2006. Separating Structural Modes and Harmonic Components in Operational Modal Analysis. *Proceeding of the 24th International Modal Analysis Conference*, St. Louis, Missouri.

Jacobsen, N.L., Andersen, P., Brincker, R. 2008. Application of Frequency Domain curve-fitting in the FDD technique. *Proceeding of 26th International Modal Analysis Conference,* Orlando, Florida.

Janssens, K Z. Kollar, B. Peeters, S. Pauwels and H. Van der Auweraer. Order-based resonance identification using operational PolyMAX*. Proceedings of 24th IMAC Conference on structural dynamics*, St. Louis, US, 30 Jan-2 Feb 2006.

Juang ,J.N., Pappa, R.S. 1985. An eigensystem realization algorithm for modal parameter identification and model reduction. *Journal of Guidance Control Dynamics*, 8(5) pp 620-627.

Kemp B.G 1996. Ambient vibration assessment of Ruskin dam: Dynamic properties. MSc (Civil) Engineering. thesis, submitted to the University of British Columbia (UBC), Vancouver, Canada

Kennedy, R. C., & Hanna, F. W. (1931). The Design of dams. New York: McGraw-Hill.

Kucukarslan, S., Coskun, S. B., & Taskin. (2005). Transient analysis of dam-reservoir interaction including the reservoir bottom effects. Journal of Fluids and Structures , 1073-1084.

Kuo, J. S.-H. (1982). Fluid Structure Interaction: Added mass computations for incompressible fluids. Berkeley: University of California.

Lardies J. and Gouttebroze S. 2002. Identification of modal parameters using wavelet transforms. *International Journal of Mechanical Science*, 44(11), pp 2263-2283.

Lemos J.V, Oliviera S and Mendes P. 2008. Analysis of the dynamic behaviour of Cabril dam considering the influence of contraction joints. *Proceedings of 7th European conference on structural dynamics* (EURODYN), Southampton, UK

Leung, A., Fok, A., Dai, H., & Su, R. (2008). The fractal finite element method for added mass type problems. International Journal for Numerical Methods in Engineering , 1194-1213.

Loh, C.H. and Tsu-Shiu, W. 1996. Identification of Fei-Tsui Arch Dam from both Ambient and Seismic Response Data. Soil Dynamics and Earthquake Engineering, 15(7):465-483.

Loh, C.-H., & Wu. (1996). Identification of Fei-Tsui arch dam from both ambient and seismic response data. Soil Dynamics and Earthquake Engineering , 465-483.

Maeso, O., & Diminguez, J. (1993). Earthquake analysis of arch dams 1: Dam-Foundation Interaction. Journal of Engineering Mechanics , 496-512.

Magalhaes F, Cunha E and Caetano E., 2009. Outline automation identification of the modal parameters of a long span arch bridge. Mechanical systems and signal processing 23 pp 316-329.

Magalhães F., Cunha A. and Caetano E. 2008. Permanent monitoring of “Infante D. Henrique” bridge based on FDD and SSI-COV methods, *Proceedings of ISMA2008*, Leuven, Belgium.

Maghous, S., Bernaud, D., Freard, J., & Garnier, D. (2008). Elastoplastic behaviour of jointed rock masses as homogenized media and finite element analysis. International Journal of Rock Mechanics & Mining Sciences .

Mendes et al., 2004. Dynamic behaviour of concrete dams monitoring and modelling. Proc. 13th World Conference on Earthquake Engineering, Vancouver, BC, Aug 1-6, 2004.

Mendes et al., 2007. Development of monitoring system to Cabril dam with operational modal analysis. *Proceedings of the 2nd Experimental Vibration Analysis for Civil Engineering Structures* (EVAC), Porto, Portugal, 2007.

Mendes, P and Oliveira, S. 2009. Influence of the intake tower behaviour on modal identification of Cabril dam. *Proceeding of the 3rd International Operational Modal Analysis Conference (IOMAC IX)* Portonovo, Italy.

Mendes, P. (2006). Development of a monitoring system to Cabril dam with operational modal ANALYSIS.

Mivehchi, M.R. Ahmadi, M.T. 2003. Effective Techniques for Arch dam Ambient Vibration Test. Application on Two Iranian Dams, International Institute of Earthquake and Seismology (IIEES), Tehran, Iran, 2003.

Mohanty, P. 2005. Operational Modal Analysis in the presence of harmonic excitations Ph.D. Thesis, Technische Universiteit Delft, The Netherlands.

Mohanty, P. and Rixen, D.J.2004. Operational modal analysis in the presence of harmonic excitation. *Journal of Sound and Vibration,* 270(1-2) pp 93-109

Moyo, P and Oosthuizen C. (2010). Ambient Vibration Survey Trials of Two Arch Dams in South Africa. *Proceeding of the 8th ICOLD European Club Symposium*, Innsbruck, Austria

O’Connor, J. P. (1985). Comparison of the observed and predicted behaviour of Roode Elsberg arch dam including the effect of tensile cracking in the concrete. Fifteenth Congress on large dams. Paris: ICOLD.

Okuma N, Etou Y, Kanzawa K, Hirata K. 2008. Evaluation of dynamic properties of an aged large arch dam. Civil Engineering Group, Research Laboratory report, Kyushu Electric Power Co. Fukuoka, Japan

Okuma, N., Etou, Y., Kanazawa, K., & Hirata, K. (2008). Evaluation of Dynamic Properties of an Aged Large Dam. Chiba: Central Research Institute of Electric Power Industry.

Oliviera et al. 2004. Damage characterization in concrete dams using output-only modal analysis. Proc of 22nd International Modal Analysis Conference (IMAC XXII) Dearborn, Michigan, USA.

Pani, P., & Battacharyya, S. (2008). Hydrodynamic pressure on a vertical gate considering fluid-structure interaction. Finite Elements in Analysis and Design , 759-766.

Parloo E, Application of frequency-domain system identification techniques in the field of operational modal analysis. PhD thesis, Department of Mechanical Engineering, Vrije Universiteit Brussel, Belgium, avrg.vub.ac.be, 2003.

Parloo E, Verboven, P, Guillaume, P, and Van Overmeire M, 2002. Sensitivity-based operational mode shape normalization. Mechanical systems and signal processing, 16(5) pp. 757-767.

Peeters B. 2000. System Identification and Damage Detection in Civil Engineering, Ph.D. Thesis. Katholieke Universiteit Leuven, Leuven, Belgium.

Peeters B., Van der Auweraer H., Guillaume P. and Leuridan J. 2004. The PolyMAX frequency-domain method: a new standard for modal parameter estimation, *Shock and Vibration*, Special Issue dedicated to Professor Bruno Piombo, 11, pp. 395-409.

Peeters B., Van der Auweraer H and Leuridan J. 2004. The PolyMAX frequency-domain method: a new standard for modal parameter estimation, *Shock and Vibration*, **11(3)**, pp. 395-409.

Peeters, B., Van der Auweraer H. PolyMAX: a revolution in Operational Modal Analysis. *Proceedings of the 1st International Operational Modal Analysis Conference*, Copenhagen, Denmark.

Peeters, B. and De Roeck, G. 2001. Stochastic system identification for operational modal analysis: a review. ASME *Journal for Dynamic Systems, Measurement, and Control,*123(4) pp 659.

Petsounis, K.A and Fassois, S.D.2001. Parametric Time-Domain Methods for the identification of vibration structures-A Critical Comparison and Assessment. *Mechanical System and Signal Processing,* 15(6) pp 1031-1060.

Poncelet F., G. Kerschen, J.C. Golinval, D. Verhelst.2007. Output-only modal analysis using blind source separation techniques, Mechanical Systems and Signal Processing Vol.21 pp. 2335-2358.

Poncelet, F., Kerschen, G., Golinval, J.C., 2008. Operational Modal Analysis Using Second-Order Blind Identification, Proceedings, International Modal Analysis Conference (IMAC), 7 pp., 2008.

Proulx, J., Paultre, P., Rheault, J., & Robert, Y. (2001). An experimental investigation of water level effects on the dynamic behaviour of a large arch dam. Earthquake engineering and Structural Dynamics , 1147-1166.

Rainieri C, 2008. Operational modal analysis for seismic protection of structures, Ph.D. Thesis, University of Naples, Naples, Italy, 2008

Rainieri C., G. Fabbrocino, E. Cosenza, 2008. An approach to automated modal parameter identification for structural health monitoring applications, in: *Proceedings of the 9th International Conference on Computational Structures Technology,* Athens, Greece, 2008.

Rainieri, C and Fabbrocino, G. 2011. Performance assessment of selected OMA techniques for dynamic identification of geotechnical systems and closely spaced structural modes, *Journal of theoretical and applied mechanics* 49, 3, pp. 825-839

Rainieri, C Fabbrocino G.. 2010 Automated output-only dynamic identification of civil engineering structures, Mechanical Systems and Signal Processing 24 (3) (2010) 678-695, doi:10.1016/j.ymssp.2009.10.003.

Ruzzene M., Fasana A., Garibaldi L and Piombo B. 1997. Natural frequencies and damping identification using wavelet transform application to real data, *Mechanical Systems and Signal Processing*, 11(2), pp. 207-218.

Samii, A., & Lofti, V. (2007). Comparison of coupled and decoupled modal approaches in seismic analysis of concrete gravity dams in time domain. Finite Elements in Analysis and Design , 1003-1012.

Sani, A. A., & Lofti, V. (2007). Linear dynamic analysis of arch dams utilizing modified efficient fluid hyper-element. Engineering Structures , 2654-2661.

Sani, A. A., & Lotfi, V. (2010). Dynamic analysis of Concrete Arch Dams by Ideal-coupled Modal Approach. Engineering Structures , 1377-1383.

Seghir, A., Tahakourt, A., & Bonnet, G. (2009). Coupling FEM and symmetric BEM for dynamic interaction of dam-reservoir systems. Engineering Analysis with Boundary Elements , 1201-1210.

Severn, R.T., Jeary A.P., and Ellis B.R. 1980. Forced vibration tests and theoretical studies

Sevim B, Bayraktar A ad Altunisk A.C. 2010. Finite element model calibration of Berke arch dam using operational modal testing. Journal of Vibration and Control, 2010. doi: 10.1177/1077546310377912

Seyedpoor, S. M., Salajegheh, E., & Salajegheh, E. (2010). Shape optimal design of arch dams including dam-water-foundation rock interaction using a grading strategy and approximation concepts. Applied Mathematical Modelling , 1149-1163.

Skourtis et al. 2004. Long term geodetic monitoring of two dams in Western Greece. *Proceedings of the 1st FIG International Symposium on Engineering Surveys for Construction Works and Structural Engineering* Nottingham, United Kingdom, 28 June – 1 July 2004

Sortis A and Paoliani P. 2005. Statistical and structural identification techniques in structural monitoring of concrete dams *Proceedings of the 73rd Annual Meeting of ICOLD* Tehran, IRAN May 1-6, 2005

Staszewski W.J. 1997. Identification of damping in MDOF systems using time-scale decomposition. *Journal of Sound and Vibration*, Vol 203(2), pp. 283-305.

Tan, H., & Chopra, A. K. (1995). Earthquake Analysis of Arch Dams including dam-water-foundation rock interaction. Earthquake Engineering and Structural Dynamics , 1453-1474.

Tiliouine, B., & Seghir, A. (1998). Fluid-structure models for dynamic studies of dam-water systems. Eleventh European Conference on Earthquake Engineering. Paris.

Toyoda, Y., Shiojiri, H., Ueda, M., & Tsunekawa, K. (2004). Dynamic analysis of an existing arch dam including joint non-linearity and dam-water-foundation rock interaction. 13th World Conference on Earthquake Engineering. Vancouver.

U.S. Army Corps of Engineers. (1994). Engineering and Design: Arch dam design. WASHINGTON DC: Department of the Army.

United States Bureau of Reclamation. (1977). Design of Arch Dams. Colorado: Water Resource Technical.

USACE. (2003). Analytical Modeling of Hydraulic Structures. Washington D.C.: Engineering and Design.

USACE. (2003). Time-History Dynamic Analysis of Concrete Hydraulic Structures. Washington DC: Engineering and Design.

USACE. (2007). Earthquake design and evaluating of hydraulic structures. Washington, DC: Engineering and Design.

Van Overschee,P. and De Moor, B. 1996. Subspace Identification for linear systems: theory-implementation and applications, Dordrecht, The Netherlands: Kluwer Academic Publishers.

Verboven P., Parloo E., Guillaume P. and Van Overmeire M. 2003. An automatic frequency domain modal parameter estimation algorithm, *Journal of Sound and Vibration*, 265, pp. 647-661.

Westergaard, H. M. (1933). Water Pressure on Dams during Earth Quakes. Transactions of American Society of Civil Engineers .

Westergaard, H. M. (1933). Water pressure on dams during earthquake. Transactions, ASCE, 418-433.

Zangar. (1952). Hydrodynamic pressure on dams due to horizontal earthquake effects. Colorado: U.S. Bureau of Reclamation.

Zhang, L, M, Brinker, R. Andersen, P. 2005. An overview of operational of modal analysis: Major developments and issues. *Proceeding of International Operational Modal Analysis Conference,* Copenhagen, Denmark.

Zienkiewicz, C., & Taylor, R. (2000). The finite element method. London: McGraw-Hill.

Zienkiewicz, O. C., Clough, R., & Seed, H. B. (1984). Earthquake Analysis procedures for concrete and earth dams: State of the art. I.C.O.L.D.